DECISION FEEDBACK EQUALIZATION FOR DIGITAL COMMUNICATION OVER THE SATURATED MAGNETIC RECORDING CHANNEL

by

Patrick Glenn Gulak

A Thesis

Submitted to the Faculty of Graduate Studies

in Partial Fulfillment of the Requirements for the Degree of

Master of Science

Department of Electrical Engineering

University of Manitoba

July 1980

Winnipeg, Manitoba
R3T 2N2

DECISION FEEDBACK EQUALIZATION FOR DIGITAL COMMUNICATION OVER THE SATURATED MAGNETIC RECORDING CHANNEL

BY

PATRICK GLEN GULAK

A thesis submitted to the Faculty of Graduate Studies of the University of Manitoba in partial fulfillment of the requirements of the degree of

MASTER OF SCIENCE

ABSTRACT

The longitudinal digital magnetic recording channel is investigated as a communications channel rather than a storage device. The problem of maximum achievable binary recording density is then transformed into a problem of maximum achievable bit rate in a given transmission medium. Bandwidth, noise sources and dynamic properties of this communication channel are characterized initially. These channel characteristics are utilized to predict the theoretical channel capacity at particular signal to noise ratios. It is shown through information theoretic concepts that present data transfer rates utilize approximately 10% of the theoretical channel capacity. Even though a substantial increase in data transfer rate appears possible, as the recording channel is stressed with higher data rates intersymbol interference (ISI) becomes a dominant limiting factor. Decision Feedback Equalization is proposed as one method of combating ISI while increasing the channel utilization. When a relatively small number of past decisions (3 to 6) are used in the feedback equalization process, reasonable performance statistics appear realizable insofar as the linear systems approach remains valid.

ACKNOWLEDGEMENTS

The author wishes to express his gratitude to his supervisor, Dr. E. Shwedyk, for his invaluable counselling, guidance and encouragement.

Thanks are also due to the Winnipeg Plant of the Burroughs Corporation for their financial and technical support. Special thanks are due to Mr. Peter Thorp, Mr. Dan Card, and Mr. Jørgen Frandsen, for their enthusiastic support of this work. Without their help and advice this thesis could not have been completed.

Financial support by the Natural Sciences and Engineering Research Council Postgraduate Scholarship Programme is gratefully acknowledged.

TABLE OF CONTENTS

Chapter 1

INTRODUCTION

1.1 Overview

Magnetic recording techniques on conventional disk drives have been developed extensively over the last decade with the result that digital packing densities above 10^5 bits per square centimeter of recording surface are now commonplace [1,2]. This has encouraged predictions [3,4] that magnetic recording will remain, throughout the next decade, the predominant mass storage medium for computers.

In order to retain a sufficiently low error rate in the face of an ever-increasing demand for higher areal densities, the development of advanced digital magnetic recording systems requires every significant system parameter to be optimally designed. To date, the design process has been largely empirical and suboptimal. The alternative is theoretically based design in terms of a continuing effort to understand the behavior of a digital magnetic recorder from the standpoint of communications theory. It has the best long term cost/benefit ratio by providing absolute bounds on performance and confidence that the design is optimum. Despite these factors, attempts to apply the results of communications theory to the subject of magnetic recording have been relatively sparse and inconclusive.

It is the aim of this thesis to provide a unified analysis of a digital magnetic recorder in terms of a digital communications channel with the intent to establish maximum channel capacity and a realistic optimum receiver architecture.

1.2 Format of the Thesis

A Burroughs type disk drive was used as a test vehicle for our analysis. This removable media device is representative of the high performance rotating memories available on the market today which utilize ferrite heads and oriented γ-Fe_2O_3 media. The recent introduction of thin-film heads and plated media technology [5,6] will help maintain the increasing trend to higher densities without affecting qualitatively the optimum receiver structures investigated in this thesis. It is in this respect that the Burroughs device provides us with a general model for all hard disk drives.

This thesis consists of two major sections. Initially, in Chapter 2, we define and characterize an equivalent communication channel model. The remainder of the thesis concentrates on a receiver design which will increase the channel utilization. In particular, Chapter 2 experimentally characterizes the digital magnetic recorder from the standpoint of communications theory. A model is developed which defines a transmitter, channel and receiver. The useful channel bandwidth, signal-to-noise ratio, the noise power density spectrum and probability density function are then characterized.

Chapter 3 establishes the maximum theoretical channel capacity, develops a decision feedback equalizer design for use in saturated magnetic recording and specifies several alternate receiver structures suggested by theory.

Chapter 4 concentrates on the decision feedback equalizer. A computer simulation is presented which utilizes our experimental channel characteristics

to predict the performance of the decision feedback equalizer.

Discussion of results, conclusions and suggestions for further work are given in Chapter 5.

Chapter 2

THE DIGITAL MAGNETIC RECORD/PLAYBACK CHANNEL

2.1 Introduction

In order to apply the concepts of communication theory, a magnetic recording system can be viewed as a communications channel which consists of an encoder, a recording medium and a decoder as shown conceptually in Figure 2.1. One can consider the transmitter to be comprised of the recording media and read head, the channel to consist of the preamplifier, and the receiver to be the necessary equalizers and decoders. This is one possible way of defining the model. In our analysis, the transmitter noise is reflected to the channel for mathematical tractability. The transmitter and channel is considered as given while the design of the receiver is to be investigated.

The principles of operation are as follows. According to the coding scheme, the encoding circuit transforms the binary input data sequence $\{a_k\}$ into the desired form of write current. This current then energizes the write head, and its gap fringing field magnetizes the recording medium, which is moving at a constant velocity v. As a result, the information is stored spatially on the medium as a series of flux transitions and the write process is complete. The read head is excited by the remanent flux stored on the magnetic medium by the write process. After the readback signal has been amplified the detection circuits then decode it back into the original binary input data sequence $\{a_k\}$, completing the readback process.

In the ordinary digital magnetic recording system saturation recording is performed; i.e., two stable states of magnetization represent the binary data to be stored. (The term "saturation" is used here to describe the case where the peak magnetization in the coating becomes approximately

equal to the remanent magnetization of the major hysteresis loop).

In the readback process of this case, the relationship between the output voltage $e(t)$[†] and the magnetization pattern $m(t)$ is given by:

$$e(t) = \left[\frac{d}{dt} m(t)\right] * h(t) \qquad (2.1)$$

where * means convolution and $h(t)$ represents the magnetic head field distribution characterized by the response due to a unit step function in $m(t)$. Figure 2.2 illustrates typical waveforms at various stages in the recording method.

As seen from Figure 2.2, $e(t)$ is a three-level sequence of -1's, 0's and +1's. For analytic convenience we may consider the readback voltage $E(t)$ due to N alternating magnetic transitions at $t=t_i$ $(i=1,2, \ldots, N)$ is given by:

$$E(t) = \sum_{i=1}^{N} (-1)^{i+1} e(t-t_i) \qquad (2.2)$$

where $e(t)$ is given by equation 2.1.

Inherent in equation 2.2 is the assumption that linear superposition is valid. This assumption is accurate only under a limited (but useful) range of conditions which we will subsequently define.

[†]It is usual to deal with temporal, rather than spatial functions. Thus, we consider the isolated output voltage $e(t)$ rather than $e(x)$. The two are interrelated as:

$$v\, e(x) = v \frac{d\phi}{dx} = \frac{dx}{dt} \cdot \frac{d\phi}{dx} = \frac{d\phi}{dt} = e(t)$$

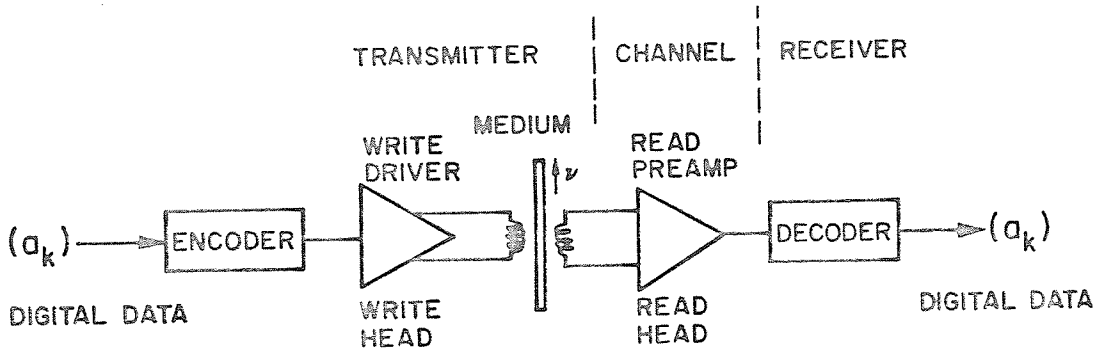

Figure 2.1 Communication Model of the Magnetic Recording Channel

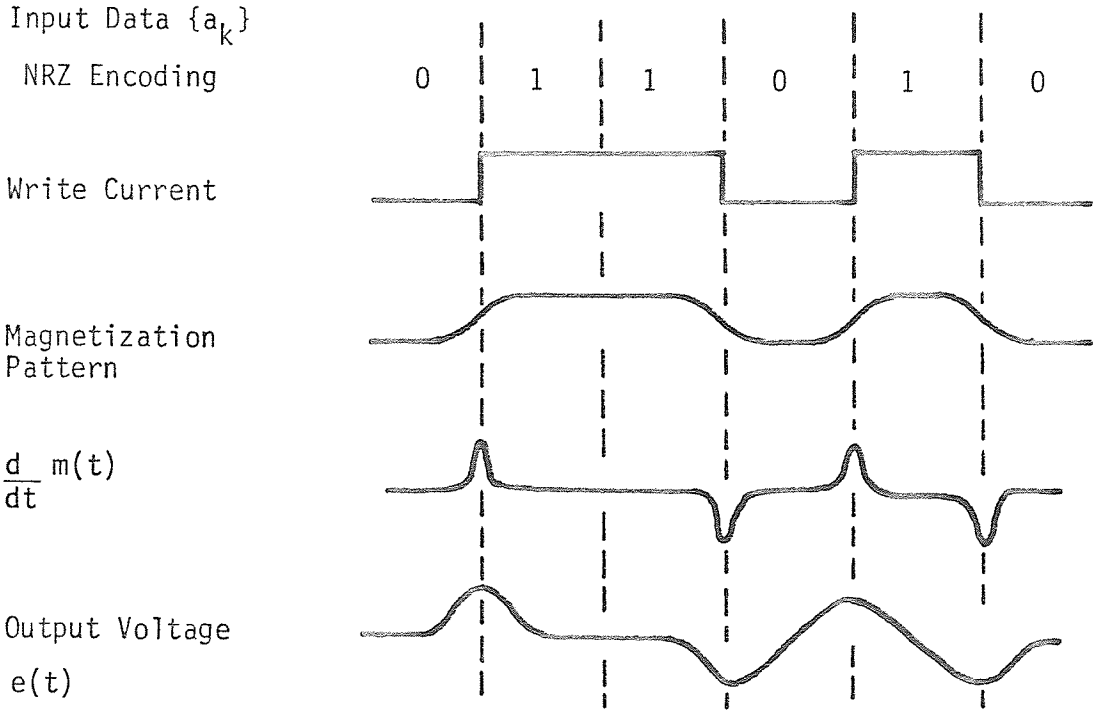

Figure 2.2 Waveforms at various stages of the recording system.

The important features which characterize the communications channel model are: the frequency response of the transmitter and channel, the validity of linear superposition, and the noise statistics. In this chapter, we will measure these channel characteristics experimentally and interpret their significance. This is a necessary prerequisite for developing an optimum receiver structure.

A Burroughs type head/disk interface was selected as the test vehicle for the investigation. The magnetic head and disk interface is similar to those which conventionally provide a density of 2389 bpcm (6060 bpi). The principal head parameters are: 0.052 mm (2.05 mil) track width, 1.52 um (60 uin) gap length and 0.90 um (37 uin) flying height at 10.8 cm (6.40 in) radius and 3600 rpm. The recording medium is a standard oriented gamma (γ) Fe_2O_3 suspended in a polymer binder. Rotational speed fluctuations are held within $\pm$ 2% peak.

The experimental measurements presented in this thesis were made on the outer recording track of the disk. It is important to note that the specific details of the measurements are a function of the position of the recording track. However, the information gleaned from one specific recording track can be used as a basis for all the others.

2.2 Characterization of the Transmitter

A digital recording channel can be considered as a synchronous baseband transmission system having a finite bandwidth [7,8,9]. The frequency response limitations of the transmitter are caused by high frequency losses in the recording and playback head material, losses due to head-to-media spacing, the thickness of the magnetic material and magnetic head gap. It should be noted that the available frequency spectrum is not only limited at the high frequency end, but has basic limitations at the low frequency end due to the lack of dc transfer through the read chain, inherent in the differentiation operation of the readback process.

For a specified recording head and recording media the read head is the key element in the transmitter. During the readback process the read head is excited by the remanent magnetic flux in the medium; consequently, the electrical loss in the read head affects the output waveform [10]. Further, the read head is generally connected to an amplifier which has a finite input impedance, thus distorting the output waveform of the transmitter.

To a first approximation, the read transducer [12] may be represented by the equivalent lumped circuit shown in Figure 2.3. The response is one ofthe family of textbook curves [11] for a second order low pass filter with a resonant frequency of f_n = 8.5 MHz and a damping factor of ζ = 0.90. The high damping factor is desirable from the standpoint of providing high frequency de-emphasis.

The output of the read head is the transmitter output in our equivalent communication channel model. Its characteristics and properties are described in the next section.

2.2.1 The Isolated Transition

(a) Functional Formulation

Central to the characterization of the transmitter is the characteristic pulse shape derived from the magnetization distribution in the transition region between oppositely magnetized regions. Several expressions have previously been chosen to represent the basic pulse analytically. Sierra [13] originally proposed the Gaussian expression e^{-t^2}. Kosters and Speliotis [14] alternately proposed a Lorentzian

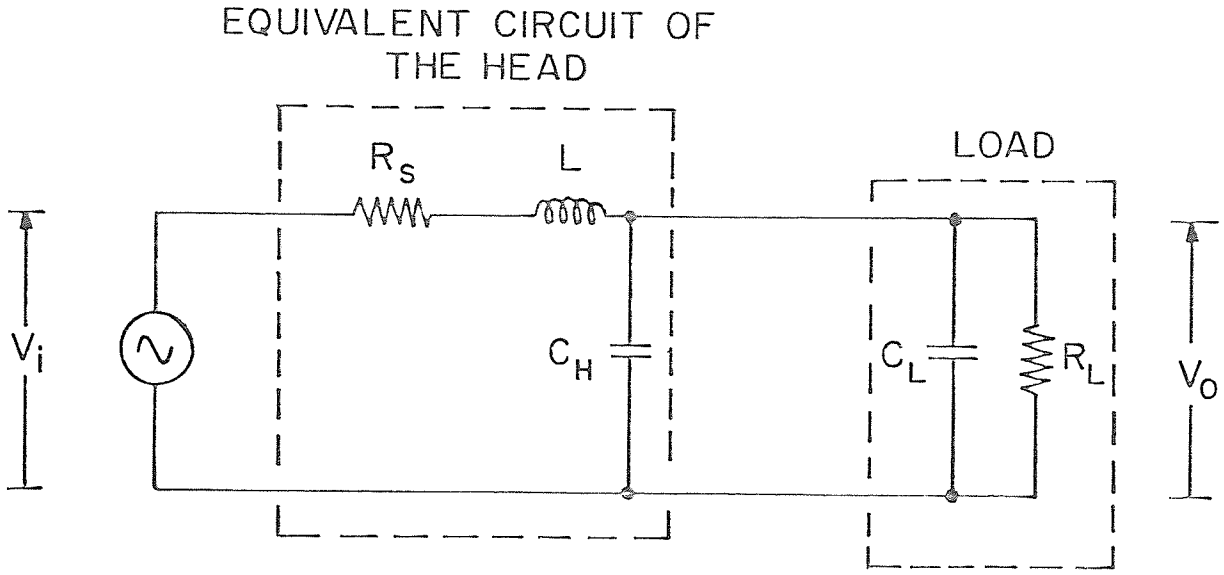

Typical Values for the Disk Drive are :

$L = 13.5\ uH$

$R_S = 15\ \Omega$

$C = C_H + C_L = 10pf + 16pf = 26pf$

$R_L = 400\ \Omega$

Fig. 2.3. Equivalent Circuit for Calculating the Electrical Loss and Loading Effect of the Read / Write Head and Amplifier Load.

representation. The latter is of the form:

$$e(t) = \frac{1}{1 + \left(\frac{t}{t_o}\right)^2}$$

where $2t_o$ is the width of the basic pulse at 50% of the maximum amplitude, universally indicated by PW_{50}. The mathematical justification for this analytic form is based on the fact that the Lorentzian is the derivative of an arctangent function which has widely been assumed as a good representation of the magnetization distribution in an isolated transition. Determined to resolve any further discussion on this topic MacIntosh [15] compared isolated pulses obtained from several currently available rotating disks memories with nine potential analytic expressions. The best least squares fit in his comparison was found to be $1/(1+t^2+t^4)$.

After extensive effort, on the part of the author, in comparing the experimentally obtained pulse shapes to the mathematical models in [15], a quartic function,

$$e(t) = \frac{a}{1+bt^2+ct^4}$$

was determined to be the best representation of the actual pulse shape. This was established by taking a photograph, from a Tektronix 466 storage oscilloscope, of isolated pulses coming directly from the read head damped with a 400Ω resistor. These waveforms were then digitized

and analyzed on a Amdahl 470/V7 computer. A least squares fit to the experimental data was performed using the Gaussian, Lorentzian and the quartic analytic expressions. Table I indicates the results of the least squares fit operation.

Most analytic expressions have little problem providing an accurate fit of the pulse above the PW_{50} amplitude level. It is the "tails" of the isolated pulse that are most difficult to fit. Hence, Table I indicates the least squares error below the PW_{50} amplitude level (i.e., the tails) in addition to the least squares error for the entire waveform.

TABLE I

Least Squares Error Between Analytic Expressions and Experimental Data for an Isolated Readback Pulse

	Least Squares Error	Least Squares Error Below PW_{50} Points
Ke^{-at^2}	0.0864	0.06710
$\frac{K}{1+bt^2}$	0.0369	0.03287
$\frac{K}{1+ct^2+dt^4}$	0.0210	0.01887

Either of these criterion indicates that the quartic function provides the best fit to the experimental data. In addition to least squares criterion, the magnitude and phase spectra of the experimental and the three analytic expressions were calculated. These amplitude spectra, which were later compared to experimental spectrum analyser results, again indicated that the quartic function provides the best fit to the experimental data. Computer generated plots of the experimental data, the least squares fit analytic expressions and the magnitude and phase spectra are shown in Figures 2.4 to 2.6 for the quartic function. The results of the other functions considered are detailed in Appendix A.

To further verify our results, a particular isolated pulse waveform was time averaged by using the oscilloscope trigger delayed sweep feature. This time averaged waveform, representing the history of a particular magnetic transition as it is read repeatedly was digitized and stored on a computer. Again a least squares fit to the experimental data was performed along with a computation of the magnitude and phase characteristics. The results (see Appendix A) indicate that the quartic function provides the best analytic description of the experimental data.

(b) Spectral Verification

To verify and complement the time domain analysis, frequency domain techniques were used.

An additional motivation for this study was encouraged by the thought that perhaps the spectral information may provide additional insight into the functional form of the tails. Experimental results of the amplitude

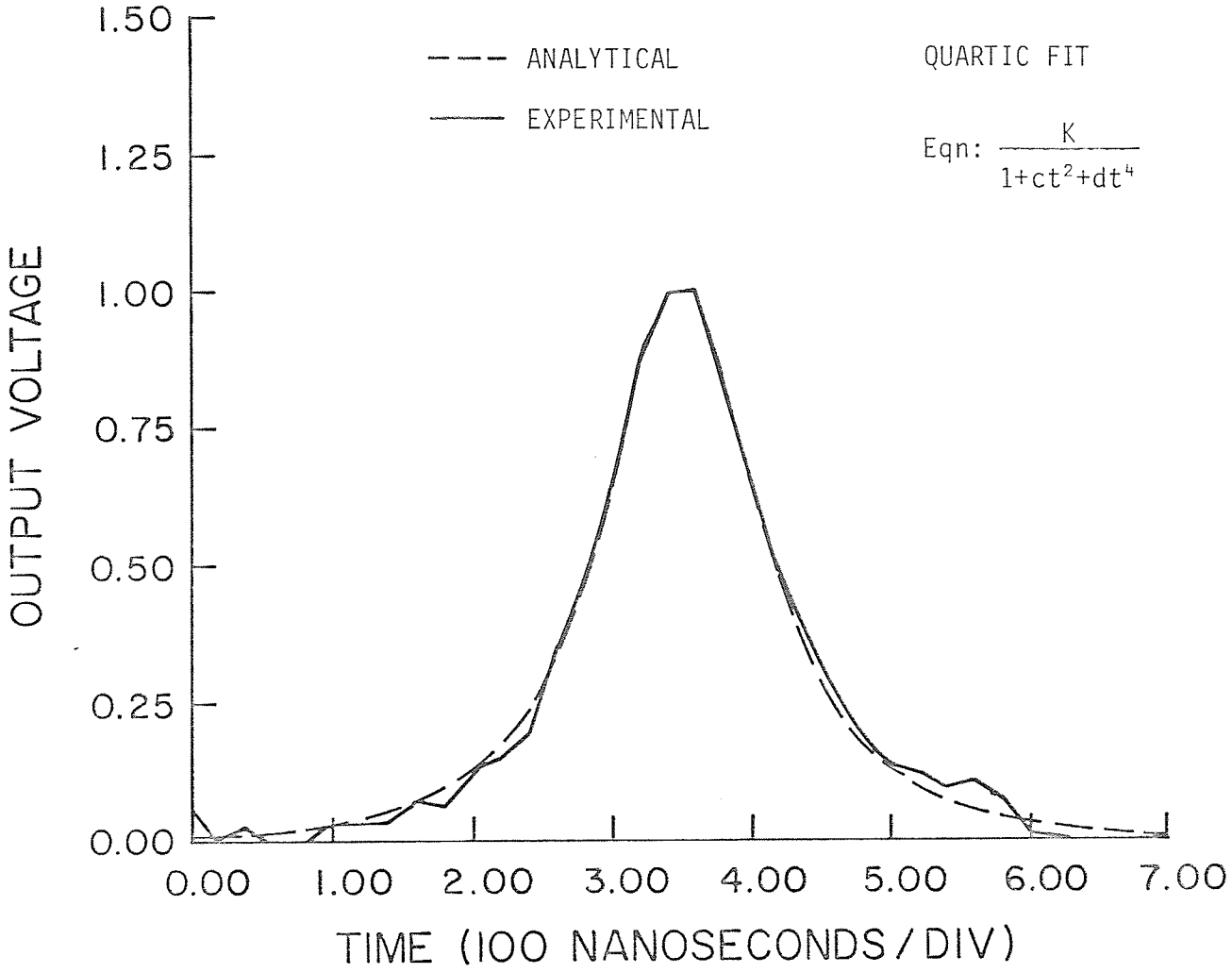

Figure 2.4 The least squares fit to the experimentally observed isolated pulse using the quartic analytic expression.

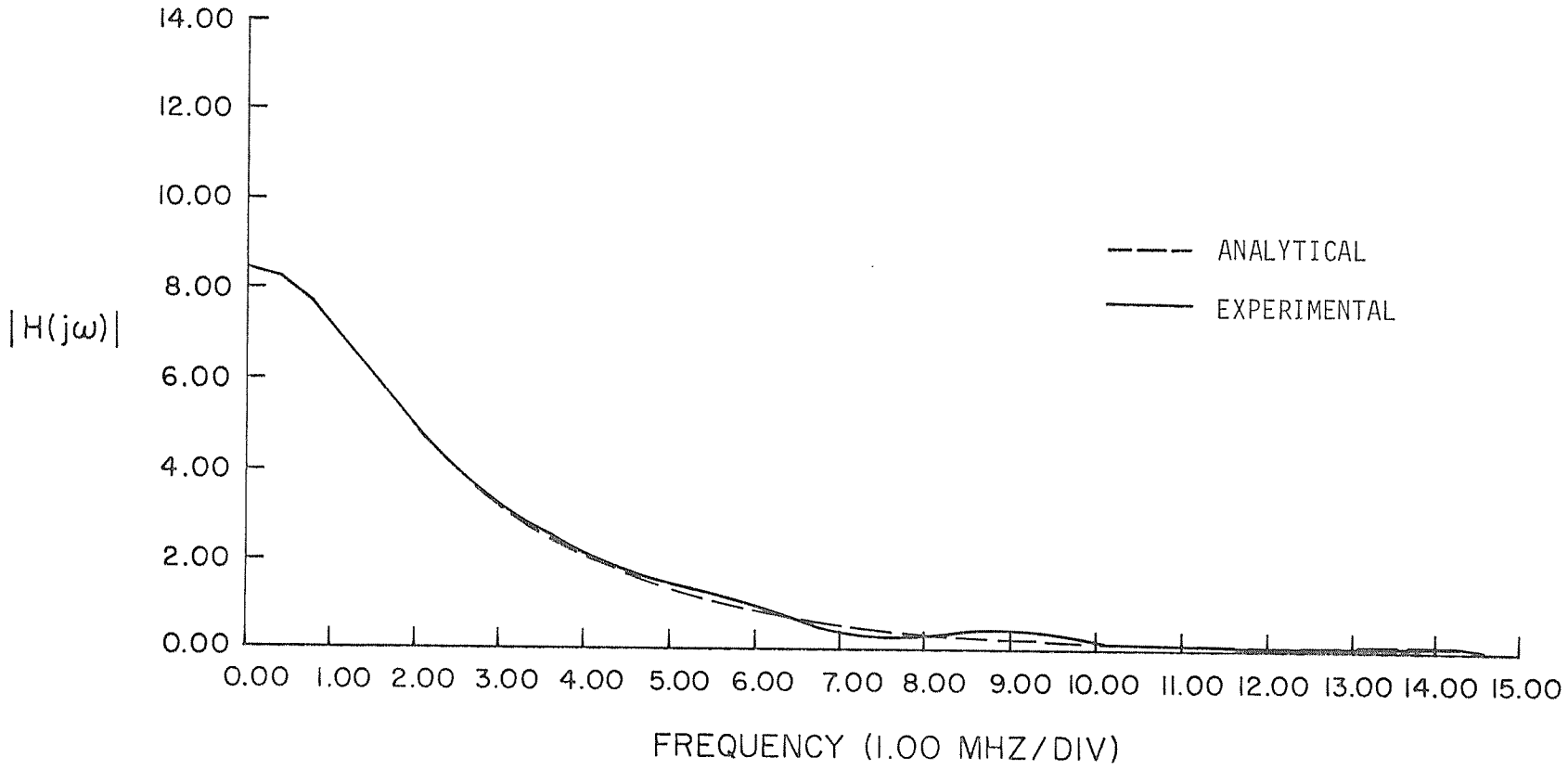

Figure 2.5 Magnitude spectrum of the quartic analytic expression and the experimentally observed isolated pulse.

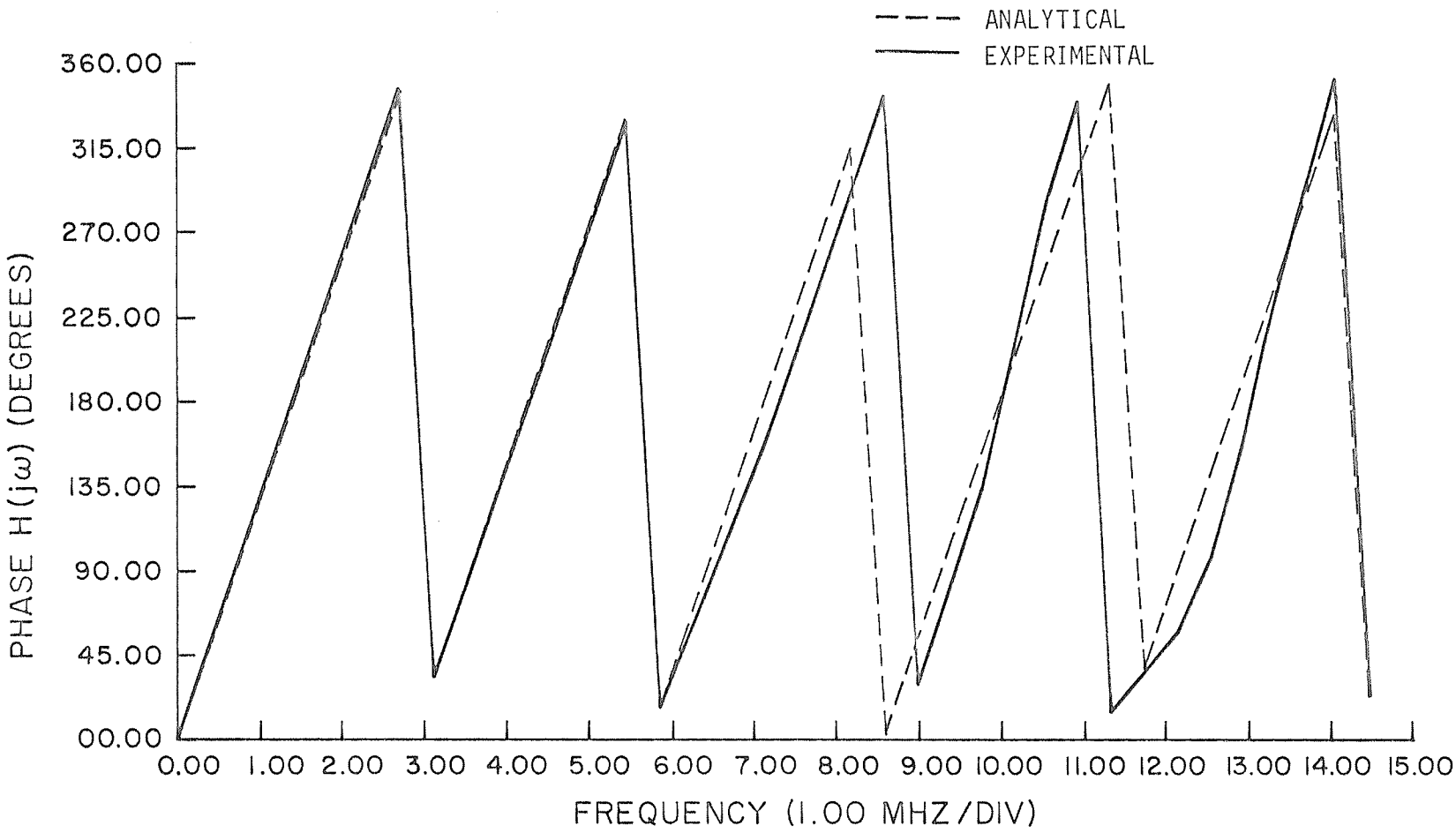

Figure 2.6 Phase spectrum of the quartic analytic expression and the experimentally observed isolated pulse.

spectra up to 10 MHz, obtained with a HP141T spectrum analyser (Figure 2.7), were digitized and subsequently encoded for use in a computer program.

The amplitude components of the frequency spectrum were combined assuming linear phase; i.e., a symmetric readback voltage. This assumption is warranted because the head output voltage due to an isolated transition is very nearly an even function [16,17]. Figure 2.8 depicts the results of the inverse Fourier transform. The reconstructed waveform has good definition in the tails and compares favourably with the analytic quartic expression.

The analysis was repeated at the output of the preamplifier (Figure 2.9). The reconstructed waveform in Figure 2.10 shows a slight pulse slimming effect. This is the result of effective high frequency emphasis due to the low frequency rolloff of the preamplifier.

(c) The Magnetization Distribution

It is apparent that an accurate description for the isolated transition is needed to be able to successfully model the high density behaviour of the magnetic medium through the use of linear superposition.

We have established previously that the quartic function provides a good description of the functional form of the isolated transition. In this section we explore the implications this has on the form of the magnetization distribution in the transition region.

Theoretical calculations of the magnetization distribution in the transition region have for the most part taken four forms. Middleton [18]

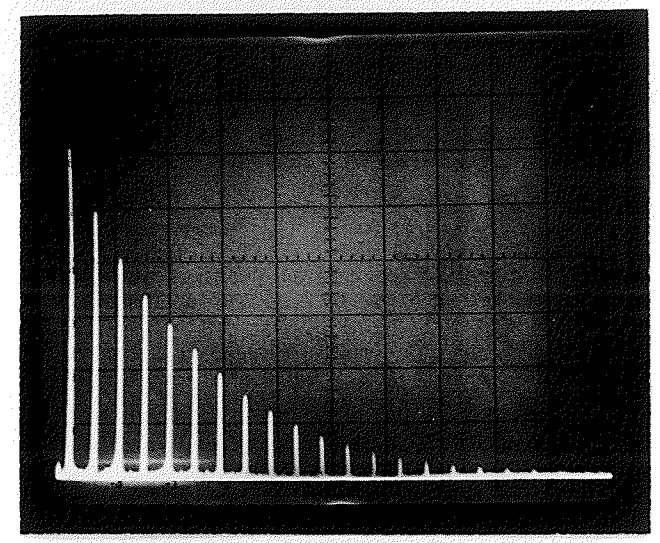

(a) Amplitude Spectrum (0-10MHz, 10kHz bandwidth,
Hor: 1MHz/div, Vert: arbitrary linear units)

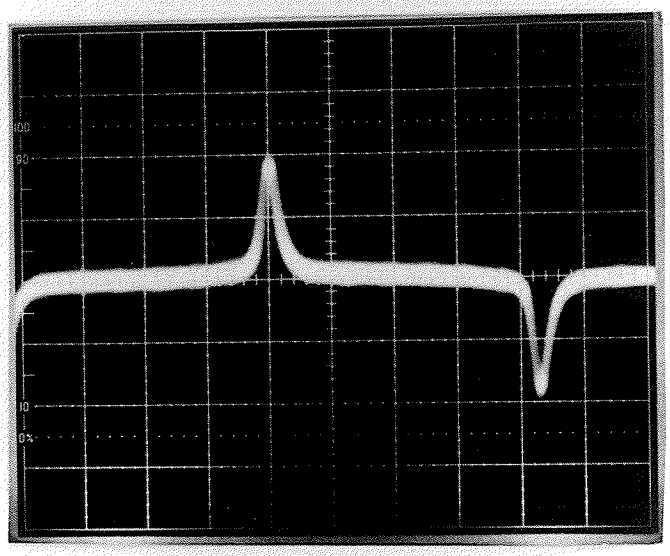

(b) Readback Voltage (0.5 μs/div, 1.0 mV/div)

Figure 2.7 Head Readback Voltage in the Time and Frequency Domains.

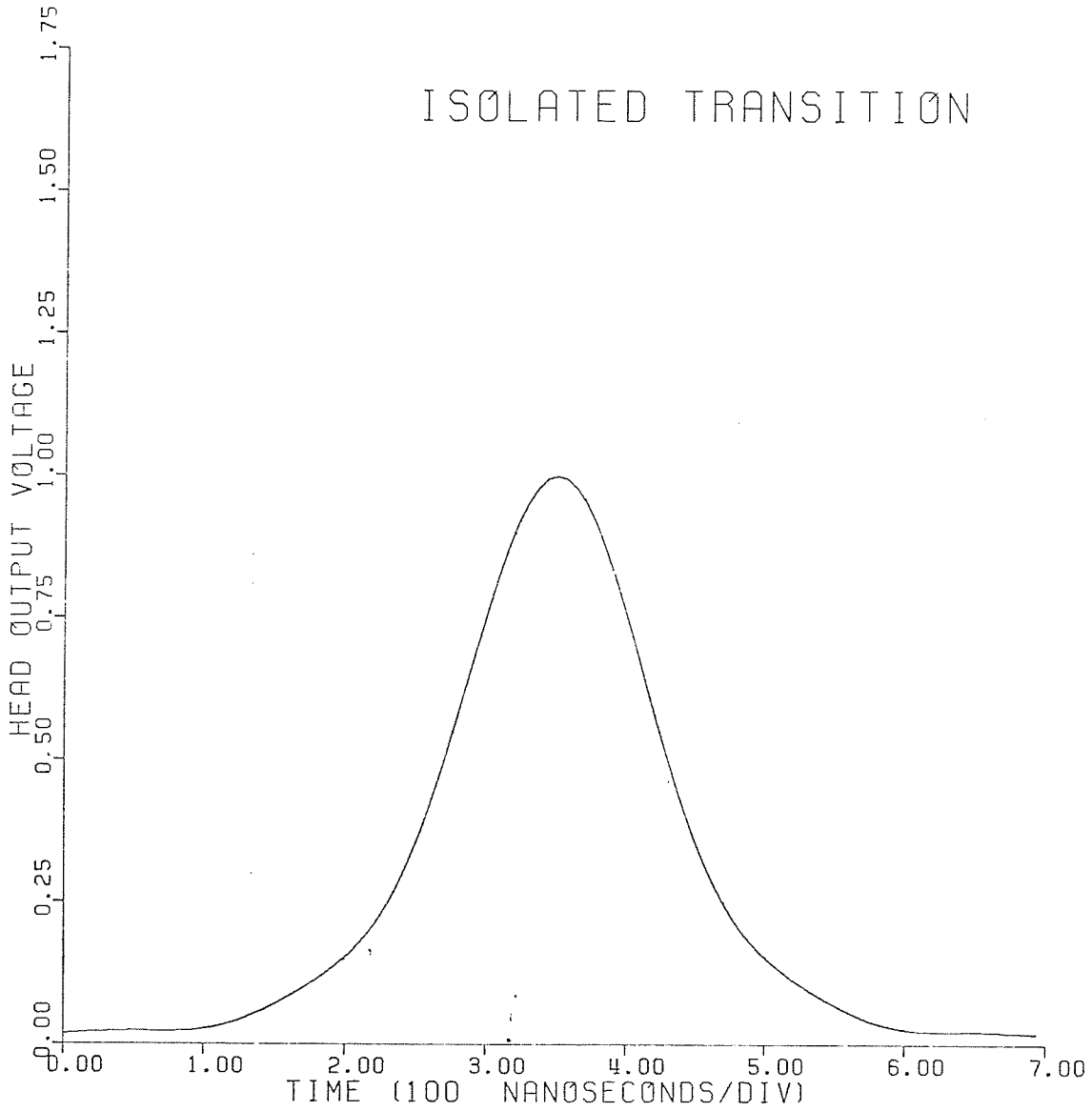

Figure 2.8 Head readback voltage obtained by the inverse Fourier transform of the magnitude spectrum depicted in figure 2.7.

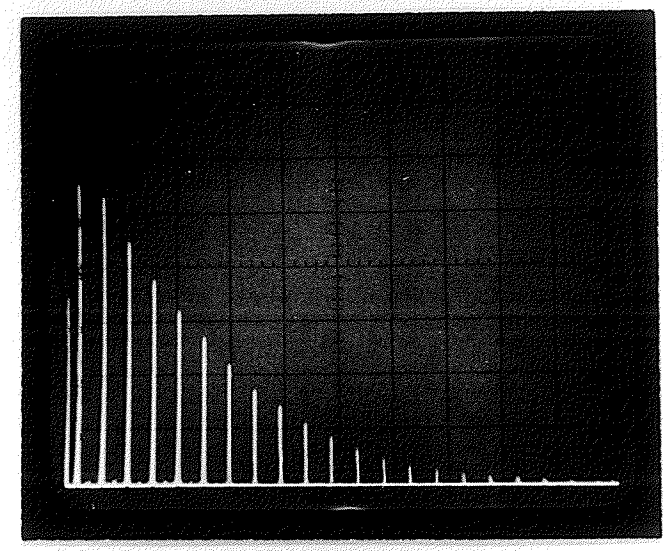

(a) Amplitude Spectrum (0-10MHz, 10kHz bandwidth,
Hor: 1MHz/div, Vert: arbitrary linear units)

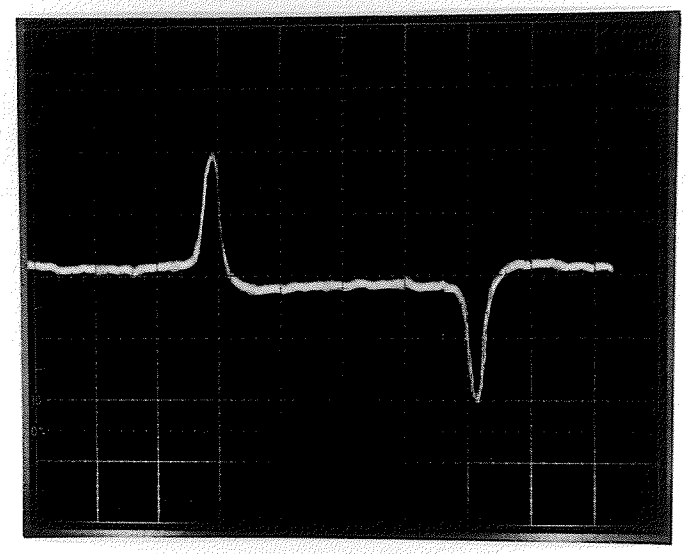

(b) Output Voltage (0.5 μs/div, 100 mV/div)

Figure 2.9 Preamplifier Output Voltage in the Time and Frequency Domains.

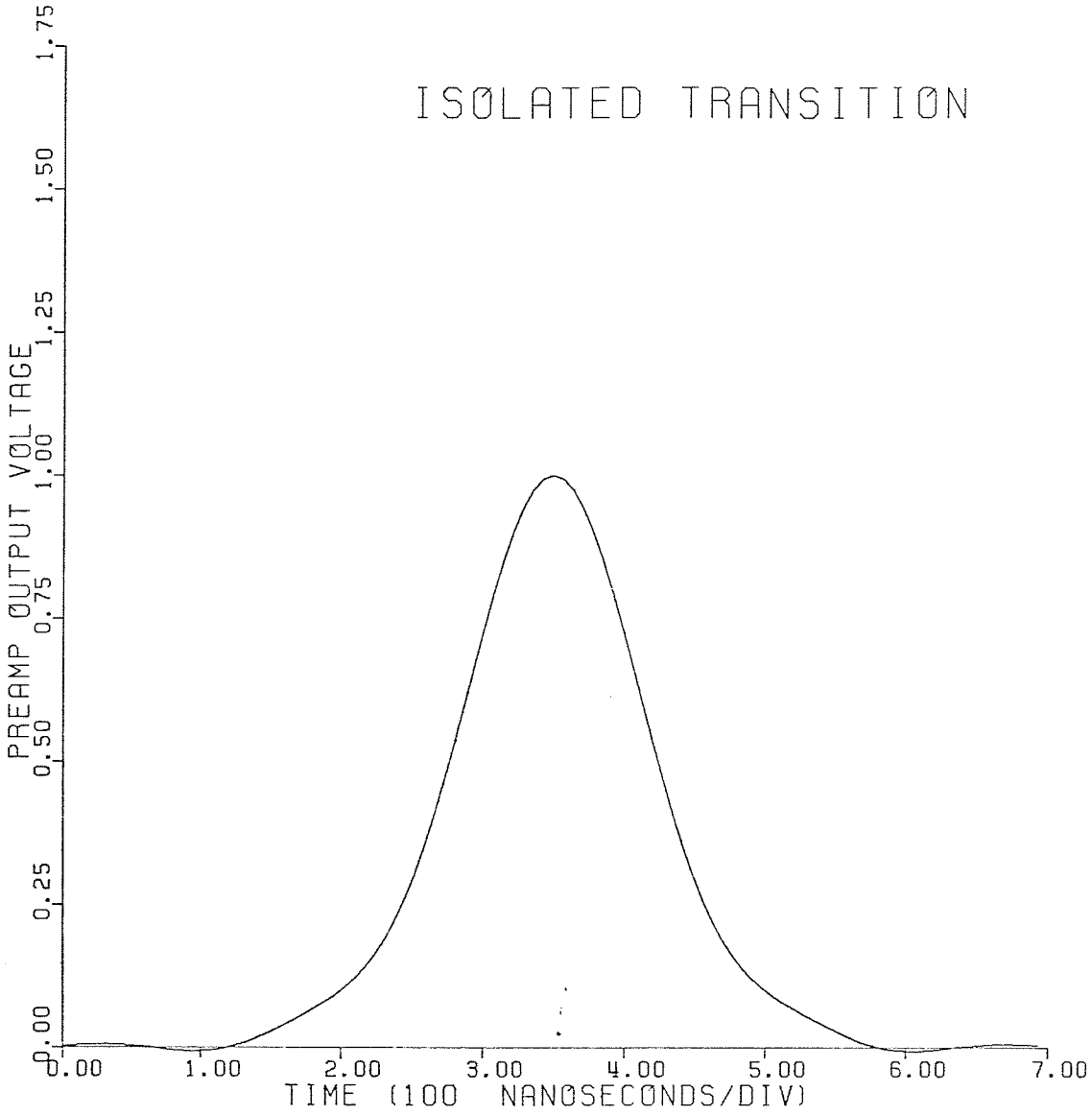

Figure 2.10 Preamplifier output voltage obtained by the inverse Fourier transform of the amplitude spectrum depicted in figure 2.9.

assumed an arctangent distribution for the transition region. Speliotis and Aharoni [18] assumed linear transitions based on demagnetizing forces and energy minimization considerations. Kostyshyn and later Mallinson [18] proposed a harmonic analysis scheme where an average demagnetizing factor was calculated for each Fourier component of the magnetization. This particular scheme is based on the assumption that the medium is linear. Iwasaki and Suzuki [18] have presented a self-consistent iterative model of the write process that does not divorce the demagnetization from the writing process as the previous theories. In this model an increment of the medium was considered to be subjected to a magnetic field composed of the sum of the head field and the demagnetizing fields due to all other (past history) increments in the medium. Though currently considered the most accurate procedure, being an iterative method it unfortunately has no analytic closed form and requires significant computing resources. The computed transitions for the various theories are illustrated in Figure 2.11.

When the head field function $h(t)$ in Equation (2.1) is an impulse (for the ideal head) the magnetization pattern is simply the integral of $e(t)$. This was the premise by which the magnetization patterns displayed in Figure 2.12 were developed. The arctangent transition,

$$m(t) = M_1 \tan^{-1} C_1 t$$

is the integral of the Lorentzian pulse, a widely accepted analytic form of the isolated pulse. The step function transition appears as a special case of the arctangent distribution when C_1 approaches infinity.

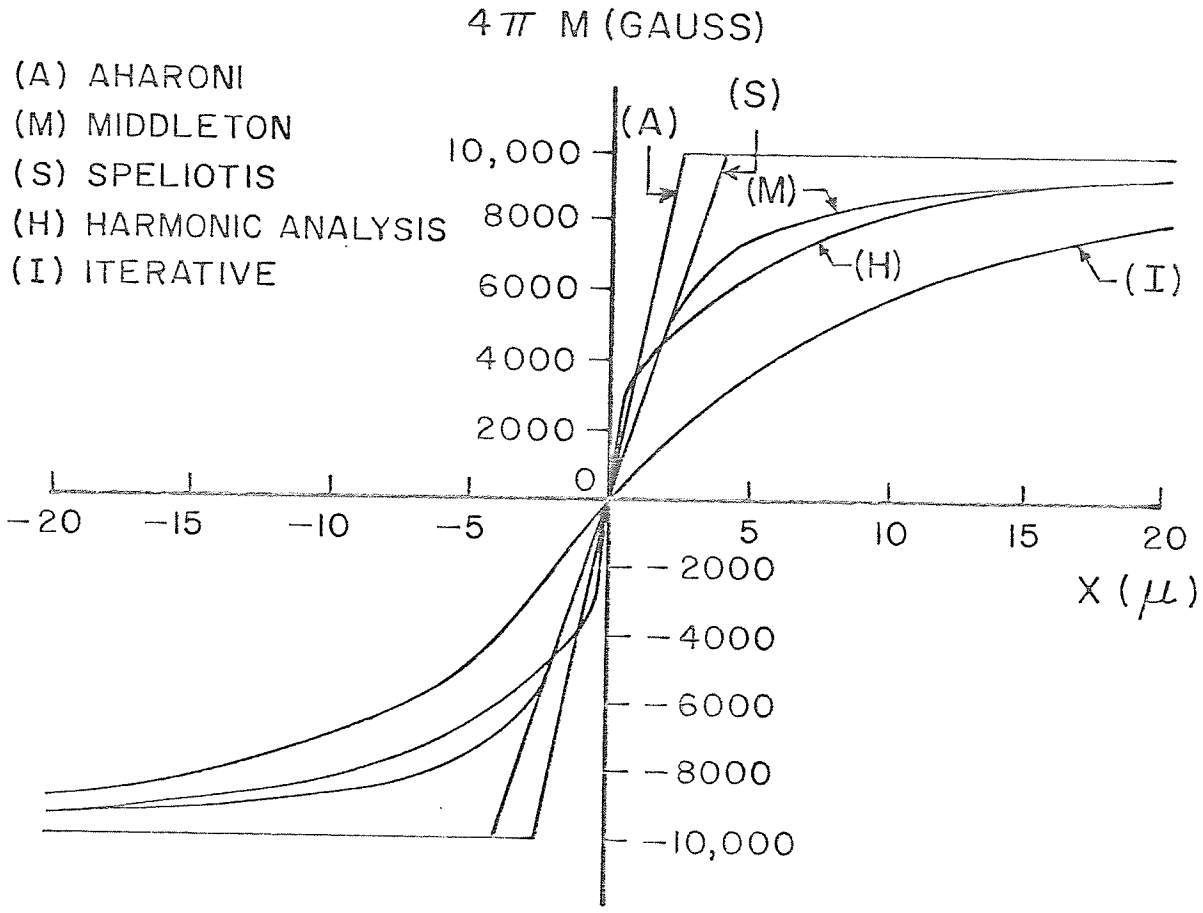

Fig. 2.11 Computed Transitions for Various Theories [18].

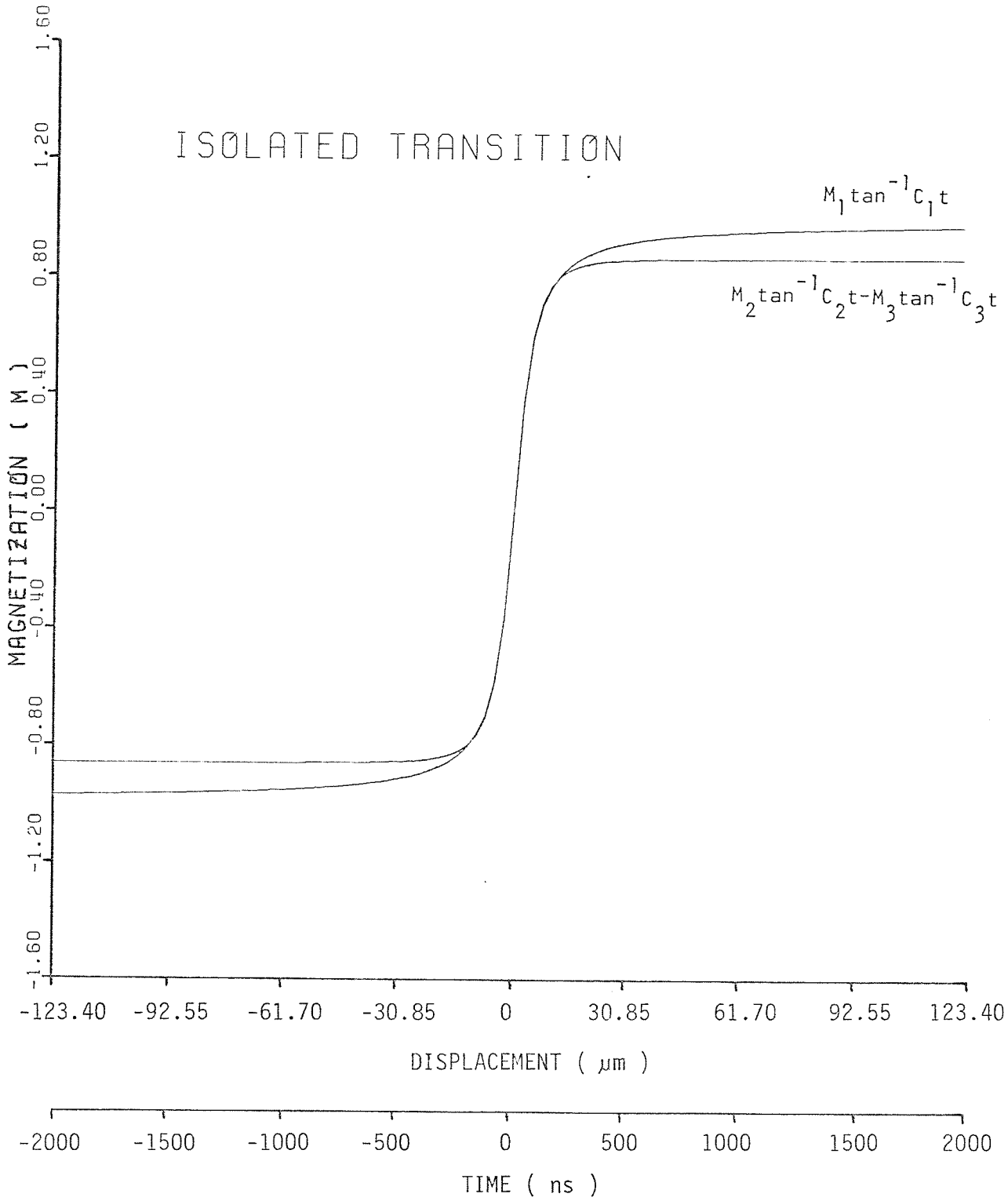

Figure 2.12 Computed Magnetization patterns for the Lorentzian and Quartic isolated pulses. Note: $M(x) = M(vt)$, x = displacement, t = time, v = 61.7 m/s.

Integrating the quartic function, which more accurately fitted our experimental data, yielded [19],

$$m(t) = M_2 \tan^{-1} C_2 t - M_3 \tan^{-1} C_3 t \quad .$$

This appears to be an even more general representation of the traditional arctangent form. The smaller asymptotic value of magnetization, as the time t (or equivalently, displacement x) approaches infinity, indicates that there is less energy concentrated in the tails, hence, adjacent bit interaction is smaller than the Lorentzian transition region would indicate.

These results are of course interpreted on the assumption that the head field distribution is an impulse function. This assumption is a good first approximation, though the head field distribution is responsible for spatial filtering of the true isolated transition [20, 21].

In summary, it appears that a potentially interesting area for further work appears to be the inversion of certain problems [22]. That is, instead of deducing the output pulse given the original magnetization, one finds the magnetization pattern which yields a specified output pulse.

2.2.2 Limits to the Application of Linear Superposition (LSP)

In the previous paragraphs where the digital recording and reproduction process was analyzed we always assumed an 'isolated' transition; i.e., the effect of adjacent pulses was considered negligible. Once the isolated reversal has been measured, the validity of superposition can be investigated directly. Superposition is essential for the successful application of linear post-equalization (receiver equalization) necessary to combat the effects of intersymbol interference (ISI) and noise.

The usual test for linearity of a magnetic record/playback channel involves recording two adjacent transitions and allowing the time of separation between these to approach zero. For absolute linearity, the net voltage at the reproduce head terminals, which is caused by a series of step-function changes in the medium magnetization is obtained by linear superposition of the individual voltage from each reversal acting on its own. This is illustrated in Figure 2.13 with a positive/negative saturation-to-saturation sequence of transitions. As long as the adjacent transitions are far from each other, there is no interaction (Figure 2.13(a)). As the transitions are moved closer to each other (Figure 2.13(b)) the interaction between the two pulses causes a change in amplitude of the resultant read-back voltage e(x). Note also that the separation between the two peaks s_2 is greater than the separation h_2 between the corresponding write current reversals. This phenomenon is known as peak shift.

Under the condition of direct two level symmetric recording, several measurements and simulations have indicated small but varying deviations from linearity [23 - 30].

The application of the superposition principle in the determination of the resultant amplitude and peak shift seems to be justified as long as the density of saturation reversals is not less than the transition length (PW_{50}) inside the medium. When the separation between reversals is much less than the transition length, the transition region will be modified by the subsequent magnetization change. At this point the non-linear nature of the writing process invalidates the basic assumptions made when applying the superposition principle.

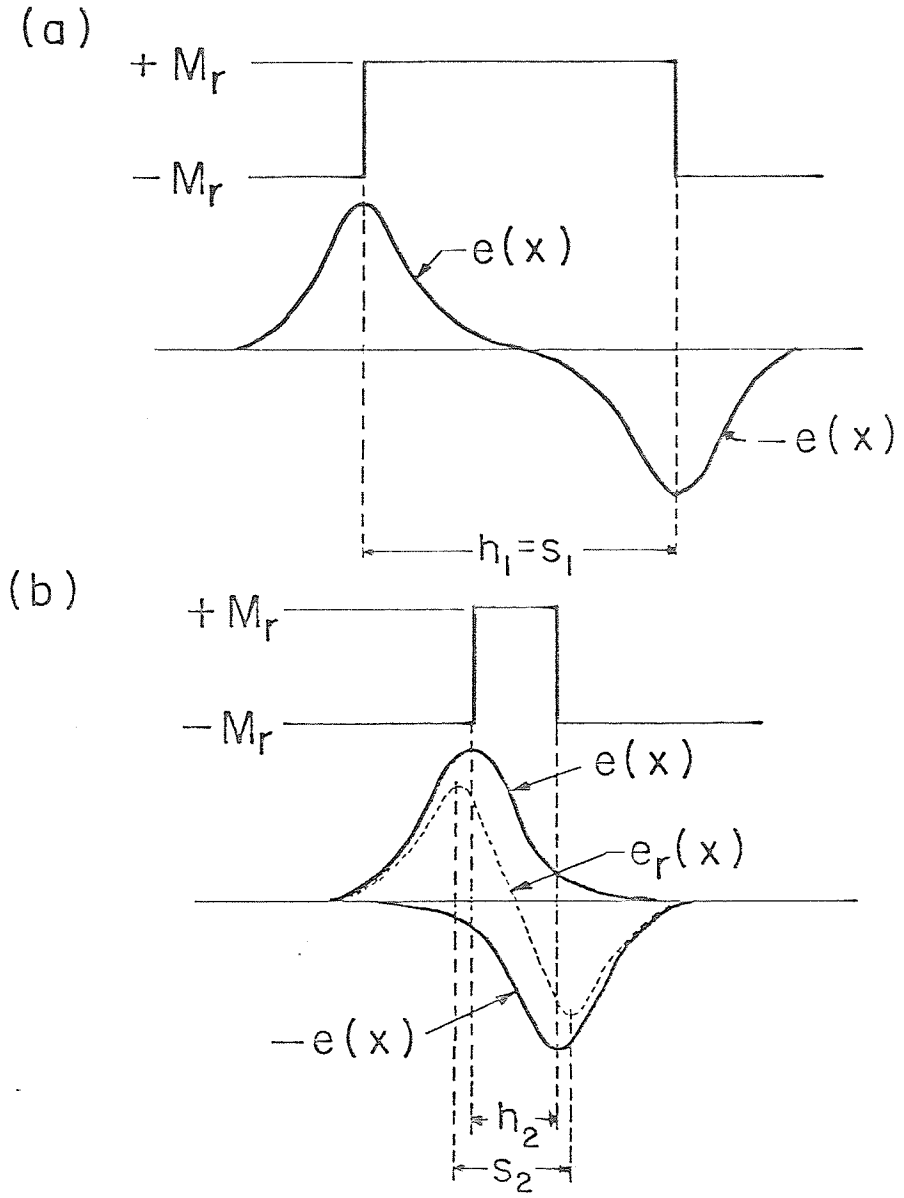

Fig. 2.13. Two Adjacent Saturation Reversals.

Tercic [25] found that for oxide disks the peak amplitude of the measured pattern and superposed one fully agreed down to a reversal distance equal to 0.5 PW_{50} using Lorentzian type pulses. Mallinson [29] shows experimental evidence of the validity of linear superposition down to a reversal distance of less than 0.2 PW_{50} on standard γ Fe_2O_3, corresponding to a linear density of 15000 bits per inch (bpi).

He concludes that to all practical purposes, LSP is valid at all bit densities, provided two conditions hold. First, it is necessary that the record-head field rise time be less than the bit interval. The crucial factor here is the field rise time and not the input current rise time. The field rise time may be deduced from observations of the voltage induced in a fine wire laid over the write head gap. The second condition is that each change in magnetization be a function only of the field causing that change. He suggests that the simplest procedure to validate this condition is to determine if the omission of a single transition in a long sequence of adjacent transitions changes the multibit waveform by exactly one isolated pulse.

In the same manner as in Figure 2.13 the output signal from two adjacent saturation reversals was experimentally studied on our magnetic recording channel. The experimental results were compared with a computer simulation ofthe linear superposition of quartic pulses. The results are detailed in Figure 2.14.

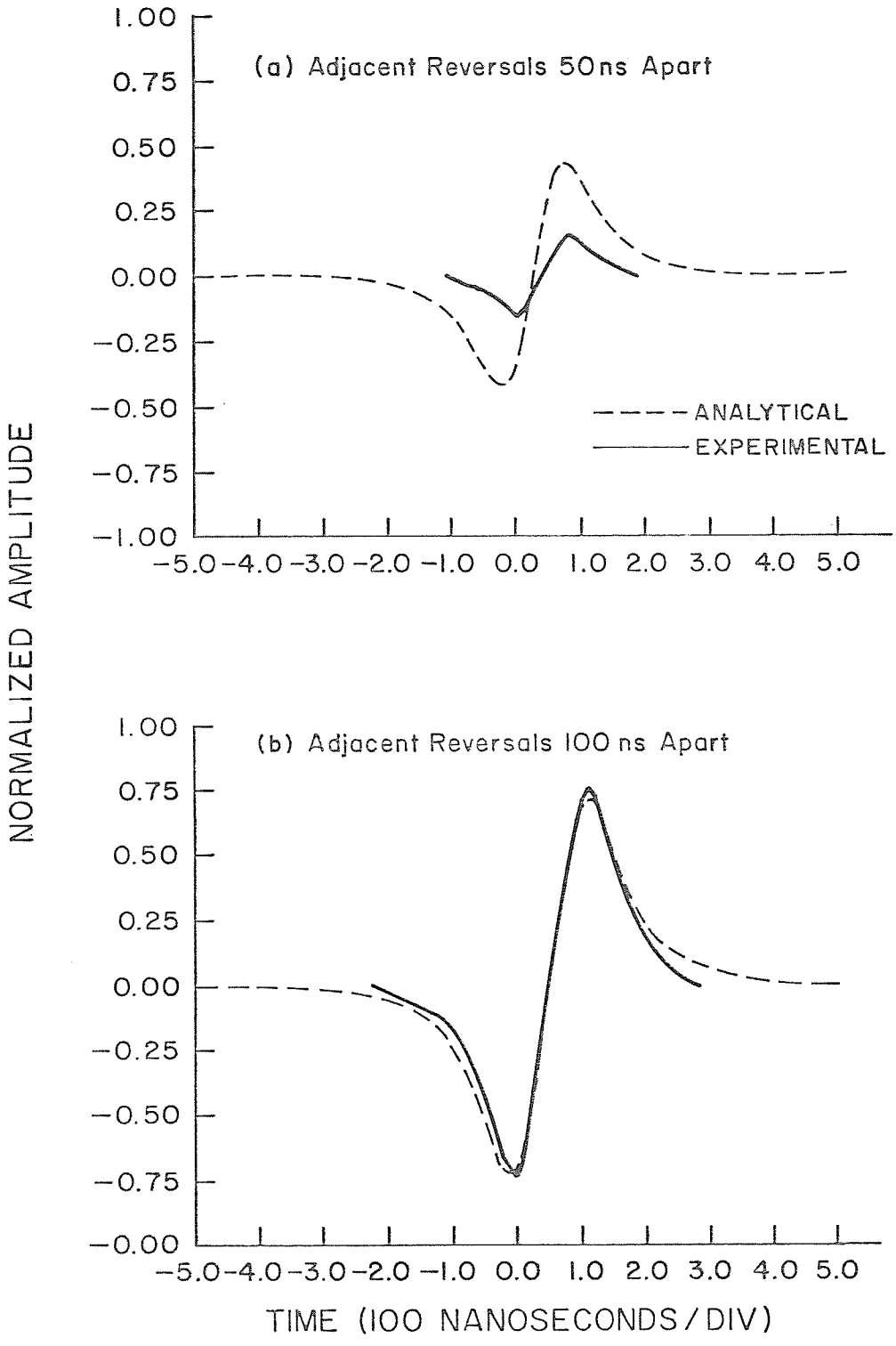

Figure 2.14 Experimentally measured and analytically calculated curves for two adjacent reversals.

As manufactured, the maximum recording density of the disk drive is depicted in Figure 2.14(b); 100 ns characteristic pulse width (PW_{50}) at 100 ns bit cells.

Agreement with the results predicted by linear superposition is excellent for low densities. But, the disparity between theoretical and experimental results increases with increasing density, especially with regard to peak shift and peak amplitude reduction.

Figure 2.15 illustrates the reduction in the amplitude of the reproduced pulse as a function of recorded transition density. As long as the minimum spacing between two saturation reversals is large and there is no interaction between pulses, the output voltage peak amplitude will remain unchanged with neglible peak shift. When the interference of adjacent pulses extends to the center of the pulse, the amplitude is reduced and the peak shift increases, as the adjacent pulse is of opposite polarity. The so-called 'head resolution' is the ratio of the head output voltage peak-to-peak at the highest bit density of interest to the head output voltage peak-to-peak at the lowest bit density of interest.

The peak shifts determined by measurement do not fully support the construction suggested by the superposition principle. It has been observed that for two adjacent transitions as shown in Figure 2.13, for which the superposition theorem predicts symmetrical shifts, the actual shifts are different for the positive and negative transitions. Kostyshyn [31] confirms that the position of the peak of the recorded transition depends upon the initial condition of the medium, the polarity of the bias in the

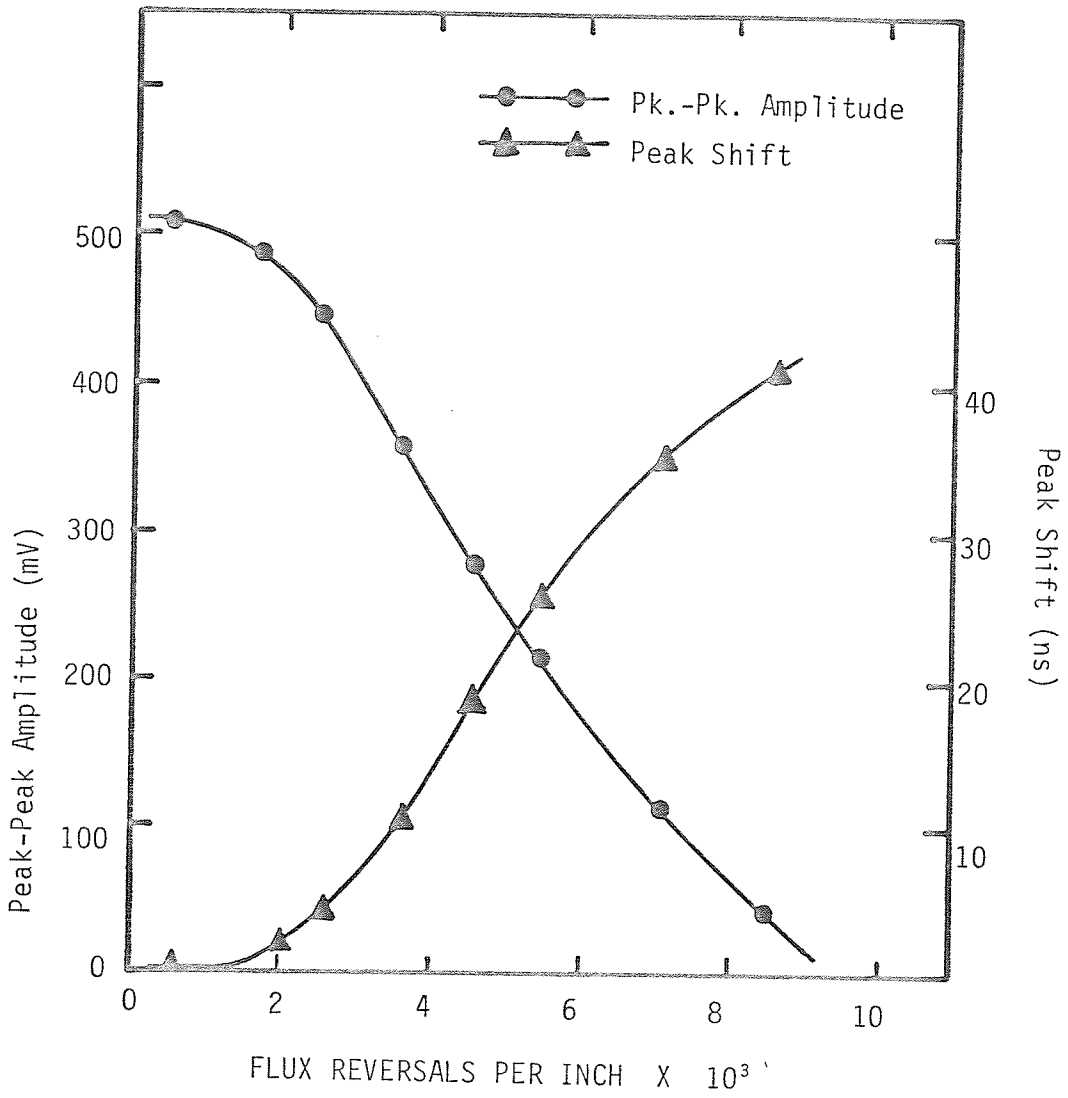

Figure 2.15 Amplitude Reduction and Peak Shift as a function of recorded transition density.

dc erase case or previously recorded data in the write over modulation case. The peak shifts resulting lead to write read delay variations which are a partial cause of system jitter. Kostyshyn concludes that by the appropriate choice of the system design parameters, particularly write current rise time, the peak shift can be substantially reduced.

The external field generated by a recorded transition is very low, thus the reproduce head can be considered as a linear element and the linear superposition principle can be applied for a fixed record level. However, the playback signal amplitude and hence the channel gain remain highly nonlinear functions of the particular record level chosen (head drive current). Writing with conventional ferrite heads requires that a high current be switched into an inductive load with only a finite voltage. Alternatively, as in our disk drive,head current rise time can be limited by the capacitance. This must constitute a finite lower limit to the flux rise time. During the finite period taken for the flux to rise the recording medium is moving past the write gap at high speed. This could cause the written transition to become broader and lower in amplitude than would be expected under ideal; i.e., zero rise-time conditions, as detailed in Figure 2.16. The media attempts to compensate for a slow current rise time since it "prefers" to be magnetized in one of two states and not somewhere in between. Other than write demagnetization, a slow current rise time may be one of the principal limitations in the validity of linear superposition.

To study the effect of finite flux rise time we investigated the head current for successively narrower write pulses. Figure 2.17 presents

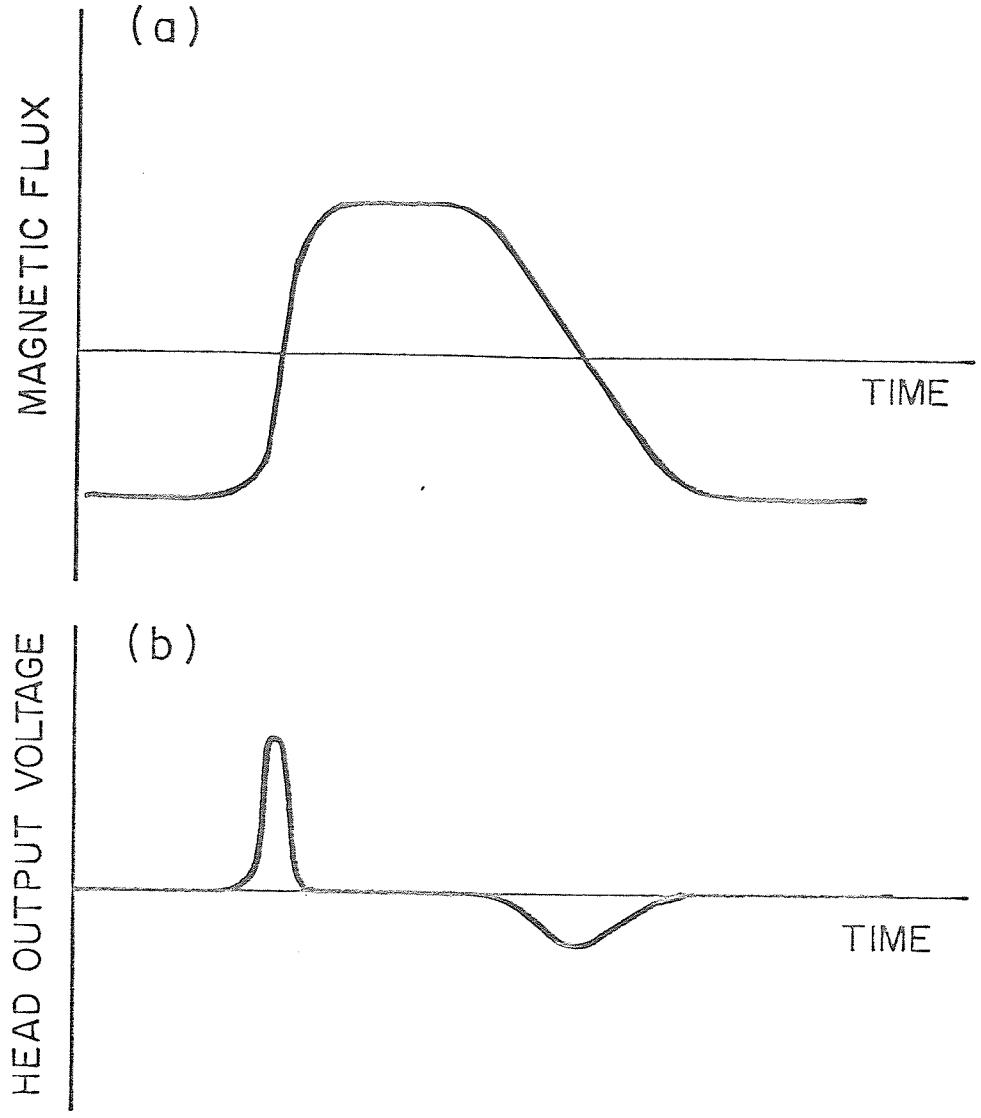

Fig. 2.16. The Effect of Finite Flux Rise Time

(a) Write-head Magnetic Flux Versus Time

(b) Read-head Output Voltage Versus Time

(a) 50 nS Write Current Pulse

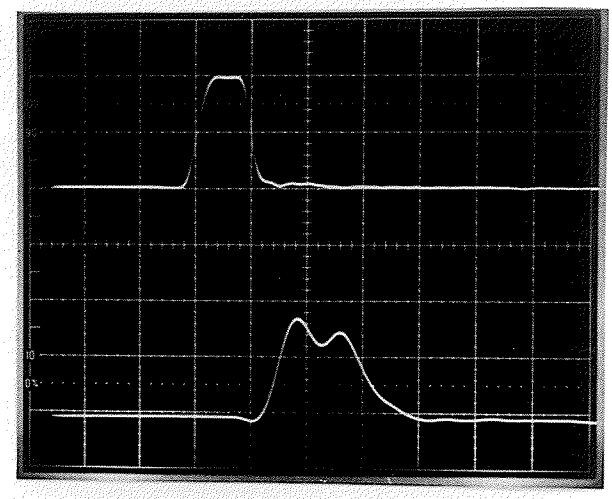

(b) 100 nS Write Current Pulse

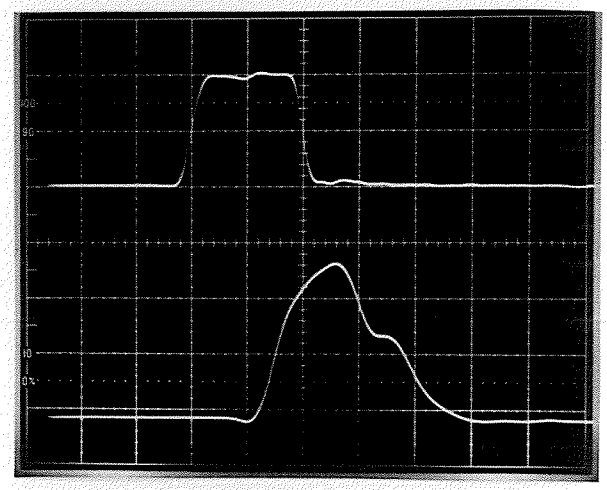

(c) 150 nS Write Current Pulse

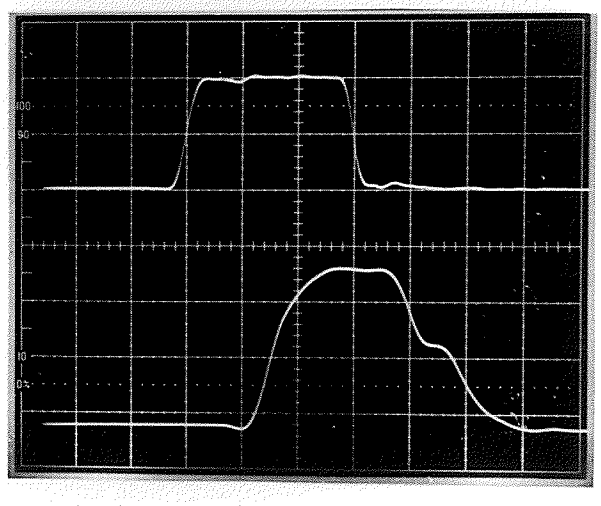

Figure 2.17 Disk Drive Head Write Driver Pulse Response
Upper trace: Input Pulse to the Write Drivers
Lower trace: Current into the Recording Head

a pictoral display of our results. It is evident that the head current rise time of 45 ns, which with no eddy current losses is the head flux rise time at best, implies that with a bit cell interval of 100 ns application of LSP is questionable. In addition for very narrow adjacent transitions (< 100 ns), the finite flux rise time limits the peak amplitude of the head current which is the source of the recorded magnetization pattern. Since the magnetic recording medium is highly nonlinear in its response to a magnetic field it is readily apparent, in our case, the deviations from linear superposition are progressively worse at higher packing densities.

Lee et al. [32] in their study of finite flux rise time have determined that there is no advantage in writing a transition with a current rise time of less than

$$t_r = \frac{2\ Mr}{H_c} \cdot \frac{\delta}{v}$$

where Mr = remanent magnetization (gauss)

H_c = coercivity (oersteds)

δ = medium thickness

v = relative head to medium velocity.

Since it will demagnetize itself to this length upon leaving the write head.

With these factors in mind, drastic improvements in linear packing densities will necessitate improvement in the write drivers and frequency response of the heads; i.e., the transmitter in our equivalent communications channel.

In summary, it must be stressed that the validity of linear superposition in no way presupposes or requires that the record process be linear. The linear superposition principle can be applied for a fixed record level down to a reversal distance of PW_{50}. The validity of linear superposition is of cardinal importance since it admits the successful application of linear post-equalization (receiver equalization) necessary to combat the effects of intersymbol interference and noise.

2.3 Characterization of the Channel

The amplitude and phase characteristics of the transmitter were characterized in the previous section. In this section we define the amplitude and phase characteristics of the preamplifier which is the channel in our equivalent communication model.

The preamplifier in the disk drive is a low noise bipolar ac coupled differential amplifier. A Bode plot, obtained experimentally, of the preamplifier displaying the magnitude and phase characteristics is shown in Figure 2.18. With an input impedance of 400Ω it has a voltage gain of approximately 200 (45dB) within the lower and upper cut off frequencies of 0.17 MHz and 10.2 MHz, respectively. Features to especially note in the Bode plot are: (i) the exceptional phase linearity above 0.5 MHz which implies a pure time delay for these frequencies; and, (ii) the lower 3dB point of 0.17 MHz. The lack of dc transfer is desirable in that it helps to alleviate the problem of baseline galloping, characterized by a non-zero output voltage midway between two separated flux transitions.

For the data rates of interest, the preamplifier introduces little

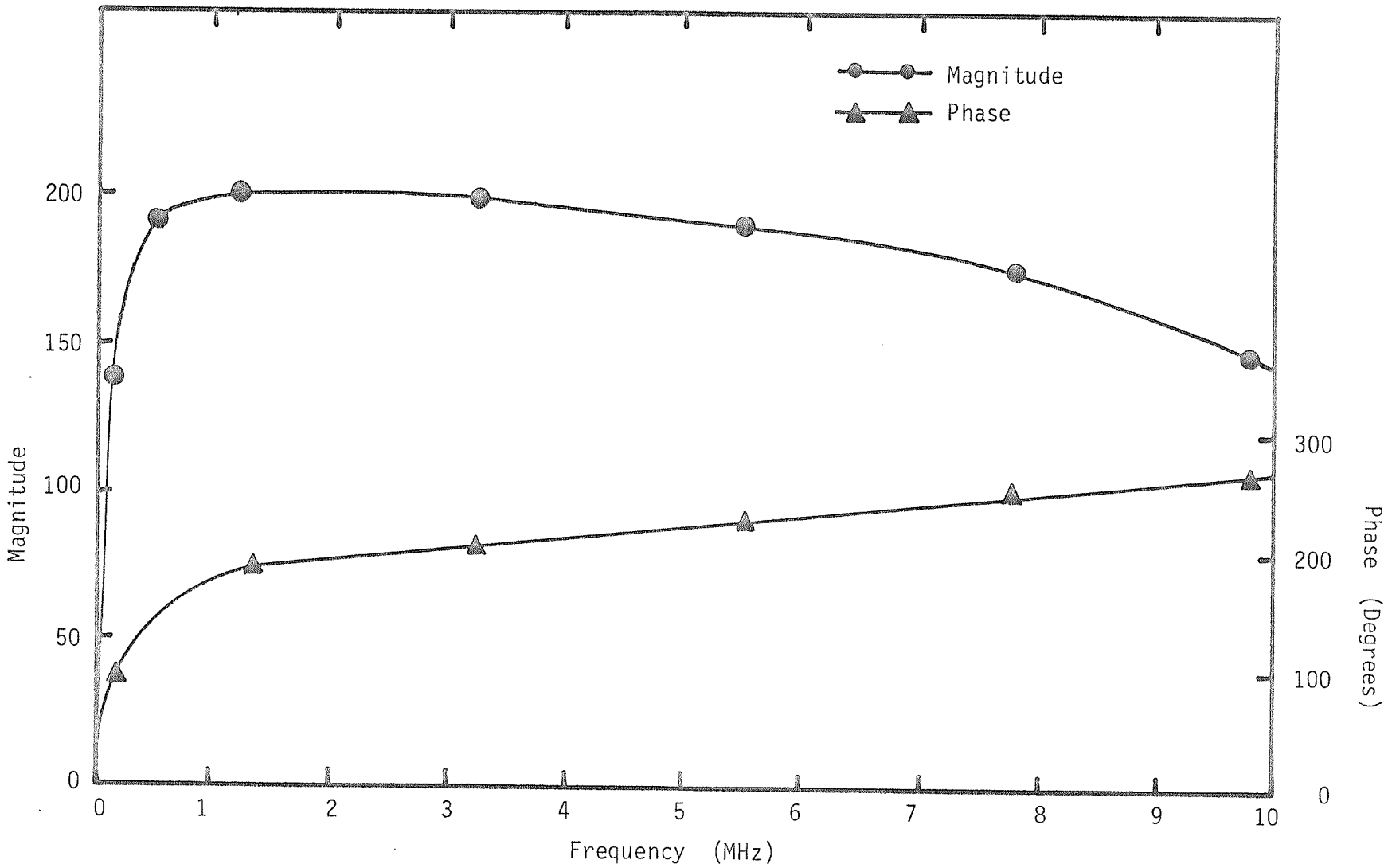

Figure 2.18 Magnitude and Phase Characteristics of the Preamplifier.

ISI on its own. The principal channel impairment is due to the noise sources. In the next section, we consider the media, head and preamplifier together as a channel noise source for simplicity.

2.4 Noise in Digital Recording

In order to utilize the techniques originally developed for conventional communications channels it is important to characterize a digital magnetic recorder in terms of its noise sources.

2.4.1 Principal Noise Sources

The principal sources of noise are:

(i) Amplifier noise.

(ii) Head Impedance Noise.

(iii) Media Noise.

These three sources define the fundamental limit to areal bit densities (track/cm x bits/cm) via their contribution to bit error rate.

The relationship between these noise sources depends on the quality and bandwidth of the preamplifier and the width of the read track. The importance of differentiating between these noise sources lies in their spectral distributions and probability densities.

(a) Head and Amplifier Noise

The amplifier (electronics) noise consists of thermal noise, shot noise, and $\frac{1}{f}$ noise. At the 1-15 MHz bandwidths currently used in magnetic recorders, the $\frac{1}{f}$ noise is negligible and hence, thermal and shot noise are predominant. The spectrum of the latter two is that of bandlimited

white noise. Hence, the noise power spectral density $p_\eta(\omega)$ (watts/cycle of bandwidth) is constant:

$$P_\eta(\omega) = \frac{N_i^2}{\omega_H} \quad 0 \leq \omega \leq \omega_H$$

where N_i^2 is the total input noise power measured up to the preamplifier high frequency cutoff ω_H.

Since the noise arises from the combined effects of many independent sources, it tends to be Gaussian.

The thermal noise due to the real part of the head impedance shunting the amplifier input impedance contributes to a head impedance noise spectral distribution which is concentrated near the resonant frequency of the head. This may be seen by considering Figure 2.3. The head inductance shorts out the thermal noise at low frequencies and the head, cable and layout capacitance shorts out the thermal noise at high frequencies.

Since the head is a passive element, and its resonance is of a fairly low Q (see Section 2.2), the assumption of bandlimited white noise is fairly accurate.

In summary, the usual assumption, warranted for the head and electronics noise is that it is white noise with a Gaussian probability density. Further the two are ergodic, independent and thus uncorrelated.

(b) Media Noise

Electronic noise tends to predominant over media noise for extremely narrow tracks and high channel bandwidths [4]. But, in well designed

recorders, the media noise is dominant [33].

The signal in a magnetic recorder relates to the mean magnetization of the particulate recording media, whereas noise arises from the deviations from the mean of the magnetization. In a bulk erased disk, the source of these deviations is the randomness of the particle magnetization directions, mechanical imperfections and the statistical variation in the number density of the particles as small volumes are sequentially scanned by the recording head [4, 34].

As the disk becomes magnetized the noise increases somewhat, probably due to nonuniform particle packing effects [34]. A noise which depends upon the signal is neither stationary nor additive. However, since the noise increase is slight (< 3dB), we shall assume that the noise is stationary and additive at all signal levels.

Most disk noise studies are performed under the dc erased or uniformily magnetized state which resembles the saturated digital state. The dc erase noise provides information about the homogeneity of the magnetic medium which is a good indicator of the suitability of the medium for use at high storage densities. Interpretation of the dc erase noise is generally done in the frequency domain by measuring its power density spectrum.

The dc erasure reported in this work consisted of the application of a dc current of sufficient amplitude in an inductive write head to saturate the medium of a Burroughs disk drive. The experimental results, are shown in Figure 2.19, of the dc erased noise of a γ - Fe_2O_3 coated aluminum substrate disk. The results were obtained with a Tektronix P6046

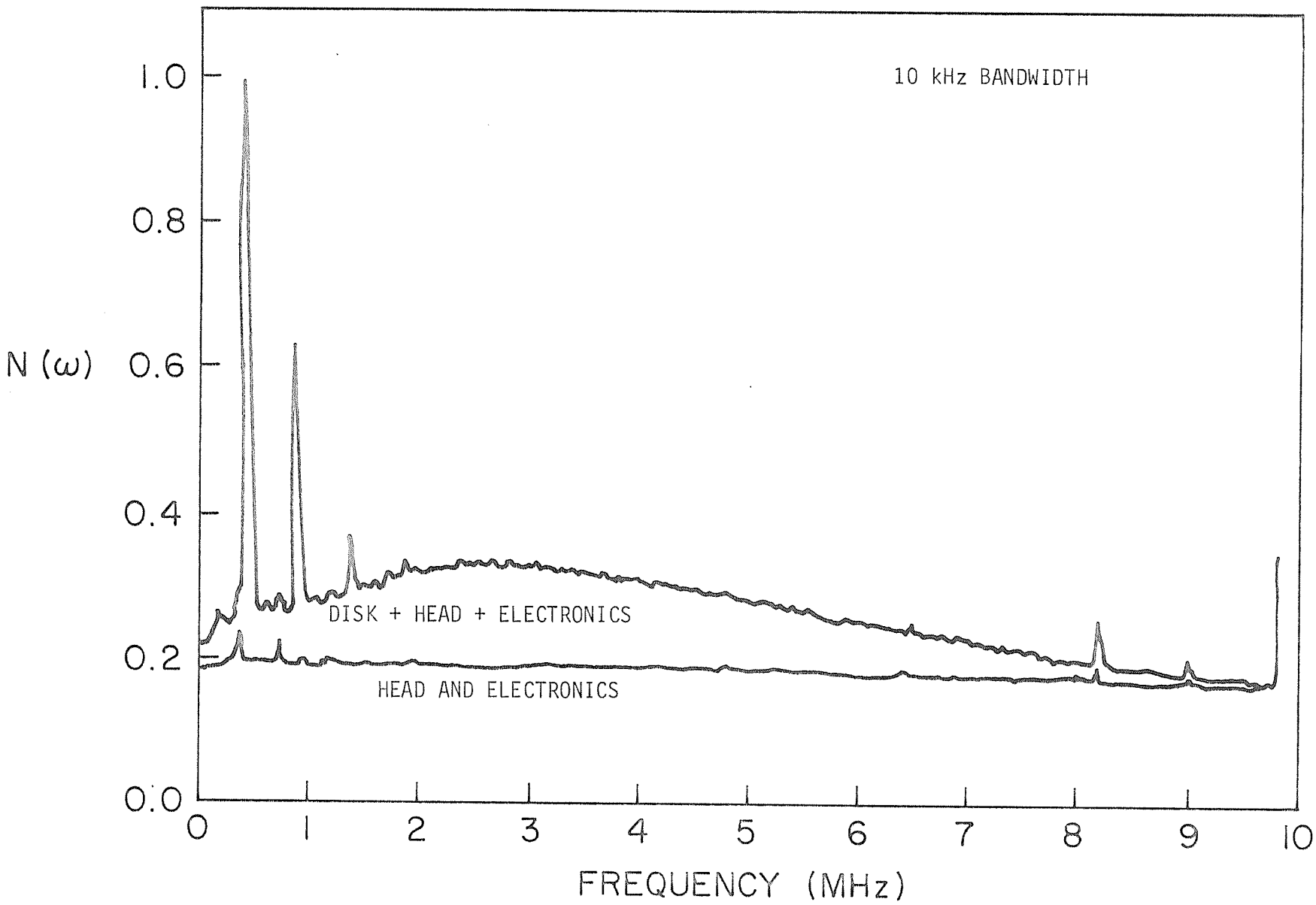

Figure 2.19 Power Density Spectrum of the Preamplifier and DC-erased Disk Noise.

differential probe with matching amplifier and an HP 141T spectrum analyser with a 8553B high frequency plugin.

As shown in Figure 2.19, the dc erased noise rises with frequency to a maximum and falls to zero rapidly. The peaks are a result of: (i) incomplete erasure of previous data (magnetization) patterns; and (ii) disk surface-substrate roughness. Head and electronics noise is also included for comparison. This result is in good agreement with [35].

The characteristic spectral shape has been referred to by Hughes [36] as chromatic and by Mallinson [37] as a so-called "blue" noise spectrum.

Su and Williams [35] note that the dc erased noise increases with increasing write current and saturates at high write currents. In addition, they found that a comparison with background noise shows an increase in noise level occurring at frequencies in the vicinity of the written signal frequency.

The noise power density spectrum due soley to the particulate nature of the medium is known [33]. However, no experimental or theoretical work has been found which attempts to determine the probability density function of the disk noise. Several authors [36 - 40] have been content with the assumption of a Gaussian probability density function.

Figure 2.20, details a circuit that was used in the experimental determination of the dc erased noise probability distribution. The output from the disk drive preamplifier was fed into a Tektronix P6046 differential probe and matching probe amplifier. The probe amplifier output in turn was connected to a first-order 10 MHz low pass filter then to the vertical channel A amplifier of a Tektronix 466 oscilloscope. The oscilloscope amplifier output served as the signal source for the circuitry illustrated in Figure 2.20. The amplifier gains were adjusted so that the

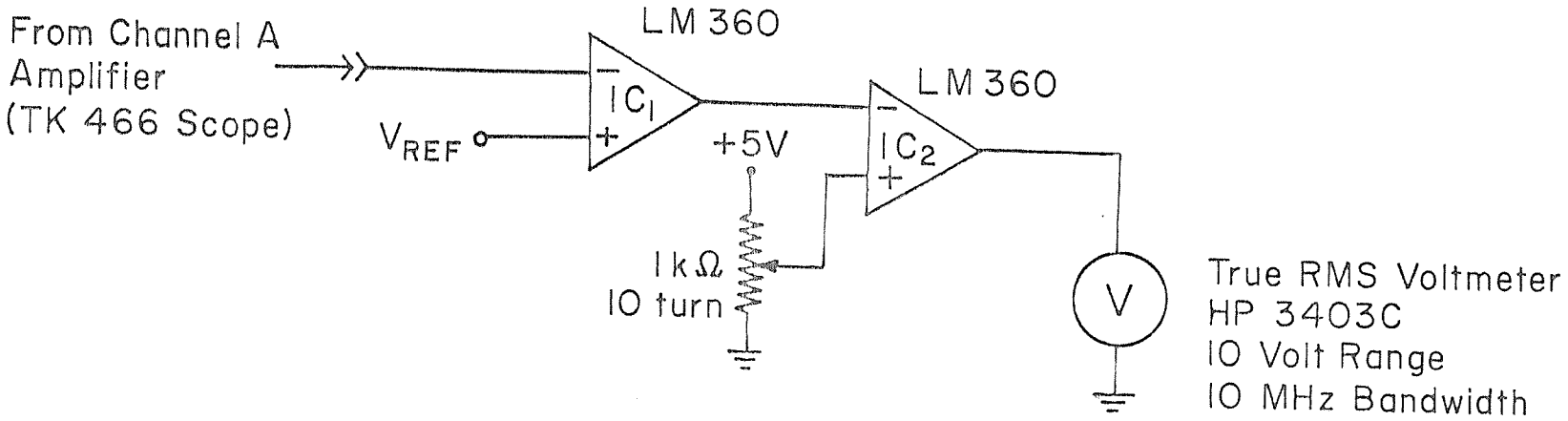

Fig. 2.20. Circuit used for the Determination of the DC-Erased Noise Probability Distribution Function

peak-to-peak noise voltage was less than 2.0 volts. The comparators are a high speed differential type having a typical response time of 15 ns and complementary TTL outputs. The IC1 output goes high (+5V) whenever input voltage is below V_{REF}, otherwise it remains at a low logic level (0V).

Depending on the magnitude and duration of the comparator overdrive the high logic level typically ranges between 3 to 4 volts. By providing additional shaping, IC2 is used to establish the required uniformity in the high and low logic levels so that the DC component of the true RMS voltmeter input gives the value of the probability distribution function for a given reference voltage V_{REF}.

The experimental results are detailed in Figure 2.21 and show the probability distributions for the head-amplifier noise and the head-preamplifier-disk noise. Taking the derivative of these functions results in corresponding probability density functions. Confidence in our results is established, when we note that the second central moment of the head and preamplifier noise measured with a true RMS voltmeter was 151 mV. From the density function in Figure 2.22 it was found to be 135 mV.

Determination of the dc erased disk noise probability distribution cannot be done directly as the head and preamplifier used to "read" the disk noise contribute noise to the measurement itself. Fortunately, simple mathematical operations can be performed to completely isolate the disk noise probability density function.

Initially, let us define the following random variables:

$X \equiv$ head impedance and amplifier noise

$Y \equiv$ dc erased disk noise

$Z \equiv X + Y$

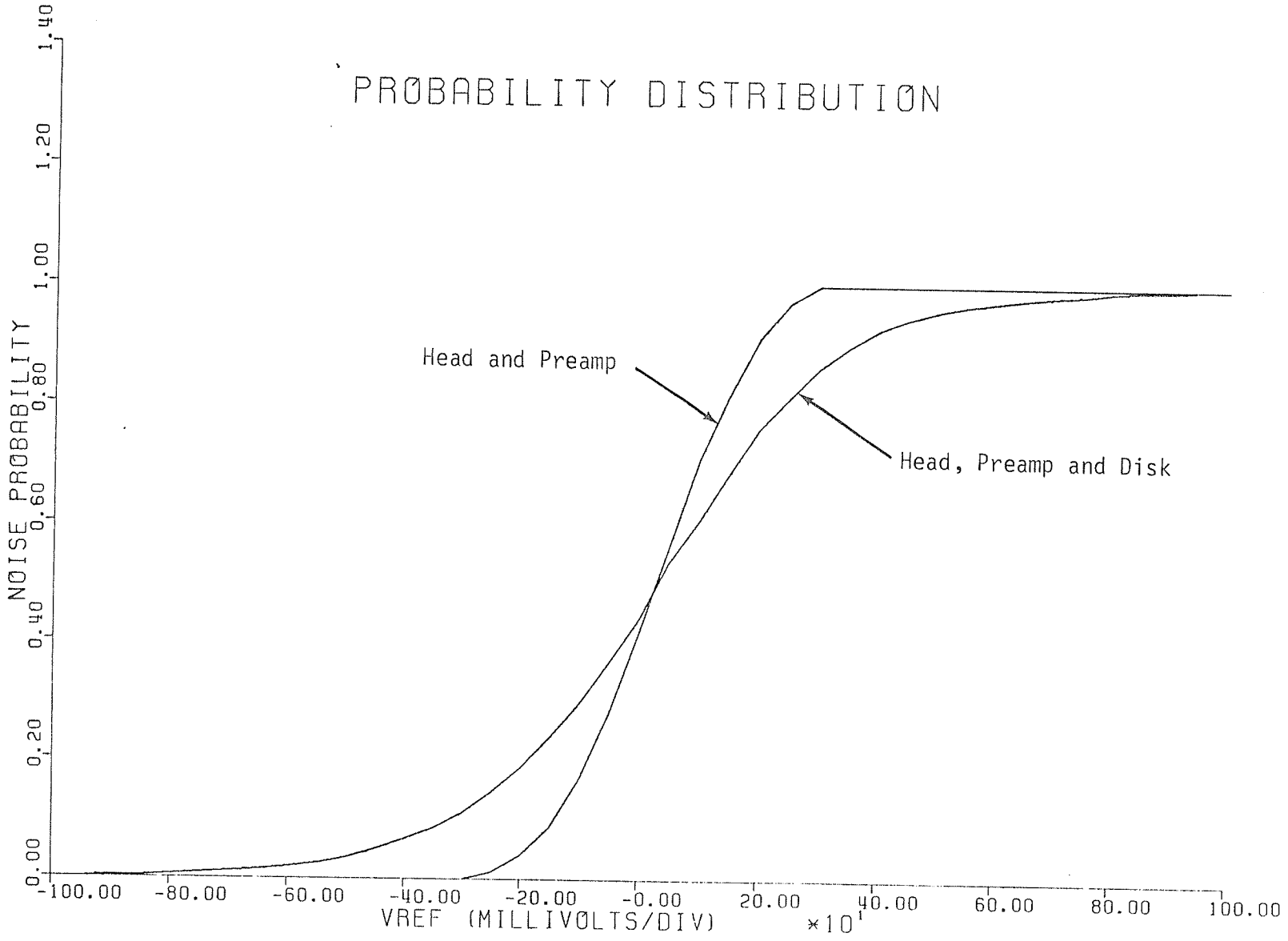

Figure 2.21 Experimentally obtained probability distributions of the head-preamplifier noise and the head-preamplifier-disk noise.

where p_x, p_y, p_z are the corresponding noise probability density functions. p_x and p_z are known while p_y is desired.

Recognizing that when two random variables are statistically independent, the form of the probability density function of their sum is simply the convolution of their individual probability density functions, we may write:

$$p_z = p_x * p_y \quad .$$

It is often easier to calculate convolution by means of Fourier transforms which, in our case, we write as a characteristic function. Hence, in terms of characteristic functions ,

$$M_z(\alpha) = M_x(\alpha) \cdot M_y(\alpha)$$

or

$$M_y(\alpha) = \frac{M_z(\alpha)}{M_x(\alpha)} \quad , \quad M_x(\alpha) \neq 0 \; .$$

The density function is regained by the inverse Fourier transform:

$$p_y(\tau) = \frac{1}{2\pi} \int_{-\infty}^{+\infty} M_y(\alpha)\, e^{-j\alpha\tau} d\alpha \quad .$$

This procedure was carried out numerically and the result showing the dc erased disk noise density is illustrated in Figure 2.22.

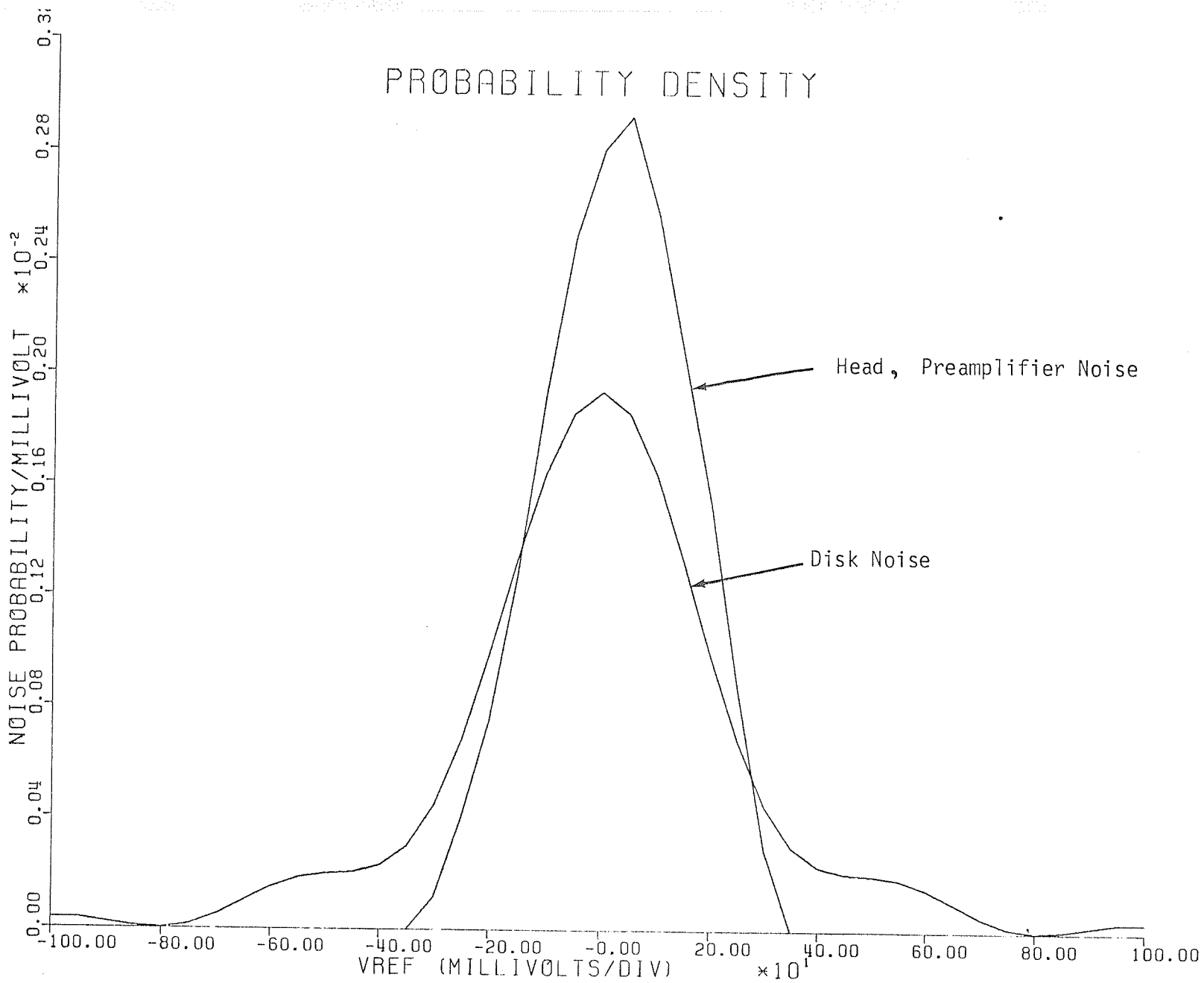

Figure 2.22 Probability density functions of the experimentally measured head-preamplifier noise and the numerically derived disk noise.

The numerical results were verified by convolving p_x and p_y and comparing with the experimental p_z. Excellent agreement, particularly in the tails, was obtained as shown in Figure 2.23.

The functional form of the dc erased disk noise probability density was determined by a least-squares-fit to potential probability density functions. The results outlined in Table II indicates that the best fit (using minimum least squares error as the criterion) is obtained with an inverse quartic approximation.

In Appendix B, Figures B.1 to B.4 indicate the quality of the fit for the probability density functions surveyed. Attention to the quality of the fit, particularly in the tails, is especially important as this will determine the accuracy of the bit error rate calculations.

It is interesting to note that the "tails" of disk noise probability density function are not monotonic decreasing. With reference to Figure 2.22 we note that the presence of a secondary lobe on either side of the central lobe. It may be argued that this is an artifact of the numerical transformations on our experimental data. However, considering the quality of the fit obtained by convolving p_x and p_y (Figure 2.23) an alternate explanation, for the secondary lobes on the tails of the density function has been proposed.

It has been suggested [41] that the dc erased disk noise probability density may be the convolution of two distinct probability densities arising from the disk structure itself. The disk surface irregularities in conjunction with the blanchard grinding marks on the aluminum substrate, which forms a regular periodic pattern, may interact with the particulate

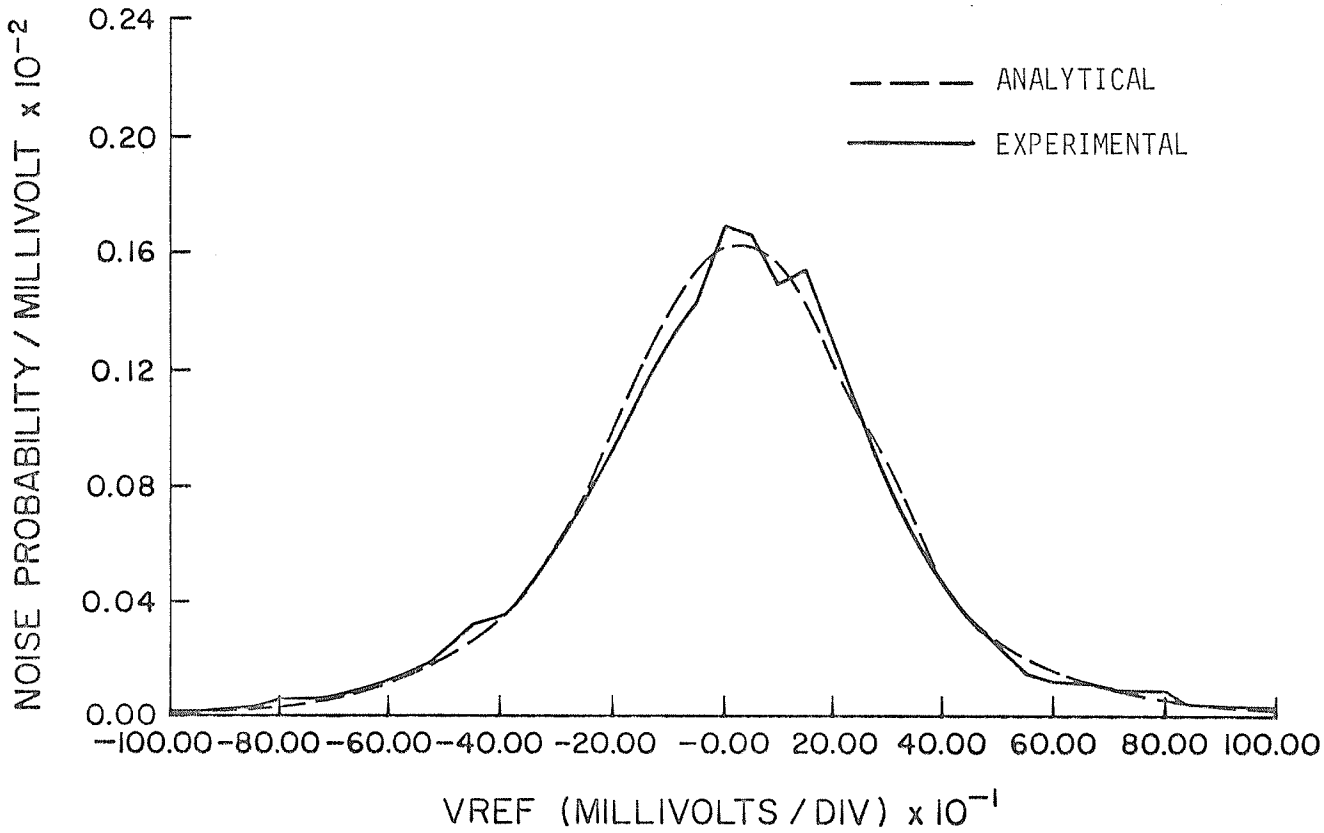

Figure 2.23 Comparison of the probability density functions of the disk head preamplifier noise obtained experimentally and through numerical convolution of the disk and head-preamplifier probability density functions of figure 2.22.

TABLE II

Determination of the Functional Form of the Disk Noise Probability Density

Probability Density Function		Least Squares Error
Inverse Quartic	$\frac{\sqrt{2\sqrt{c}+b}}{\pi\,(1+bx^2+cx^4)}$, $\left\lvert\frac{b}{2\sqrt{c}}\right\rvert < 1$	0.9982×10^{-7}
Gaussian	$\frac{1}{\sqrt{2\pi}\,\sigma}\, e^{-x^2/2\sigma^2}$	0.5468×10^{-6}
Laplacian	$\frac{1}{a}\, e^{-2\lvert x\rvert/a}$	0.4442×10^{-6}
Lorentzian	$\frac{1}{\pi}\,\frac{a}{a^2+x^2}$	0.3970×10^{-6}

or grain noise of the γ - Fe_2O_3 layer which the central limit theorem (law of large numbers) would suggest has a Gaussian distribution.

Electron microphotographs of the disk surface and underlying substrate layer along a radial profile of the disk structure are shown in Figure 2.24.

The substrate profile indicates that there is a significant periodic variation in the oxide volume residing above, with its consequent effect on the mean magnetization that is sequentially scanned by the recording head. Moreover, the periodicity is of a wavelength comparable to the wavelength of an isolated transition. The surface profile consists of scratches, pits and microprotrusions, most of which are small relative to present trackwidths and transition lengths. Morrison [42] has indicated that there is only a very slight correlation between surface roughness and signal envelope roughness. Ogawa et al. [43], by an auto-correlation analysis, observed a remarkably periodic fluctuation in the recording media surface. They warn the periodicity itself should not be regarded as a noise source, because the period is about 110 um and a noise frequency corresponding to it is less than 0.5 MHz. Nevertheless, neither the roughness nor the noise drops as long as the periodicity remains in the surface roughness. However, studies considering substrate roughness have not been found in the literature.

Our results suggest a correlation between surface-substrate roughness and noise probability density, hence with bit error rate. This may indicate the need for improved roughness specifications of the media substrate and of the recording media itself. It would be interesting to

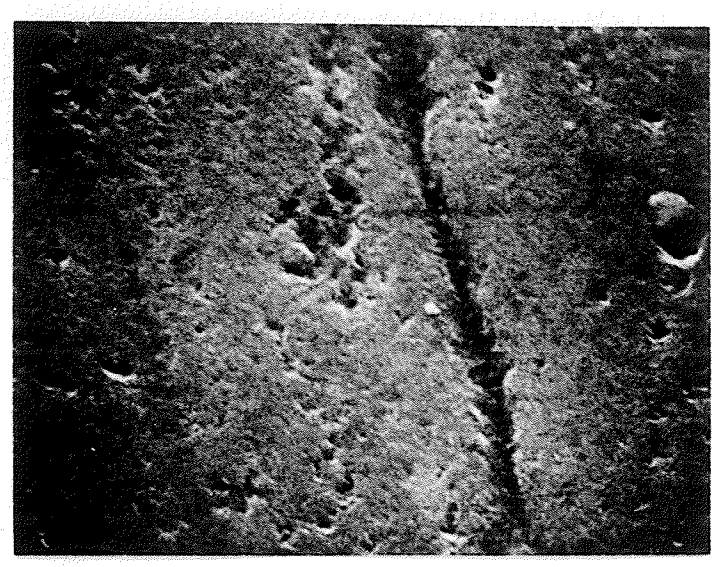

Oxide Surface

Magnification 4000X

Surface Roughness:
0.025 μm maximum
arithmetic average

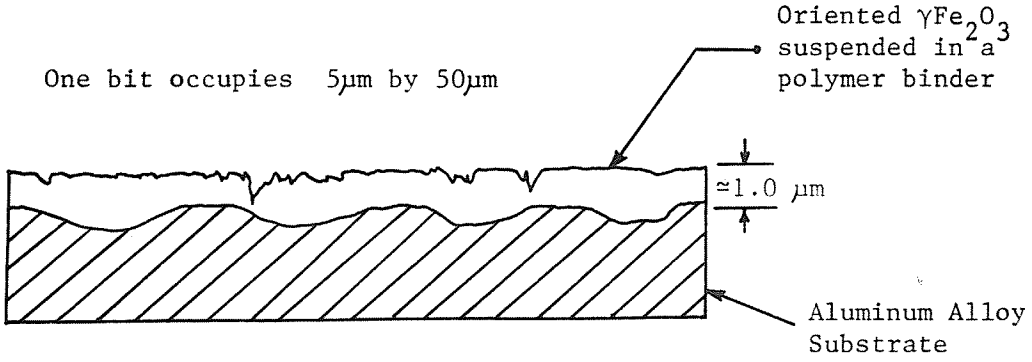

RADIAL PROFILE

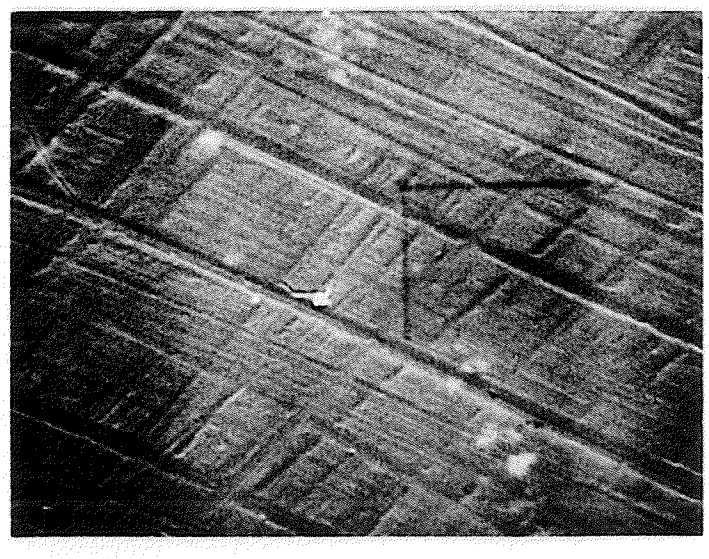

Substrate Surface

Magnification 1600X
1.0 μm = 1.6 mm

Figure 2.24 Disk Surface and Disk Substrate Profile

investigate the noise probability density function with a substrate that was electropolished or had a metallic epitaxial layer (for smoothness) deposited on it before coating with the $\gamma - Fe_2O_3$ layer, though adhesion of the oxide may be a formidable problem.

2.4.2 Auxiliary Noise Sources

In addition to the noise sources mentioned previously the recording channel may be plagued by auxiliary noise sources that are difficult to analyse mathematically. Typical sources include: adjacent-track interference, [44] tracking errors, incomplete overwrite of previously recorded data, head to media spacing variations (separation losses) and nonuniformities in the magnetic media. From the viewpoint of fading channel communications theory these variations are by no means intrinsic to recording systems. The probability density function of some of these types of noise sources may make them somewhat benign. However, the difficulty in proper characterization and mathematical tractability has prevented any significant analytical work with these types of noise sources. Kiwimagi [45] has suggested the coding techniques utilized may affect the significance of these auxiliary noise sources.

Though the noise spectrum illustrated in Figure 2.19 has been modified by multiplicative noise sources due to spatial parameter variations and magnetic nonuniformities mentioned above, the SNR computed soley on the basis of the principal noise sources is often within 6 dB of that measured [4].

Chapter 3

RECEIVER DESIGN

3.1 Introduction

The signal processing techniques utilized in many of the saturated magnetic recording systems in existence today were developed primarily by intuition and experiment. This approach has been so successful that more mathematical methods for the receiver design have been neglected. Of course, the success of intuitive designs is not the only reason for a lesser interest in more mathematical approaches. Mathematical system analysis and design requires at the outset a set of physically meaningful assumptions which, in turn, produce an accurate and mathematically tractable model. Even if such a model is available, the mathematical design problem to be solved is frequently quite complex.

In spite of the aforementioned drawbacks, there is much to be gained by taking a more mathematical or analytical approach to system design. First, an analytical formulation of the problem allows the relationships between existing receivers to be more clearly defined and highlights the assumptions upon which existing designs are based. Second, an analytical formulation can produce new system design approaches which, when modified by intuition and experiment, can lead to practically important receiver designs for the future.

It is the purpose of this section to take a more mathematical or analytical approach to saturated magnetic recording receiver design, with emphasis on the decision feedback equalizer. More specifically the goals

of this section are to establish the maximum channel capacity of the digital magnetic recording channel, to develop a decision feedback equalizer for use in saturated magnetic recording and to specify several alternate receiver structures suggested by theory.

3.2 Channel Capacity

3.2.1 Concepts Based on Information Theory

According to Shannon [46], the absolute maximum capacity (C) of a channel of bandwidth (B) at which vanishingly small probability of error can be achieved is related to its wideband signal-to-noise ratio (SNR) by the expression

$$C = B \log_2 (1+SNR) . \tag{3.1}$$

Three factors are assumed (i) the system is equalized flat; (ii) the noise has a Gaussian distribution; and, (iii) that the noise has a flat ("white") power spectrum.

Following Gallager [47], a more general representation of Shannon's theorem which accommodates arbritrary system transfer functions $H(\omega)$ and noise spectra $N(\omega)$ is:

$$C = \frac{1}{2\pi} \int \frac{1}{2} \log_2 \frac{|H(\omega)|^2 D}{N(\omega)} \, d\omega \tag{3.2}$$

where D is defined by the "water filling" formulation:

$$S = \int \left[D - \frac{N(\omega)}{|H(\omega)|^2} \right] d\omega \ . \qquad (3.3)$$

In this formulation, the integrals are taken over the range (or ranges) of ω where the integrand of (3.2) is positive and S is the input signal average power.

Gilbert [48] has calculated the channel capacity of a burst noise binary channel. The burst noise model provides a good characterization of errors due to variations in head-to-media spacing, tracking errors and media dropouts. However, the capacity of the burst noise channel exceeds only slightly, the capacity of a "classical" noisy binary channel and will not be considered further.

3.2.2 Capacity Estimates of the Disk Drive

Using modified-frequency-modulation (MFM) encoding [49], the 1F and 2F bounding frequencies are 2.42 MHz and 4.84 MHz, respectively, corresponding to a bit transfer rate of 9.68×10^6 bits/sec. This occurs with an all one's or all zero's pattern with a raw error rate of 6×10^{-11} at a signal to noise ratio of approximately 30 dB.

The Shannon capacity, given by (3.1), for a bandwidth of 10 MHz is presented in Table III. Using the data presented in the previous sections of this chapter, the results due to Gallager, given by (3.2) and (3.3), are presented in Table III, for comparison.

The results of Table III, implies that only 10% of the maximum channel capacity is presently being utilized.

It is important to note that the capacity estimates include two fundamental assumptions. First, the analysis assumes that the design of the transmitter (recording media and read head) is under our control. Secondly, the capacity theorems guarantee that signal sets exist which afford communication with arbitrarily low error probability. After establishing the signal set that is appropriate, the recording medium and read head must be designed with the corresponding performance characteristics. This is not a trivial problem.

TABLE III

Channel Capacity of the Burroughs Disk Drive

Capacity (Mbits/sec)

SNR	Shannon	Gallager	Presently
10	43.92	31.10	-
20	76.51	66.00	-
30	109.70	99.35	9.68

3.3 Receivers for Channels with Intersymbol Interference

The increasing availability of low cost digital systems has created a demand for more efficient methods of digital data transmission. This demand has promoted a sustained research effort concentrated on the problem of digital communications through linear channels that exhibit intersymbol interference. The remainder of this chapter will attempt to utilize the knowledge gained in this research effort to develop an optimum receiver architecture for the digital magnetic recording channel discussed in Chapter 2. The material is principally tutorial in nature and is more fully developed in Lucky *et al.* [54].

To develop a meaningful receiver architecture we focus on the optimum structure of the pulse amplitude modulation (PAM) system when the channel characteristics are known exactly. The simplest type of PAM system employs fixed transmitting and receiving filters, $F(\omega)$ and $R(\omega)$, respectively, and a sampler and threshold detector as shown in Figure 3.1. Every T seconds the transmitter maps (an independent and equally likely) symbol a_n into a given waveform marking its amplitude proportional to the data value. The channel, assumed to be linear and time invariant, operates upon the trans-

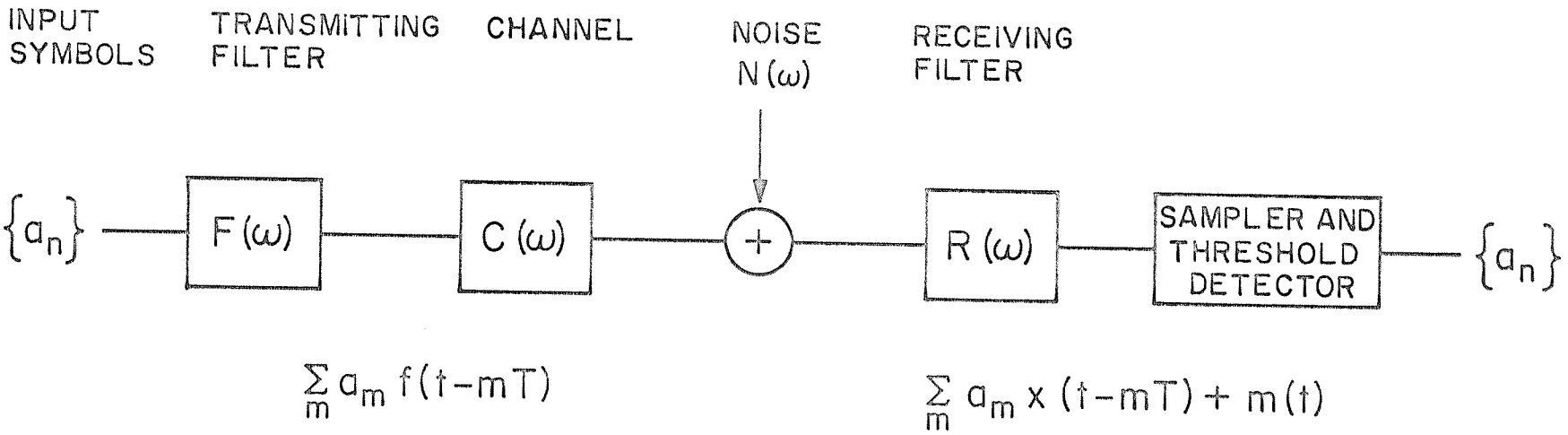

Fig.3.1 PAM System with Simple Threshold Detection

mitted waveform and delivers to the receiver a time dispersed version of it.

3.3.1 The Matched Filter

If a single pulse $a_0 f(t)$ were to be transmitted through a perfect channel $C(\omega)$, that is $C(\omega) = 1$, the optimum detection scheme in this case of no intersymbol interference, consists of a noise filter and a filter matched to the received pulse shape followed by a threshold detector. The optimum noise filter has a transfer function equal to the reciprocal of the noise power spectrum $N(\omega)$. When the additive noise at the receiver input is white; i.e., its spectrum is flat over the frequency band of interest, the noise filter or prewhitening filter can be omitted in the optimum receiver. The optimum receiver for a fixed channel transfer function $F(\omega)$ then contains a cascade filter with component transfer functions:

$$R(\omega) = \underbrace{\frac{1}{N(\omega)}}_{\text{noise filter}} \underbrace{F^*(\omega)}_{\text{matched filter}}$$

where * denotes complex conjugation. The matched filter receiver is also known as a correlation receiver [46] because of its mathematical analogy. In practical applications, signal delay must be introduced in order to make these filters realizable.

The transversal filter or tapped-delay-line (TDL) filter [50] is an important filter structure for the implementation of the matched filter or other receiver (equalizer) structures. It is attractive primarily because of its ease of implementation in either the analog or the digital form.

The TDL filter shown in Figure 3.3 consists of a tapped delay line with signal multiplications (attenuation) by the tap weight h_i for each tap. All the attenuator output signals are then summed. The optimum receiver can then be realized by a cascade of two such parallel TDL filters: one with tap weights adjusted to form the noise filter, the second one with tap weights adjusted to form the matched filter. Since the cascade of two bandlimited linear filters is another bandlimited filter, in some applications it is more convenient to employ one TDL filter to realize $R(\omega)$ directly.

Implementation can be viewed most easily in the time domain. The impulse response may be written:

$$h(t) = \sum_{n=-N}^{N} h_n \, \delta(nT) \tag{3.4}$$

where the number of taps is $2N + 1$, h_n is the attenuator setting of the n^{th} tap and $\delta(nT)$ is the Dirac delta function. The corresponding Fourier transform can be written

$$H(\omega) = \sum_{n=-N}^{+N} h_n \, e^{jn\omega T} \quad . \tag{3.5}$$

It can be seen from Equation (3.5) that the spectral response is periodic in frequency. Specifically, the amplitude response is even about frequencies $\frac{2n\pi}{T}$ and the phase response is odd about the same frequencies. A more detailed analysis is given in [51].

Two practical limitations are worth noting. In practice, signals cannot be both time and frequency limited so that finite length TDL filters can only approximate the ideal solution. Secondly, the inevitable

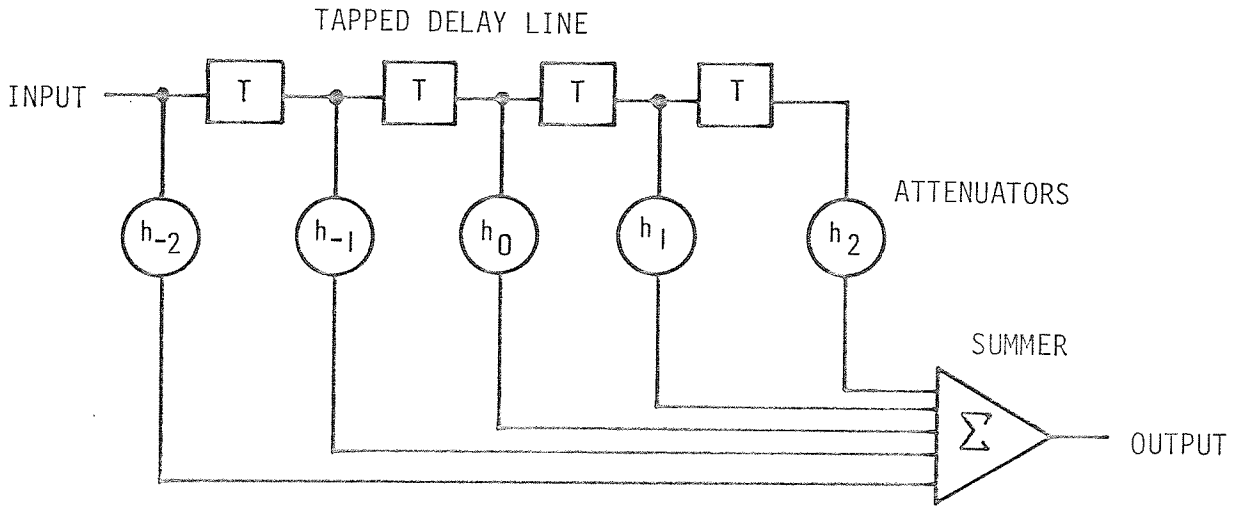

Figure 3.2 Direct Form Realization of a Transversal Filter.

inaccuracies in implementing the desired weighting coefficients results in a departure of the actual frequency response from the predesigned frequency response. Gersho et al. [52] has recently shown that under very general conditions the maximum error $\Delta H(\omega)$ in frequency response is given asymptotically by

$$\max_{\omega} |\Delta H(\omega)| = \sigma\sqrt{n \log n} ,$$

where n is the number of taps, σ is the rms coefficient inaccuracy, and log denotes the natural logarithm. One advantage of the TDL filter is the convenience in adjusting the tap weights as a means of tracking the channel and noise spectrum variations [53].

When a sequence of pulses which overlap in time is transmitted, the simple receiver described in this section is no longer optimum unless, as in the ideal channel situation, the individual pulses do not interfere with each other in the process of matched filter detection. Development of a method to deal with pulses which overlap in time leads us to a discussion of the zero-forcing equalizer.

3.3.2 The Zero-Forcing Equalizer

For imperfect channels exhibiting intersymbol interference, the optimum linear receiver can be factored as a matched filter followed by a transversal filter with tap spacings equal to the symbol interval T. The quantizer as a threshold device then operates on the equalized signal to decide which symbol was transmitted. The tap gains of the transversal filter are set optimally according to the measure of performance being

used [54]. For example, if only intersymbol interference is being removed completely (a so-called "zero-forcing" mode of operation), the tap gains are adjusted such that the system transfer function $X(\omega) = F(\omega)\ C(\omega)\ R(\omega)$ satisfies the Nyquist criterion.

The criterion of removal of intersymbol interference does not uniquely specify $X(\omega)$ unless the bandwidth is limited to the Nyquist band

$$\left[-\frac{\pi}{T} , +\frac{\pi}{T} \right] .$$

One class of Nyquist characteristics which has been extensively studied is the so-called raised-cosine characteristic.

The action of the zero-forcing equalizer is such that the matched filter establishes an optimum signal-to-noise ratio (SNR) irrespective of the residual ISI at its output. The transversal filter then eliminates or at least reduces the intersymbol interference (by making the equivalent Nyquist channel response constant) at the expense of diminishing the SNR.

The major advantage of a linear equalizer is its ease of implementation and analysis. For this reason they are commonly being used in communication systems where intersymbol interference is a prime limitation to performance.

3.3.3 The Decision Feedback Equalization

If symbols of a data sequence are correlated by ISI, a better way than making symbol-by-symbol decisions is to base decisions on the entire data sequence received. Receivers can be built with a performance advantage because the correlation introduced by ISI between successive sample values

is of a discrete nature in the sense that a data symbol can be disturbed by adjacent data symbols only in a finite number of ways. Receivers that perform sequence decisions exhibit structures of varying complexity. Decision feedback equalization (DFE), though nonlinear, is attractive because it can be as easily implemented as a linear equalizer. Its nonlinearity comes only from the quantizer as a decision device.

The classic structure of this receiver is shown in Figure 3.3. Initially, the received signal is processed by a prewhitening and matched filter. A linear feed forward filter (FFF) then processes the received signal and its output is sampled at time intervals of T seconds. The sampler output is then the sum of a linear combination of several transmitted symbols plus a noise term. The receiver makes decisions every T seconds on a symbol-by-symbol basis. At the time a decision is to be made on the n^{th} transmitted symbol the feedback filter (FBF) forms a linear combination of the previously estimated symbols, assumed to be correct, and cancels the intersymbol interference produced by them at the sampler output. The result is then applied to a quantizer to determine the closest possible data value. Several techniques for the design of the FFF and FBF have been presented in the literature [55,56]. George et al. [57] has developed an adaptive DFE algorithm for time varying channels.

The prewhitening and matched filters serve to maximize the signal-to-noise ratio. The feedforward filter processes the signal to reduce the intersymbol interference of all future symbols while the feedback filter subtracts the interference due to all past symbols. (In contrast, a linear equalizer reduces the effect of past and future symbols).

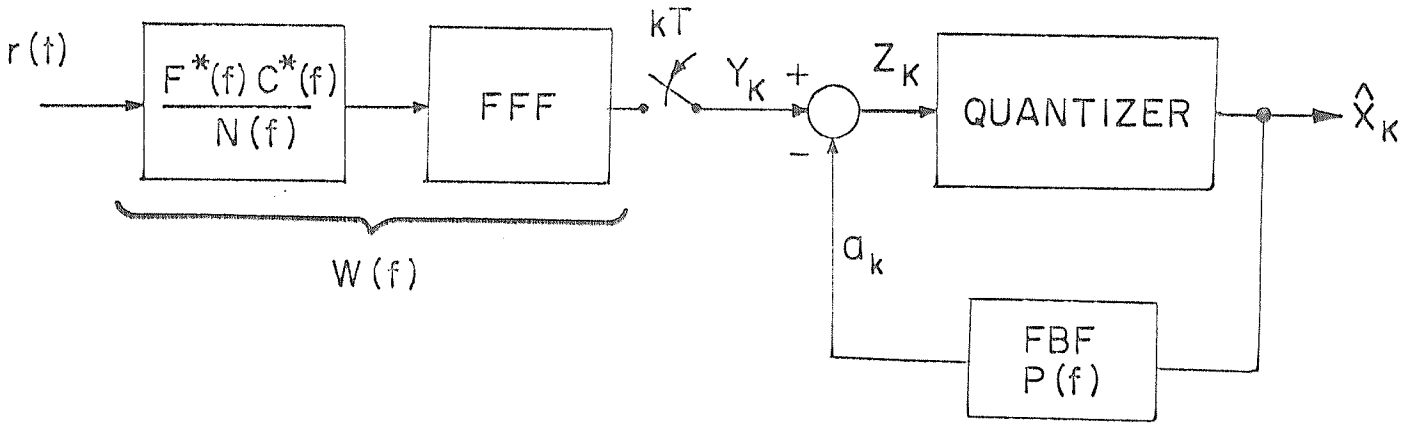

Fig. 3.3. Classic Decision Feedback Equalizer Structure

The analysis of the DFE has always been performed on the assumption that the past decisions are error-free making the mathematics more tractable. When an error is made by the receiver the output of the FBF is no longer the desired value and the probability of subsequent errors is increased with the result that errors tend to occur in bursts. The receiver will reset to its optimum state when N consecutive correct decisions are made. (Where N is the number of feedback taps). For practical signal-to-noise ratios, the probability of this event is large enough that the use of decision feedback provides a net improvement in performance over linear equalization.

The error propagation mechanism is more severe when the tap weights and the number of feedback taps are large. Bounds on the error propagation mechanism have been developed through a Markov chain analysis [58,59]. The results demonstrate that the decision feedback equalizer has a lower error probability than the linear zero-forcing equalizer when there is both a high signal-to-noise ratio and a fast rolloff of the feedback tap gains. Tomlinson [60] has invented a method of avoiding the error propagation problem by subtracting out interference from past digits in the transmitter. Dieulus [61] proposes digital sum feedback as an alternate method of controlling the error propagation.

The error propagation phenomenon, though important is not especially critical in magnetic recording because of the standard implementation of burst-error correction codes. Results in the literature [62] demonstrates that, if the error propagation is neglected, the DFE always has an advantage, and often a substantial advantage, over purely linear equalization.

This has been the incentive for the recent development of DFE modems for satellite, coaxial cable and optical data links [63,64,65,66].

3.3.4 Alternate Structures and Considerations

Decision Feedback Equalization, by nonlinear processing attempts to avoid noise enhancement which would otherwise occur if ISI were eliminated by linear filtering. Several alternate nonlinear receiver structures of varying complexity have been proposed which are competitive, performance-wise, with decision feedback equalization.

When ISI is present, observation of the entire sequence received is optimum in the decision theoretic sense [46]. Unfortunately, the receiver complexity grows exponentially with message length. Chang and Hancock [67] develop receiver structures for making minimum probability of error decisions about L consecutive symbols on the basis of the complete message received. The attractive feature of the algorithm is that the number of computations increases only linearly with the message length.

A new nonlinear receiver structure known as the Maximum Likelihood Sequence Estimator (MLSE) was introduced by Forney [68]. The MLSE algorithm works by assigning a state for each intersymbol interference combination. Because of the one-to-one correspondence between the states and the ISI, the maximum likelihood source sequence can be found by determining the trajectory of states. The receiver consists of a whitened matched filter, a symbol rate sampler and a recursive nonlinear processor that employs the Viterbi algorithm. The receiver is unacceptably complex for most realistic channels as the computations and storage required for processing the received signals grow exponentially with the channel

memory. Vermeulen [69] proposed a reduced state Viterbi dedector to reduce the complexity.

A survey of the Viterbi algorithm is given by Forney [70] and a microprocessor implementation is given by Wilson et al. [71]. Its applicability to receivers for channels with intersymbol interference and correlative level coding (partial-response) coding was suggested by Kobayashi [72]. Application of the Viterbi algorithm to digital magnetic recording systems has been suggested [73]. Adaptive versions of Forney's receiver have been proposed [74] and its combination with decision feedback equalization has been suggested [75]. In comparison with Viterbi receivers there are indications [76] that decision feedback receivers may offer more robust performance on channels with phase jitter.

Sometimes ISI is introduced deliberately for purposes of spectral shaping, in so-called partial response systems [54]. The detector structure is the same as that of a decision feedback equalizer [77]. Nakagawa et al. [78] indicate that the partial response detection method promises the largest areal density among three detection methods studied.

Wood and Donaldson [79] warn that partial response techniques are a liability on digital magnetic recording channels, as are decision feedback or Viterbi receivers which require an implicit knowledge of the incoming signal level. This is in contrast to [57,73,74,78].

Soft decision demodulation has been proposed [80,81] as an additional method of improving channel error rates. In conventional receiver structures, when a decision variable (quantizer input) is close to the decision boundary, this decision is unreliable. An improved decision may

be obtained by using a soft decision demodulator which outputs not only the binary estimate but also a reliability number indicating the quality of the estimate. When an unreliable estimate is indicated, a predictor estimate or interpolator estimate is used rather than the received sample containing a potential serious error.

An important element in the design of all the receivers mentioned is the transversal filter. The transversal filter is the direct form realization of the class of Finite Impulse Response (FIR) non-recursive digital filters. A transposed form [51], though it has an equal number of multiplier (attenuator) and delay elements, offers substantial algorithmic advantages in a practical analog or digital implementation. In addition to direct form and transposed form FIR digital filters, direct form and transposed form network implementations exist. Direct form network implementations, which allow a reduction in multiplications by a factor of two, while doubling the delay elements, look attractive from the standpoint of digital implementation on microprocessors or bit-slice processors. A digital implementation which avoids algebraic multiplications is suggested by Yan et al. [82].

There is presently much interest in finding suboptimum nonlinear receivers that will provide significant performance advantages over linear equalization without the discouraging complexity of the optimum solutions. In this context the decision feedback equalizer appears to be a reasonable compromise. The next chapter investigates the use of the DFE for the saturated magnetic recording channel.

Chapter 4

A DECISION FEEDBACK EQUALIZER FOR SATURATED MAGNETIC RECORDING

4.1 Introduction

The decision feedback equalizer (DFE) has been shown to provide a significant improvement in performance over the linear equalizer for highly dispersive channels which is the case in the saturated magnetic recording channel.

The action of the DFE is to feedback a weighted sum of past decisions to cancel the ISI they cause in the present signaling interval. Three performance criteria have been used to derive optimum systems; 1) minimize the noise variance under a "zero forcing" (ZF) constraint; i.e., insist that all ISI is cancelled; 2) minimize the mean square error (MMSE) between the true sample and the observed signal just prior to the decision threshold; and, 3) minimize the probability of error.

Belfiore [83] introduced a decision feedback structure different from the classical one and used it to show that both the ZF and MMSE decision feedback signal processing are analogous to the general problem of linear prediction. He showed that the decision feedback equalizer can be realized as the optimum linear equalizer followed by an estimator of a random distortion sequence (one-step linear predictor). This model will be used throughout our analysis and is shown in Figure 4.1.

4.2 Design Methodology

In the design, which follows Belfiore [84] closely, consider the

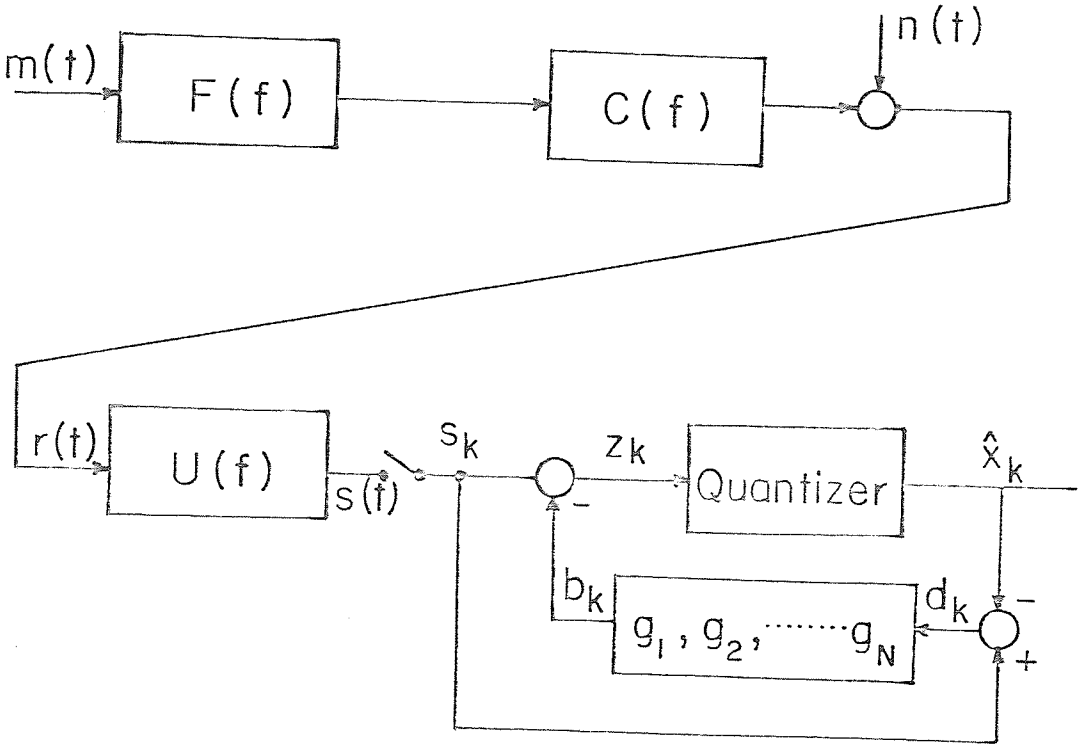

Fig. 4.1. The Channel Model and Decision Feedback Equalizer

transmitter as fixed (i.e., known media, playback head and preamplifier) and the optimum DFE receiver is to be determined. Capital letters will be used for frequency domain functions and lower case for time domain functions. A subscript will be used when the time function is a sampled data sequence. All sums are $-\infty$ to $+\infty$ and all integrands are over the whole real line unless otherwise noted. The transfer functions F, C and U are assumed linear and time invariant. We do not put a causality constraint on these transfer functions. Their impulse responses can be closely approximated in real life by the introduction of a delay in the system. In our case we avoid delayed sampling and hence can base our decision on the transmitted symbol x_k on a sample of $s(t)$ taken at the time $t = kT$. It is further assumed that the receiver has perfect knowledge of the transmitter F and channel C and operates in perfect synchronism with the transmitter. The noise $n(t)$ is stationary, zero-mean, Gaussian with double-sided spectral density $N(f)$. The system is time dispersive and hence introduces ISI. The object of the receiver is to decide which symbol, of a three-level sequence of -1's, 0's and +1's, was transmitted on a symbol-by-symbol basis. The decision device consists of an appropriate three level quantizer. The performance criteria used is to minimize the MSE between z_k and x_k with the constraint that all ISI is eliminated. The number of feedback taps will be a finite number N treated as a system parameter with the two limiting cases $N \to 0$ (the linear equalizer) and $N \to \infty$.

Initially, we specify the transmitter $F_n(f)$ and $C_n(f)$ and noise characteristics $N_n(f)$ where for brevity we have used $F_n(f)$ for $F(f+\frac{n}{T})$, etc. These characteristics can be obtained from the experimental data detailed

in Figures 2.7(a), 2.18, and 2.19 respectively.

Minimization of the MSE between z_k and x_k with the constraint that all ISI is eliminated leads to the following sequence of operations [83]: After choosing the number of feedback taps N evaluate:

$$a_k = T \int_{-\frac{1}{2T}}^{+\frac{1}{2T}} \left[\frac{1}{T} \sum_n \frac{|F_n(f)\, C_n(f)|^2}{N_n(f)} \right]^{-1} \exp\,(j2\pi fkT)\, df$$

for k = 0, 1, 2, ..., N

which defines the periodic feedforward filter

$$U(f) = \frac{F_n^*(f)\, C_n^*(f)}{N_n(f)} \left[\sum_k a_k \exp\,(-j2\pi fkT) \right] .$$

The optimum g_k's are then given by

$$[g_1, g_2, \ldots, g_N]^T = A^{-1}\, [a_1, a_2, \ldots, a_N]^T$$

where A is an NXN non-singular Toeplitz matrix with entries

$$(A)_{m,n} = a_{m-n} \qquad 1 \leq m, \quad n \leq N \quad .$$

This defines the optimum feedback filter

$$G(f) = \sum_{n=1}^{N} g_n \exp\,(-j2\pi kfT).$$

Implementation of the FBF and FFF in the classic DFE structure can be accomplished by the respective transformations:

$$P(f) = - G(f)$$

$$W(f) = U(f) [1 - G(f)].$$

Note that the feedback tap weights $\{g_k\}$ and $\{p_k\}$ are identical in magnitude; hence, any error propagation is the same in both systems. Note also there could be a situation where W(f) is square integrable but U(f) is not and, hence, the structure in Figure 3.3 is realizable but the structure in Figure 4.1 may not be.

Figure 4.2 shows a decision feedback equalizer for N = 3 proposed for use in digital magnetic recording. Several factors influence the choice of the number of feedback taps (N) required. The error propagation phenomenon is more severe when the tap weights and the number of feedback taps are large. A decision feedback equalizer with a modest number of taps performs almost as well as one with an infinite number. In addition, for channels which are only slightly time dispersive (e.g., ISI which extends only to immediately adjacent symbols) we would expect N to be small.

4.3 The Simulation Algorithm

A computer program was written in Fortran (Appendix C) to implement the decision feedback equalizer of Section 4.2. Originally, a CSMP program [84] was written to simulate the DFE algorithm. CSMP proved to be a poor medium in which to run the simulation due to the significant computing resources required (40 ms/cycle) and was abandoned in favor of the Fortran implementation.

The transmitter and channel characteristics were obtained from the experimental data presented in Chapter 2. The transmitted sequence of

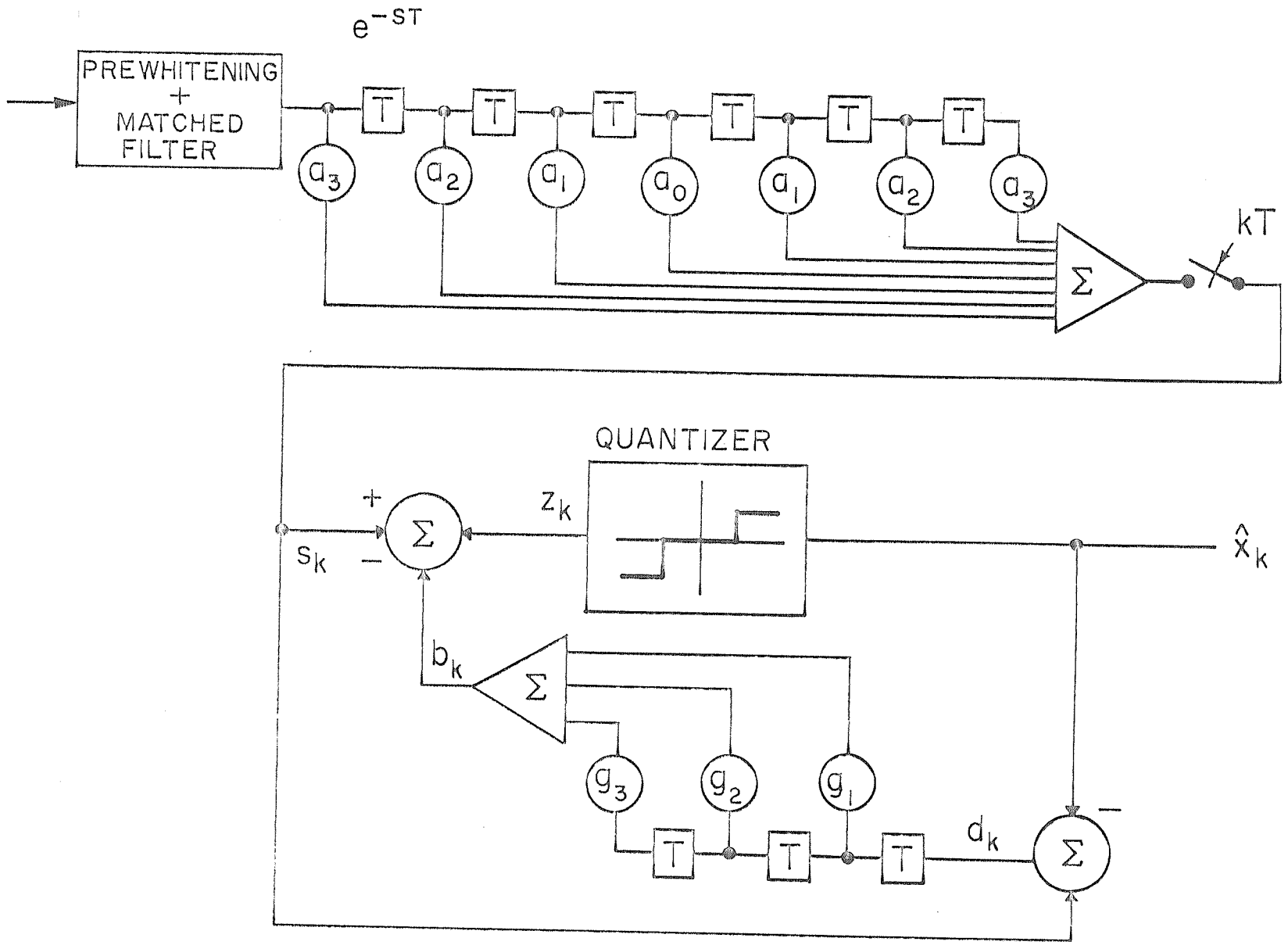

Fig. 4.2. The Decision Feedback Equalizer (N=3)

symbols was determined by a 512-bit pseudo-random number generator (Appendix D) which was subsequently encoded into a binary MFM data sequence. This data sequence defined the analog waveform of the transmitter by the corresponding linear superposition of quartic pulses. (Each symbol extended over a 13 T period with T = 100 ns). The channel noise was obtained from a pseudo-random number generating procedure GGUN given in [85]. The power density spectrum of the noise sequence resulting from multiplicative congruential pseudo-random number generators as given in [85] has been determined in the literature as being essentially white [86]. An appropriate difference equation was written to transform the power density spectrum of the noise to correspond with the experimental measurements.

The analysis was done for a decision feedback equalizer structure consisting of 7 feedforward taps, 3 feedback taps for T = 100 ns and 13 feedforward, 6 feedback taps for T = 100 ns and T = 50 ns. This corresponds to a data transfer rate of 5 MHz and 10 MHz respectively, the lowest and highest bounding frequencies for the MFM encoding currently used in the Burroughs disk drive.

The simulation was set up to terminate after the transmission of 10^7 symbols. One of the limitations typical to this type of simulation is computer time. On an Amdahl 470/V7 digital computer, the program discussed here required about 21.24 μs per processed symbol (of which 11.8 μs could be attributed to the random noise generator).

4.4 Simulation Results

The bit error rate (BER) of a communications channel is a valuable

criterion to use in evaluating its performance. The BER is used as the basis through which the DFE is evaluated in terms of its suitability for application in the digital magnetic recording channel.

In the DFE, many of the symbol errors are members of the same error event (error propagation mechanism) and hence are not independent. In fact, Belfiore [83] has shown that the total number of errors P_E is bounded by the number of burst errors P_e as,

$$P_E \leq P_e \, M^N$$

where M is the number of PAM levels, N is the number of feedback taps.

Throughout this thesis the BER is calculated on the basis of P_e only. The BER curves presented in this section are based on the number of times, x, that an appropriate error event has occurred in m transmitted symbols. For a small sample of error events it would be unreasonable to claim that the estimate $\hat{P}_e = \frac{x}{m}$ is exactly equal to the probability of error P_e that would be obtained from the observation of an infinite number of transmitted symbols. Hence, it would seem desirable to accompany the estimate $\hat{P}_e$ with some statement as to how close we might reasonably expect the estimate to be to the true P_e. This can be done by using confidence intervals. In cases where P_e is close to 0 (or 1) we are interested in one-sided confidence intervals of the form $P_e < C$; that is, we are interested mainly in finding an upper confidence limit for P_e. When P_e is small and m is large, we approximate the binomial distribution with a Poisson distribution rather than a normal curve.

Hald [87], has shown that an approximate $1-\alpha$ upper confidence limit is given by $\frac{1}{2m} \cdot \chi^2_\alpha$, where χ^2_α is the chi-square distribution and the number of degrees of freedom equals $2(x+1)$. For example, for $x = 10$ burst errors, $m = 10^6$ transmitted symbols (i.e., $\hat{P}_e = 10^{-5}$) and $\alpha = 0.01$ for a confidence level of 99%, we obtain the following one-sided confidence interval,

$$P_e < \frac{40.28}{2\ (10^6)} = 2.014 \times 10^{-5}$$

where 40.28 is the value of $\chi^2_{0.01}$ for $2(10+1) = 22$ degrees of freedom. Had we used the normal distribution rather than the Poisson distribution to approximate the binomial distribution, we would have obtained a more optimistic interval $0 < P_e < 1.7 \times 10^{-5}$.

Assuming that one cannot afford more than one minute (i.e., $60/(21.24 \times 10^{-6}$ cycles) of computer time per run along with the observation of at least 10 error events, simple evaluation of $\hat{P}_e = 10/(60/21.24 \times 10^{-6}) \cong 3.54 \times 10^{-6}$ shows that in practice 5×10^{-6} is the lowest error probability attainable by this method (5×10^{-7} if one is allowed to use 10 minutes of computer time per run, etc.). Furthermore, for a large sample size ($m > 10^3$) based on the observation of at least 10 error events, at the confidence level of 99% we would establish the following bound

$$P_e < 2\hat{P}_e$$

The simulation results for three DFE feedback taps and $T = 100$ ns corresponding to a data rate of 5 MHz for MFM encoding are presented in

Figure 4.3. Initially, lower and upper performance bounds are established. The matched filter and simple quantizer discussed in Section 3.3.1 provides the upper bound. The theoretical lower bound for no inter-symbol interference (additive noise considerations only) is provided by the familiar Q function. The performance of the receiver considering additive noise only (i.e., the dc-erased disk - no magnetic flux transitions) defines the quiescent error rate. The quiescent BER follows Q(x) closely by a constant, a necessary (but certainly not a sufficient condition) for establishing some confidence in the simulation.

The DFE provides approximately a 6 dB improvement over the matched filter plus simple quantizer at a 20 dB SNR. For a SNR greater than 25 dB DFE may achieve competitive error rates with the present disk drive (albeit at half the present density).

Above 15 dB SNR the feedback operation ($s_k - b_k$) improves the BER. This is logical since the feedback process is disturbed less by random noise. Conversely, the feedback process provides little benefit for a SNR < 15 dB.

The results corresponding to the doubling of the number of feedback taps (N = 6) is presented in Figure 4.4. The DFE (N = 6) realizes a 1.5 dB improvement over the case N = 3, as the ISI due to the entire symbol period can be taken into account. All the other results for N = 6 are consistent with the case N = 3.

A sensitivity analysis to component tolerances is an important criterion in evaluating the merits of a practical engineering design. The effect on the BER of varying all the feedforward and feedback taps $\pm$ 10% was used as a crude sensitivity indicator. The results are presented in

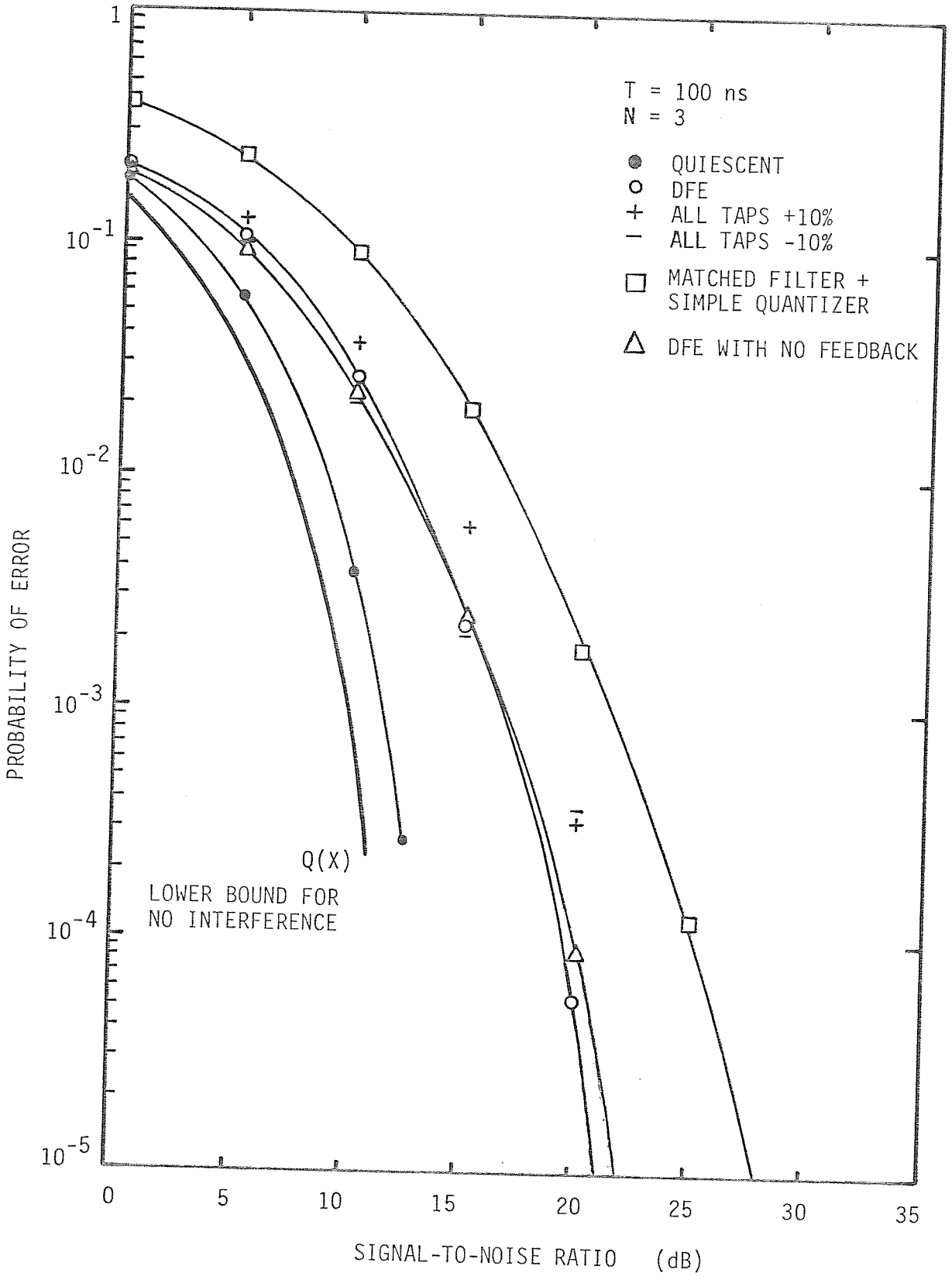

Figure 4.3 BER for 5MHz MFM data transfer rate and 3 feedback taps.

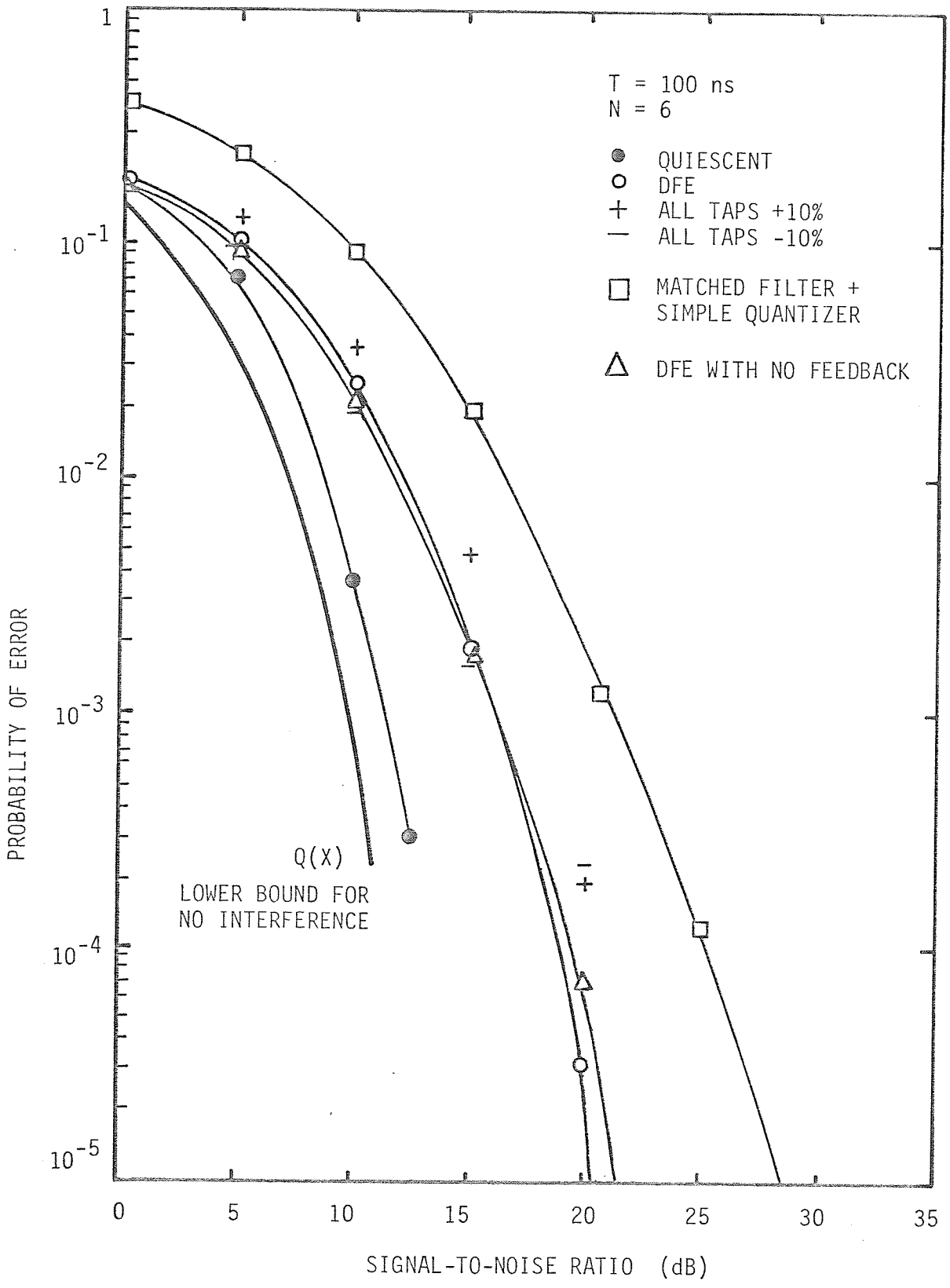

Figure 4.4 BER for 5MHz MFM data transfer rate and 6 feedback taps.

Figure 4.5 and Figure 4.6. The effect on the BER appears more pronounced as the SNR increases indicating that component tolerances (or quantization errors in digital implementations) may be a potential limitation at high SNR. A more rigorous sensitivity study in conjunction with reference [52] is needed.

In addition, the sensitivity of the three-level quantizer thresholds was studied. The effect of varying the input threshold levels is presented in Figure 4.5. A $\pm$ 10% variation in input threshold levels increases the BER by a minimum factor of three. Doubling the number of feedback taps in turn reduces the error rate by at least 15% for the same variation in input threshold level. The effect of varying the output amplitude, shown in Figure 4.6, is much less dramatic. A $\pm$ 10% variation in output amplitude increases the error rate by no more than 15%. Doubling the number of feedback taps in turn reduces the error rate by 10% for the same variation in output amplitude.

In order to evaluate the merits of using DFE it is important to compare its performance to that of the existing Burroughs receiver. The receiver consists of a 4th order low pass filter, which closely corresponds to an appropriate matched filter approximation, followed by a differentiator and zero-crossing detector. The differentiator is responsible for approximately 2 dB of noise enhancement [36]. This is more than offset by the ability of the receiver to handle some fading of the readback signal (usually due to media dropouts). In the simulation that follows we retain the Burroughs matched filter approximation and replace the differentiator and zero-crossing detector by an appropriate threshold detector. The performance results are

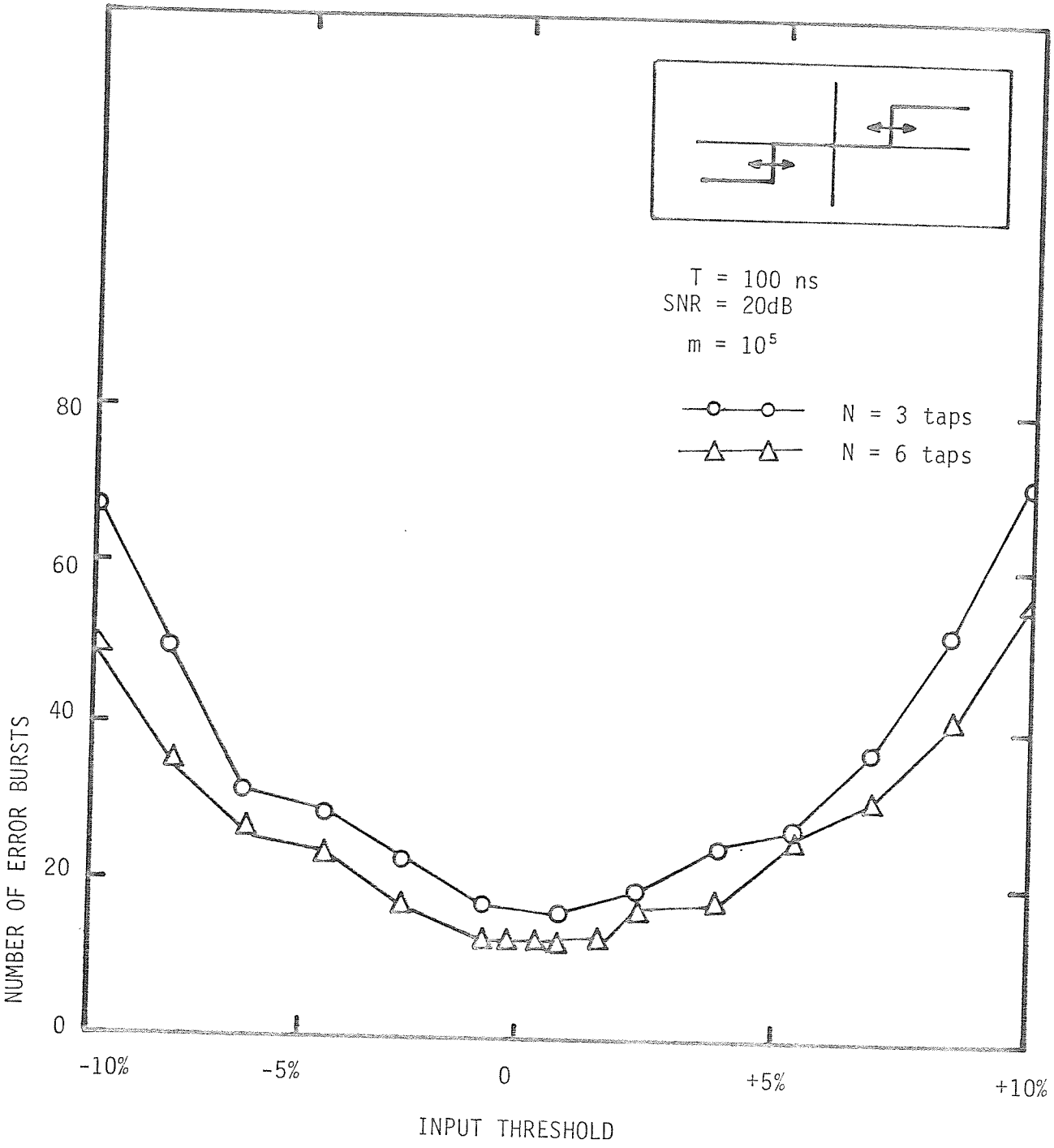

Figure 4.5 Effect of varying the input threshold of the three-level quantizer.

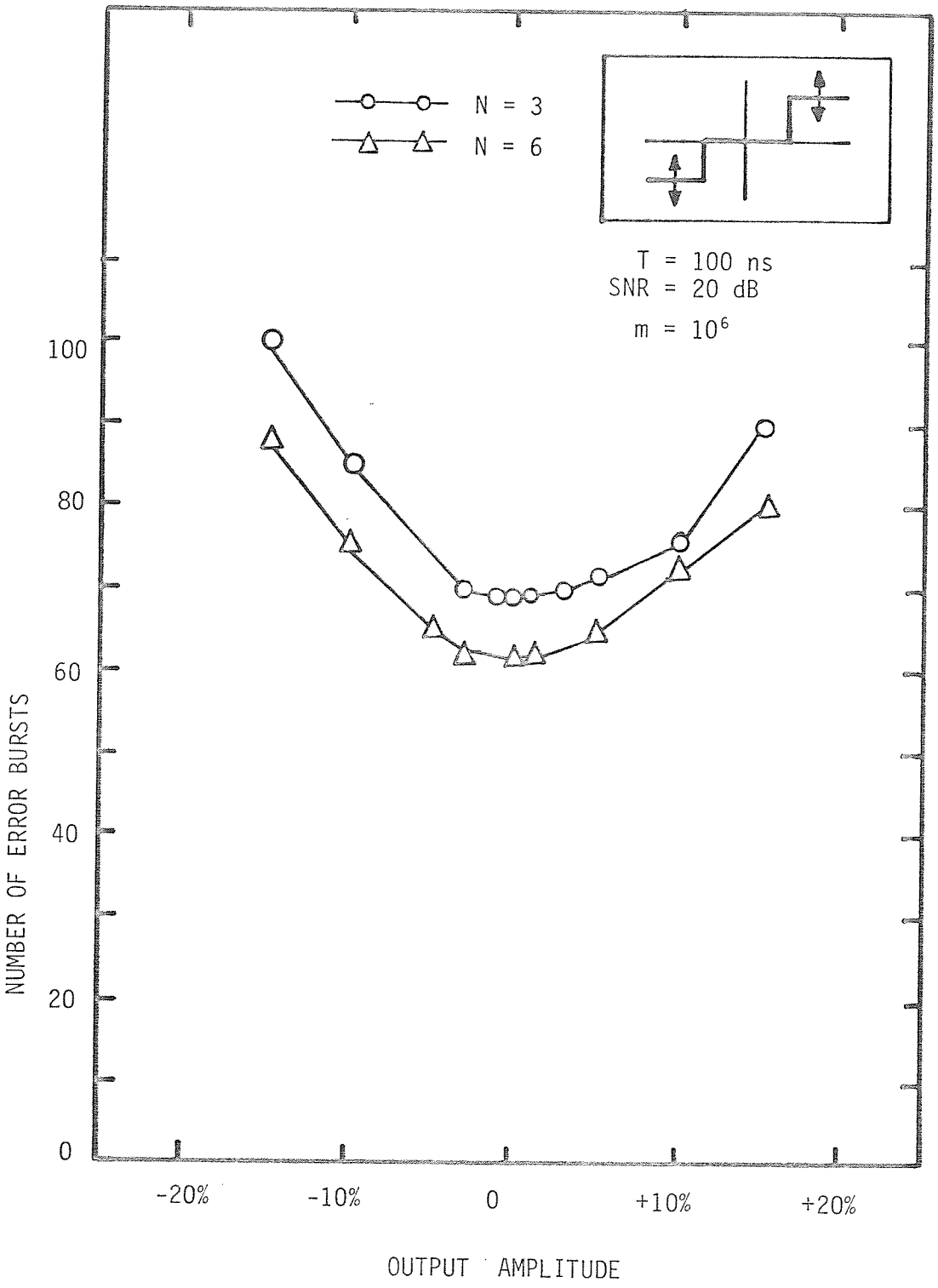

Figure 4.6 Effect of varying the output amplitude of the three-level quantizer.

then compared to those of the DFE receiver.

The simulation results for six DFE feedback taps and T = 50 ns, corresponding to a data rate of 10 MHz for MFM encoding, are presented in Figure 4.7. As before, the theoretical lower bound for no-intersymbol interference is provided by the familiar Q function. The DFE with 6 feedback taps always enjoys a performance advantage over the Burroughs matched-filter approximation. However, the practical implementation of the Burroughs receiver exhibits a $\hat{P}_e = 10^{-11}$ at a SNR of approximately 30 dB. The simulation results for the same receiver exhibits a $\hat{P}_e = 10^{-5}$ at a SNR of 32 dB. The large discrepancy suggests a deficiency in the simulation model used to describe the saturated magnetic recorder. The characterization of the noise as Gaussian may account for this discrepancy. The Gaussian noise assumption and the superposition of isolated pulses in the simulation clearly defines the SNR. However, the SNR of the Burroughs disk drive (as measured with a true RMS voltmeter) includes not only the Gaussian noise of the head and electronics but also the disk noise and the noise due to auxiliary sources. Experimentally, the power density spectrum and the probability density function indicates the significance of these auxiliary noise sources. In addition, Su and Williams [35] found an increase in noise level occurring at frequencies in the vicinity of the written signal frequency. This also makes a direct SNR comparison with the simulation difficult. Improving the noise characterization is discussed in the conclusions.

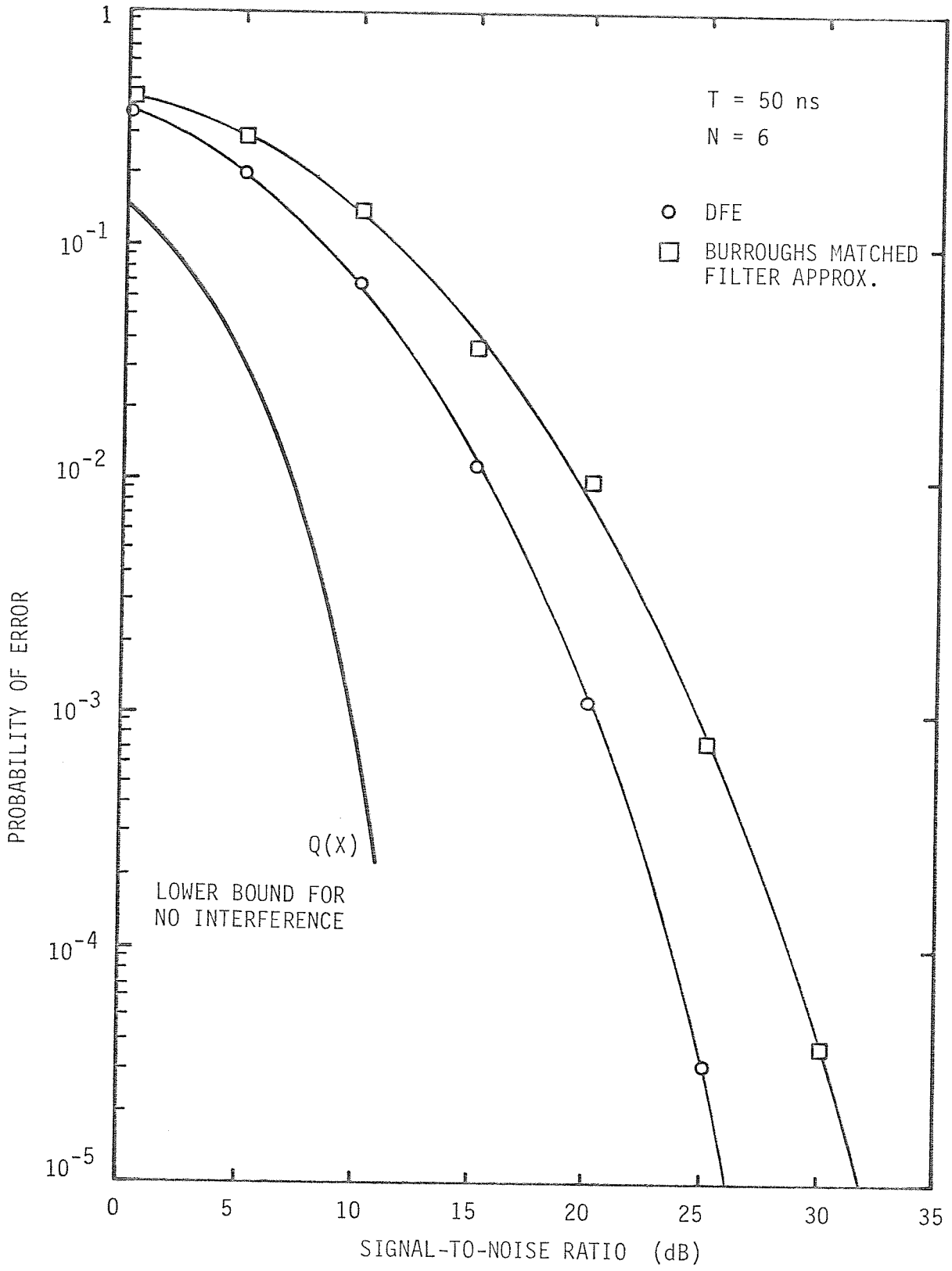

Figure 4.7 BER for 10MHz MFM data rate and 6 feedback taps.

Chapter 5

CONCLUSIONS AND SUGGESTIONS FOR FUTURE WORK

The analysis of digital recording and reproduction in the previous sections has led, in spite of the complex processes involved, to some reasonably accurate approximations.

We found that the readback voltage of the isolated transition could be accurately approximated by a quartic function:

$$\frac{K}{1 + at^2 + bt^4} \quad .$$

In addition, the validity of linear superposition has been verified down to a reversal distance of PW_{50}. The validity of linear superposition is of cardinal importance since it admits the successful application of linear post-equalization (receiver equalization) necessary to combat the effects of intersymbol interference and noise. As the linear bit density increases, distortion introduced by writing demagnetization and bit-to-bit interactions reduces the accuracy of the linear system approach. The merits of linear equalization are then questionable.

The functional form of the dc-erased disk noise probability density can best be approximated by:

$$p(x) = \frac{\sqrt{2\sqrt{c} + b}}{\pi (1 + bx^2 + cx^4)} \quad , \quad \left| \frac{b}{2\sqrt{c}} \right| < 1 \quad .$$

A further analysis of the dc-erased disk noise probability density suggests a correlation between surface-substrate roughness and noise probability density and hence with bit error rate. This may indicate the need for improved roughness specifications of the media substrate and of the recording media surface.

With regard to the absolute maximum capacity of a communications channel at which vanishingly small probability of error can be achieved, only 10% of the maximum channel capacity is presently being utilized on the Burroughs disk drive.

As the recording channel is stressed with higher data rates, inter-symbol interference (ISI) becomes a dominant limiting factor. To combat this effect in the saturated magnetic recorder use of a DFE in the receiver is proposed.

When a relatively small number of past decisions (3 to 6) are used in the feedback equalization process, the simulation results by themselves indicate that a performance improvement relative to the existing Burroughs receiver appears realizable. However, it is important to qualify this statement in view of the fact that the simulation results for the Burroughs matched filter approximation do not correspond to the performance statistics of the hardware implementation of the device itself. One major factor may account for this discrepancy. The Gaussian noise assumption in the simulation model may not be an accurate representation of the noise process of the disk drive. Indeed, our experimental measurements indicate that the noise could be more accurately modelled as the convolution of Gaussian noise with quartic noise. Furthermore, if we could model one component

of the noise source, such as caused by mechanical imperfections, poor servo-tracking, inter-track interference or incomplete overwrite, as a sinusoidal (for example) type of noise, examination of its probability density function indicates that for the same SNR it is quite benign up to some threshold. Unfortunately, very little theory exists to handle optimum receiver design in the presence of non-Gaussian noise.

Assume for the sake of argument that a more accurate representation of the noise process in the magnetic recorder when implemented in the computer simulation improves the BER simulation curve of the Burroughs matched-filter approximation in Figure 4.7, so that it corresponds closely with the actual performance measurements. Likewise, assume a corresponding improvement in the BER curve for the DFE. The simulation results then indicate that the DFE appears to maintain a 5 dB performance advantage at a SNR of 25 dB. However, the DFE must still prove itself in terms of its robustness to phase jitter, fades and synchronization. In addition, a thorough sensitivity analysis of the feedforward and feedback filter taps along with a more complete characterization of the DFE burst error statistics is needed. Due to the significant computing resources required, a thorough computer simulation of these effects may be a formidable problem. An obvious solution is the construction of a prototype for use on an actual disk drive. Considering the simplicity of the receiver itself, an equivalent microprocessor simulation operating at a kHz symbol rate may be an attractive alternative that provides the required flexibility at reasonable cost.

An important extension of this work would investigate the application of partial response signaling or other types of spectrum shaping codes which are matched to the channel. The decision feedback equalizer is a possible receiver for such codes which may increase the channel utilization.

In conclusion, the simulation results have consistently shown that DFE provides a significant performance advantage over the current Burroughs receiver. However, there are indications that the model is deficient, particularly in the noise characterization, in that current performance statistics cannot be reproduced. Improved modelling of the channel impairments would allow a more definitive evaluation of DFE as applied to digital communication over the saturated magnetic recording channel. Considering its ease of implementation, even at high data rates, decision feedback equalization is worth some further consideration insofar as the linear system approach remains valid.

REFERENCES

[1] Durniak, A., Eight inch hard disks set to go, Electronics, June 21, 1979, p. 83.

[2] Arnold, W.F., and Durniak, A., Denser disk drives poised for surge, Electronics, June 21, 1979, p. 86.

[3] Dreyfack, K., Thin film makes head read/write, Electronics, June 7, 1979, pp. 76-78.

[4] Mallinson, J.C., Tutorial review of magnetic recording, Proceedings of IEEE, Vol. 64, No. 2, February 1976, pp. 196-208.

[5] Yencharis, L., Thin-film, multiturn heads push disk recording densities way up, Electronic Design, March 1, 1980, pp. 30-31.

[6] Yencharis, L., IBM's thin-film heads squeeze disk capacity to record levels, Electronic Design, March 1, 1980, pp. 60-63.

[7] Haynes, M.K., Experimental determination of the loss and phase transfer functions of a magnetic recording channel, IEEE Transactions on Magnetics, Vol. Mag.-13, No. 5, September 1977, pp. 1284-1286.

[8] Hopner, E., Recent advances in magnetic recording technology affecting the storage densities and transfer rates of digital mass memories, Mitteilungen Agen Switzerland, No. 10, September 1969, pp. 48-51.

[9] Jacoby, G.V., Signal equalization in digital magnetic recording, IEEE Transactions on Magnetics, Vol. Mag.-4, No. 3, September 1968, pp. 302-305.

[10] Chu, W.W., A computer simulation of electrical loss and loading effect in magnetic recording, IEEE Transactions on Electronic Computers, Vol. EC-16, No. 4, August 1967, pp. 430-434.

[11] Roberge, J.K., Operational Amplifiers: Theory and Practice, John Wiley & Sons, Inc., Toronto, 1975, p. 87.

[12] Walker, P.A., A systems overview of transducers, Advances in magnetic recording - Annals of the New York Academy of Sciences, New York, Vol. 189, January 3, 1972, pp. 144-169.

[13] Sierra, H.M., An analytical estimate of bit shift and bit crowding in digital magnetic recording, IBM Technical Report, TR02.245, January 24, 1963, pp. 1-17.

[14] Kosters, A.J., and Speliotis, D.E., Predicting magnetic recording performance by using single pulse superposition, Intermag 1971, IEEE Transactions on Magnetics, September, 1971, p. 544.

[15] Macintosh, N.D., A superposition-based analysis of pulse slimming techniques for digital recording, Video and Data Recording Conference, Southampton University, July 1979, pp. 1-3.

[16] Potter, R.I., Analysis of saturation magnetic recording based on arctangent magnetization transitions, Journal of Applied Physics, Vol. 41, No. 4, March 14, 1970, pp. 1647-1651.

[17] McCary, R.O., The saturation magnetic recording process, IEEE transactions on magnetics, Vol. Mag.-7, No. 1, March 1977, pp. 4-16.

[18] Curland, N. and Speliotis, D.E., A theoretical study of an isolated transition using an iterative hysteretic model, IEEE Transactions on Magnetics, Vol. Mag-6, No. 3, September 1979, pp. 640-645.

[19] Gradshteyn, I.S., and Ryzhik, I.M., Tables of Integrals Series and Products, Academic Press, New York, 1979, p. 67.

[20] Sebestyen, L.G., Digital magnetic tape recording for computer applications, Chapman and Hall, London, England, 1973, pp. 59-93.

[21] Best, D.T., Digital magnetic recording principles, Technical Bulletin 1018, Ferroxcube Corp., Saugerties, New York, pp. 1-14.

[22] Mallinson, J.C., Applications of Fourier transforms in digital magnetic recording theory, IEEE Transactions on Magnetics, Vol. Mag-10, No. 1, March 1974, pp. 69-77.

[23] Morrison, F.R., and Speliotis, D.E., Study of peak shift in thin recording surfaces, IEEE Transactions on Magnetics, Vol. Mag-3, September 1967, pp. 208-211.

[24] Tjadan, D.L.A., Some Notes on 'Superposition' in Digital Magnetic Recording, IEEE Transactions on Magnetics, Vol. Mag-9, September 1973, pp. 523-537.

[25] Tercic, E.J., Superposition measurements with a flux sensitive head in digital magnetic recording, IEEE Transactions on Magnetics, Vol. Mag.-9, September 1973, pp. 335-338.

[26] Chi, C.S., and Speliotis, D.E., Dynamic self-consistent iterative simulation of high bit density digital magnetic recording, IEEE Transactions on Magnetics, Vol. Mag-10, September 1974, pp. 764-768.

[27] Mishimoto, K., Nagao, M., Suganuma, Y., and Tanaza, H., Computer simulation of high density multiple transitions in magnetic recording, IEEE Transactions on Magnetics, Vol. Mag-10, September 1974, pp. 769-777.

[28] Kosters, A.J., and Speliotis, D.E., Predicting magnetic recording performance by using single pulse superposition, IEEE Transactions on Magnetics, September 1971, p. 544.

[29] Mallinson, J.C., Theory of linear superposition in tape recording, IEEE Transactions on Magnetics, Vol. Mag-5, No. 4, December 1969, pp. 886-890.

[30] Chi, C.S., and Speliotis, D.E., The isolated pulse and two-pulse interactions in digital magnetic recording, IEEE Transactions on Magnetics, Vol. Mag-11, No. 5, September 1975, pp. 1179-1181.

[31] Kostyshyn, B., The write process in magnetic recording, IEEE Transactions on magnetics, Vol. Mag-7, No. 4, December 1971, pp. 880-885.

[32] Lee, J.E., and Truman, N.N., The effect of finite flux rise-time on recording performance, IEEE Transactions on Magnetics, Vol. Mag-6, No. 1, March 1970, pp. 95-100.

[33] Mallinson, J.C., A unified view of high density digital recording theory, IEEE Transactions on Magnetics, Vol. Mag-11, No. 5, September 1975, pp. 1166-1169.

[34] Mallinson, J.C., Maximum signal-to-noise ratio of a tape recorder, IEEE Transactions on Magnetics, Vol. Mag-5, No. 3, September 1969, pp. 182-186.

[35] Su, J.L., and Williams, M.L., Noise in disk data recording media, IBM Journal of Research and Development, November 1974, pp. 570-575.

[36] Hughes, G.F., and Schmidt, R.K., On noise in digital recording, IEEE Transactions on Magnetics, Vol. Mag-12, No. 5, November 1976, pp. 752-754.

[37] Mallinson, J.C., On extremely high density digital recording, IEEE Transactions on Magnetics, Vol. Mag-10, No. 2, June, 1974, pp. 368-373.

[38] Tahara, Y., and Miura, Y., Peak shift caused by Gaussian noise in digital magnetic recording, Electronics & Communications in Japan, Vol. 59-C, No. 10, 1976, pp. 77-86.

[39] Stevenson, T.J., Disk file optimization, IEEE Transactions on Magnetics, Vol. Mag-11, No. 5, September 1975, pp. 1237-1239.

[40] Byers, R.A., Theoretical signal-to-noise ratios for magnetic tape heads, IEEE Transactions on Magnetics, Vol. Mag-7, No. 2, June 1971, pp. 254-259.

[41] Card, Dan, Personal Communication, Burroughs Corporation - Computer Peripheral Products Division, Winnipeg Plant, Winnipeg, Manitoba, November 9, 1979.

[42] Morrison, J.R., and Speliotis, D.E., Electron probe analysis of recording surfaces, IEEE Transactions on Magnetics, Vol. Mag-5, No. 3, September 1969, pp. 325-326.

[43] Ogawa, K., and Ogawa, S., Noise reduction of magnetic coated disk, IEEE Transactions on Magnetics, Vol. Mag-15, No. 6, Nov. 1979, pp. 1555-1557.

[44] Ichiyama, Y., Theoretical analysis of bit error rate considering intertrack crosstalk in digital magnetic recording equipment, IEEE Trans. on Magnetics, Mag-15, No. 1, Jan. 1979, pp. 899-906.

[45] Kiwimagi, R.G., and McDowell, J.A., Channel coding for digital recording, IEEE Transactions on Magnetics, Vol. Mag-10, No. 3, September 1974, pp. 515-518.

[46] Wozencraft, J.M., and Jacobs, I.M., Principles of Communication Engineering, John Wiley, New York, 1965, pp. 321-341.

[47] Gallager, R.C., Information Theory and Reliable Communication, John Wiley, New York, 1968, pp. 383-390.

[48] Gilbert, E.N., Capacity of a burst-noise channel, Bell System Technical Journal, Vol. 39, No. 5, 1960, pp. 1253-1265.

[49] Mallinson, J.C., Miller, J.W., Optimal Codes for Digital Magnetic Recording, The Radio and Electronic Engineer, Vol. 47, No. 4, April 1977, pp. 172-176.

[50] Kallmann, H.E., Transversal filters, Proceedings of the IRE, July 1940, pp. 302-310.

[51] Oppenheim, A.V., and Schafer, R.W., Digital signal processing, Prentice Hall, New Jersey, pp. 455-165.

[52] Gersho, A., Gopinath, B., Odlyzko, A., Coefficient inaccuracy in transversal filters, The Bell System Technical Journal, Vol. 58, No. 10, Dec. 1979, pp. 2301-2316.

[53] Rudin, H., Automatic equalization using transversal filters, IEEE Spectrum, January 1967, pp. 53-59.

[54] Lucky, R.W., Salz, J., Weldon, E.J., Principles of data communication, McGraw Hill, Toronto, 1968, Chapters 4, 5, 6.

[55] Roza, E., A practical approach to decision feedback receivers with conventional filters, IEEE Trans. on Communications, Vol. Com-26, No. 5, May 1978, pp. 679-689.

[56] Salazar, A.C., Design of transmitter and receiver filters for decision feedback equalization, Bell System Technical Journal, Vol. 53, No. 3, March 1974, pp. 503-523.

[57] George, D.A., Bowen, R.R., Storey, J.R., An adaptive decision feedback equalizer, IEEE Trans. Comm., Vol. Com-19, No. 3, 1971, pp. 281-292.

[58] Duttweiler, D.L., Mazo, J.E., Messerschmitt, D.G., An upper bound on the error probability in decision-feedback equalization, IEEE Trans. on Information Theory, Vol. IT-20, No. 4, July 1974, pp. 490-497.

[59] Belfiore, C.A., Decision feedback equalization - A unified approach, Ph.D. Thesis, University of Minnesota, March 1976, 182 pages.

[60] Tomlinson, M., New automatic equalization employing modulo arithmetic, Electronics Letters, Vol. 7, Nos. 5/6, March 25, 1971, pp. 138-139.

[61] Dieulus, V.A., Coding for the control of intersymbol interference in baseband channels, Ph.D. Thesis, University of Illinois at Urbana-Champaign, 1978, pp. 61-64.

[62] Messerschmitt, D.G., A geometric theory of intersymbol interference, The Bell System Technical Journal, Vol. 52, No. 9, November 1973, pp. 1483-1539.

[63] Kern, D.R., and Mosen, P., Megabit digital troposcatter subsystem (MDTS), GTE Sylvania, Needham MA, and Signatron, Lexington MA, Final Report Ecom-74-0040-F.

[64] Roza, E., Thyl, J., Doorn, W., A novel concept for a hybrid 140 Mbits/sec system, IEEE Transactions on Communications, Vol. Com-27, No. 10, October 1979, pp. 1584-1592.

[65] Watanabe, K., Inoue, K., Sato, Y., A 4800 bit/sec microprocessor modem, IEEE Trans. on Communications, Vol. Com-26, No. 5, May 1978, pp. 493-498.

[66] Messerschmitt, D.G., Linear and decision feedback equalization for digital fiber optic systems, IEEE International Symposium on Circuits and Systems, Houston, Texas, April 28-30, 1980, Wa/S-11.5.

[67] Chang, R.W., Hancock, J.C., On receiver structures for channels having memory, IEEE Trans. on Information Theory, Vol. IT-12, No. 4, October 1966, pp. 463-468.

[68] Forney, G.D., Maximum-likelihood sequence estimation of digital sequences in the presence of intersymbol interference, IEEE Trans. on Information Theory, Vol. IT-18, May 1972, pp. 363-378.

[69] Vermeulen, F.L., Low complexity decoders for channels with intersymbol interference, Ph.D. Thesis, Stanford University, 1975.

[70] Forney, G.D., The Viterbi Algorithm, Proc. IEEE, Vol. 61, March 1973, pp. 268-278.

[71] Wilson, M., Crozier, S., Moreland, K., Camelon, J., McLane, P., Microprocessor implementation of the Viterbi detector, Proceedings of the National Telecommunications Conference, Washington, D.C., November 27-29, 1979, pp. 25.5.1 - 25.5.4.

[72] Kobayashi, H., Correlative level coding and maximum likelihood decoding, IEEE Trans. Information Theory, Vol. IT-17, pp. 586-594, September 1971.

[73] Kobayashi, H., Application of probabilistic decoding to digital magnetic recording systems, IBM Journal of Res. and Development, January 1971, Vol. 15, pp. 64-74.

[74] Magee, F.R., Proakis, J.G., Adaptive maximum likelihood sequence estimation for digital signaling in the presence of intersymbol interference, IEEE Trans. Information Theory, Vol. IT-19, January 1973, pp. 120-124.

[75] Lee, W., A maximum likelihood sequence estimator with decision feedback equalization, IEEE Trans. on Communications, Vol. Com-25, No. 9, September 1977, pp. 971-979.

[76] Falconer, D. and Magee, F., Evaluation of decision feedback equalization and Viterbi Algorithm detection for voice band data transmission - Part I, IEEE Transactions on Communications, Vol. Com-24, No. 10, October 1976, pp. 1130-1139.

[77] Kabal, P., Pasupathy, S., Partial-response signaling, IEEE Trans. on Communications, Vol. Com-23, No. 9, September 1975, pp. 921-934.

[78] Nakagawa, S., Yakayama, K., Katayama, H., A study on detection methods of NRZ recording, IEEE Trans. on Mag., Mag-10, No. 1, Jan. 1980, pp. 104-110.

[79] Wood, R.W., Donaldson, R.W., The helical-scan magnetic tape recorder as a digital communication channel, IEEE Trans. on Magnetics, Vol. Mag-15, No. 2, March 1979, pp. 935-943.

[80] Jayant, N.S., Steele, R., Chan, N., Schmitt, C., On soft decision demodulation for PCM and DPCM encoded speech, IEEE Trans. on Comm., Vol. Com-28, No. 2, February 1980, pp. 308-311.

[81] Kabayashi, H., Tang, D.T., On decoding of correlative level coding systems with ambiguity zone detection, IEEE Trans. Communication, Vol., Com-19, No. 4, August 1971, pp. 467-477.

[82] Yan, T. and Yao, K., A multiplication free solution for linear minimum mean-square estimation and equalization using the branch-and-bound principle, IEEE Transactions on Information Theory, Vol. IT-26, No. 3, May 1980, pp. 318-326.

[83] Belfiore, C.A., and Park, J.H., Decision feedback equalization, Proceedings of the IEEE, Vol. 67, No. 8, August 1979, pp. 1143-1156.

[84] System/360 Continuous System Modeling Program - User's Manual, GH20-0367-4, Janaury 1972.

[85] IMSL Library 1, Edition 6, International Mathematical and Statistical Libraries, Inc., Houston, Texas, July 1977.

[86] Lewis, P.A., Goodman, A.S., and Miller, J.M., A pseudo-random number generator forthe system/360, IBM Systems Journal, Vol. 8, No. 2, 1969, pp. 136-146.

[87] Hald, A., Statiscal Theory with Engineering Applications, John Wiley & Sons Inc., New York, 1952, Chapter 21, 22.

[88] Peterson, W.W., Error Correcting Codes, M.I.T., Press, Cambridge, Massachusetts, 1970, pp. 251-270.

APPENDIX A

Least Squares Fit to the Experimentally Observed Isolated Pulse

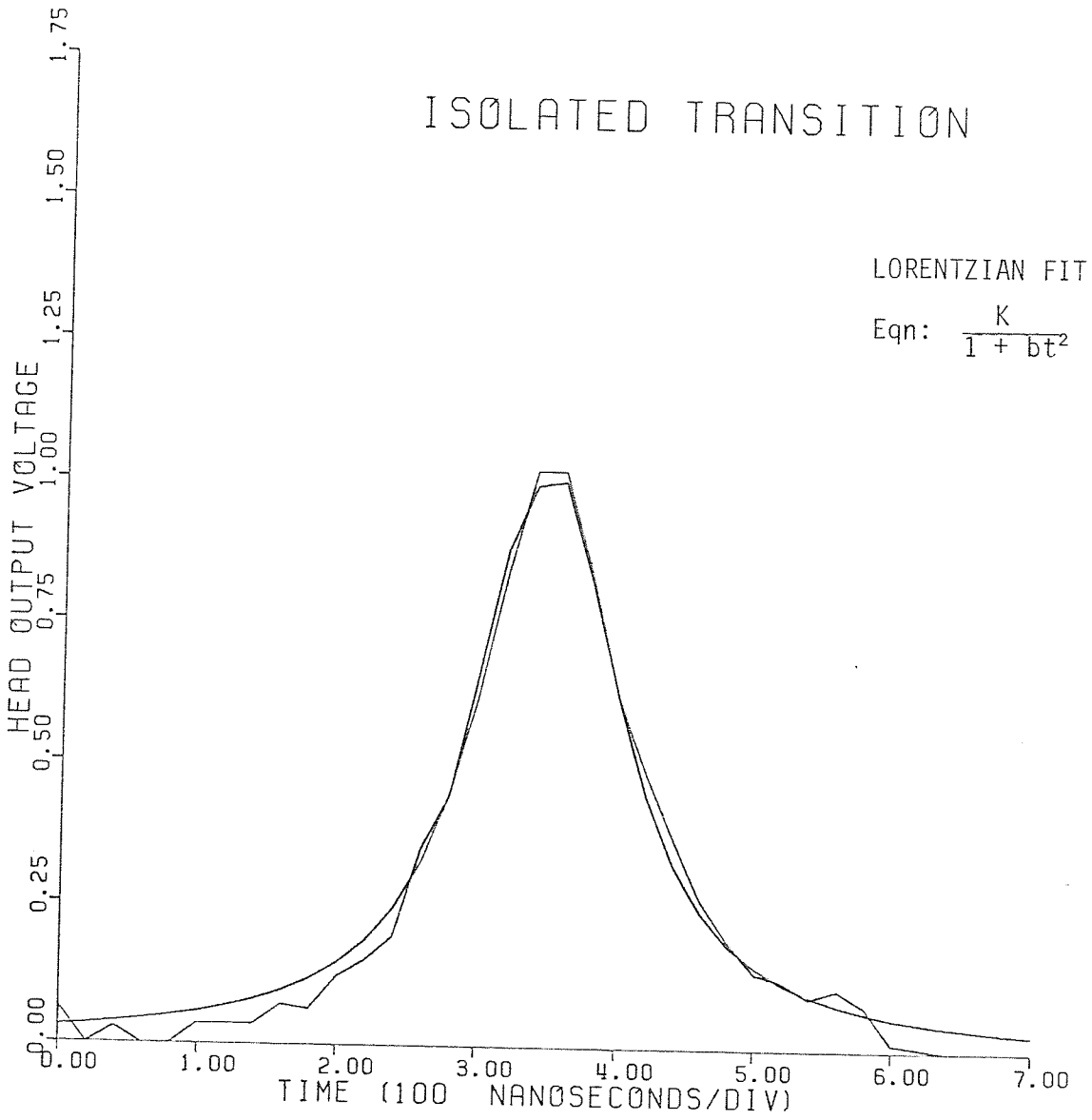

Figure A.1 The least squares fit to the experimentally observed isolated pulse using the Lorentzian analytic expression.

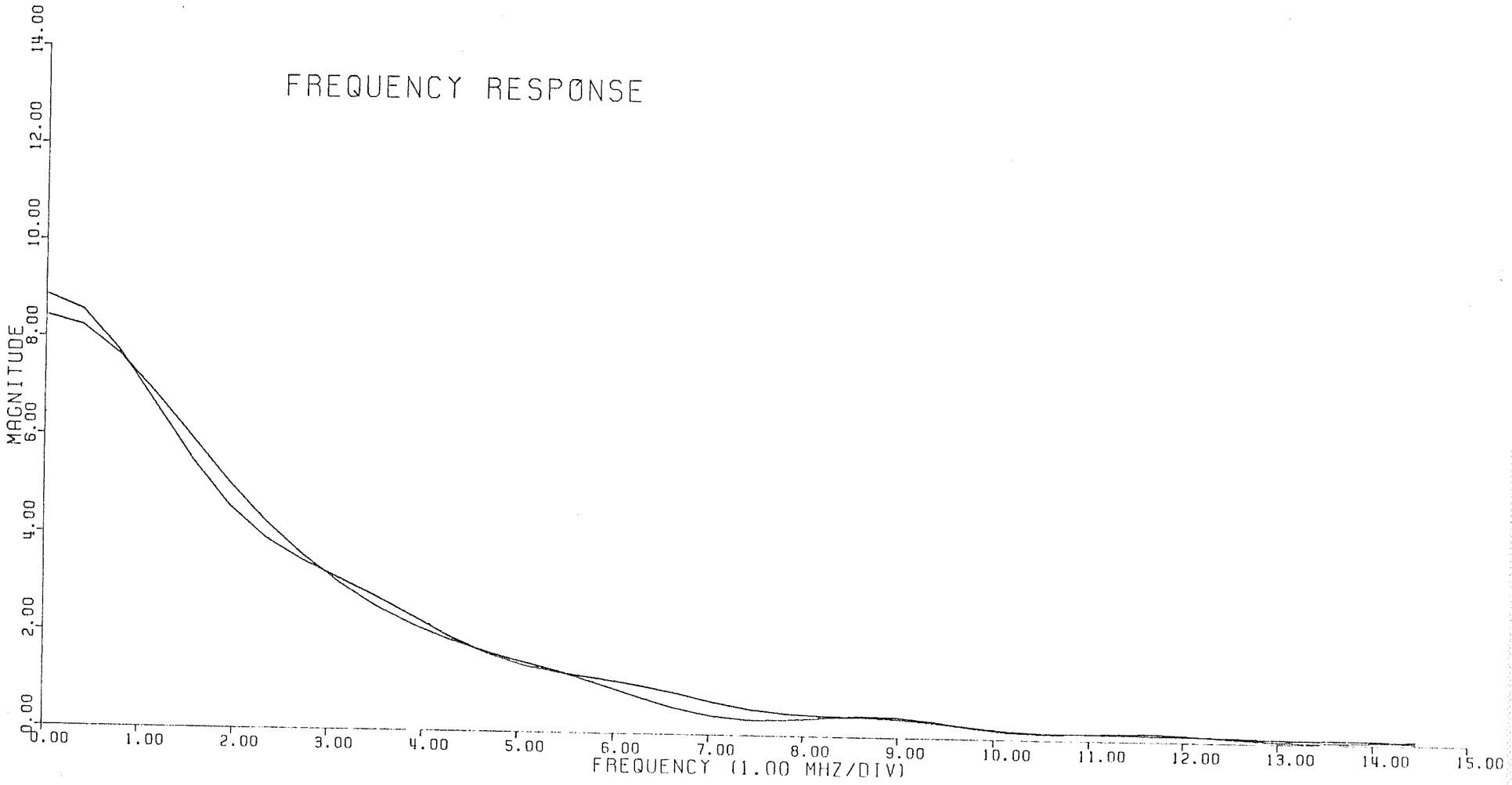

Figure A.2 Magnitude spectrum of the Lorentzian analytic expression and the experimentally observed isolated pulse.

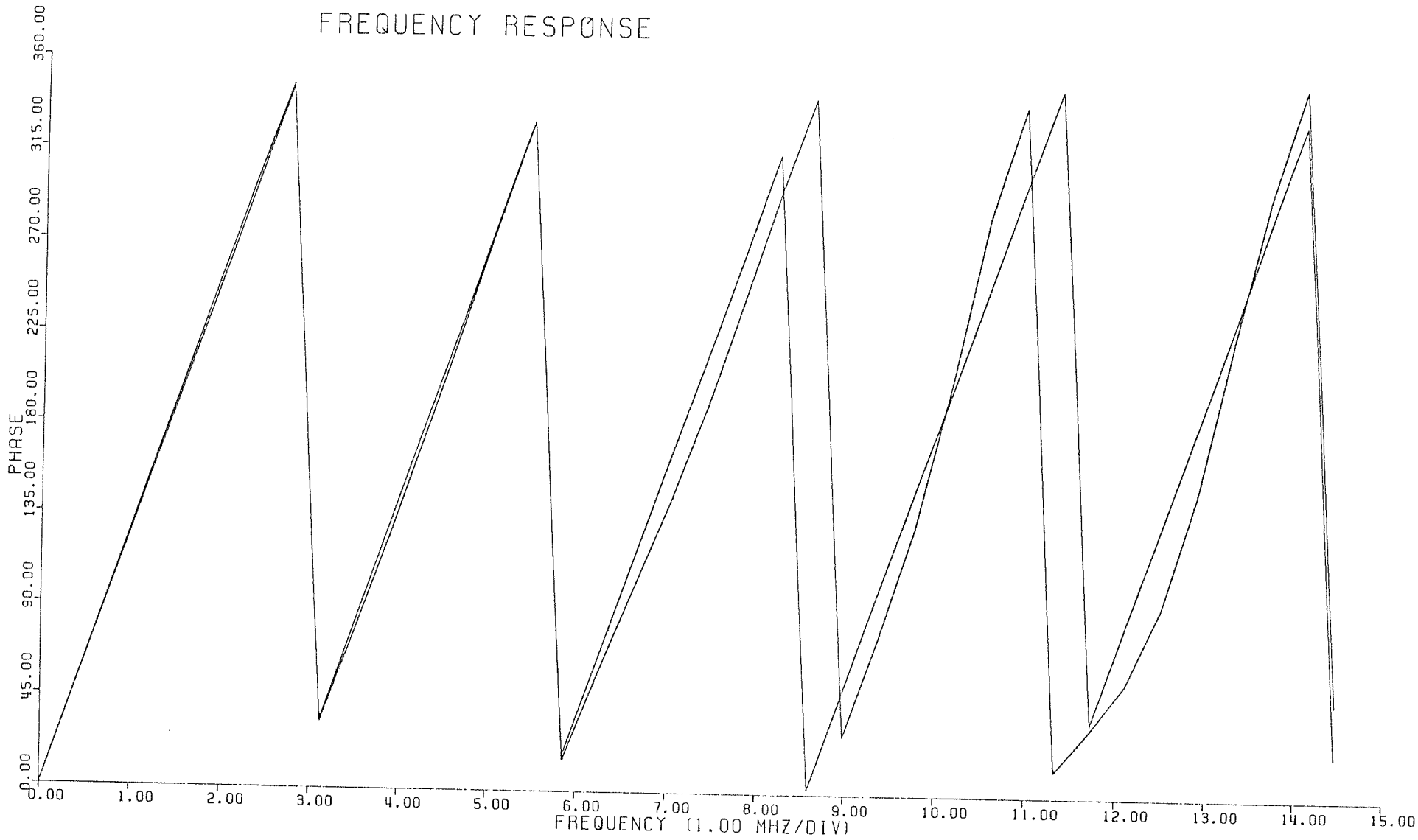

Figure A.3 Phase spectrum of the Lorentzian analytic expression and the experimentally observed isolated pulse.

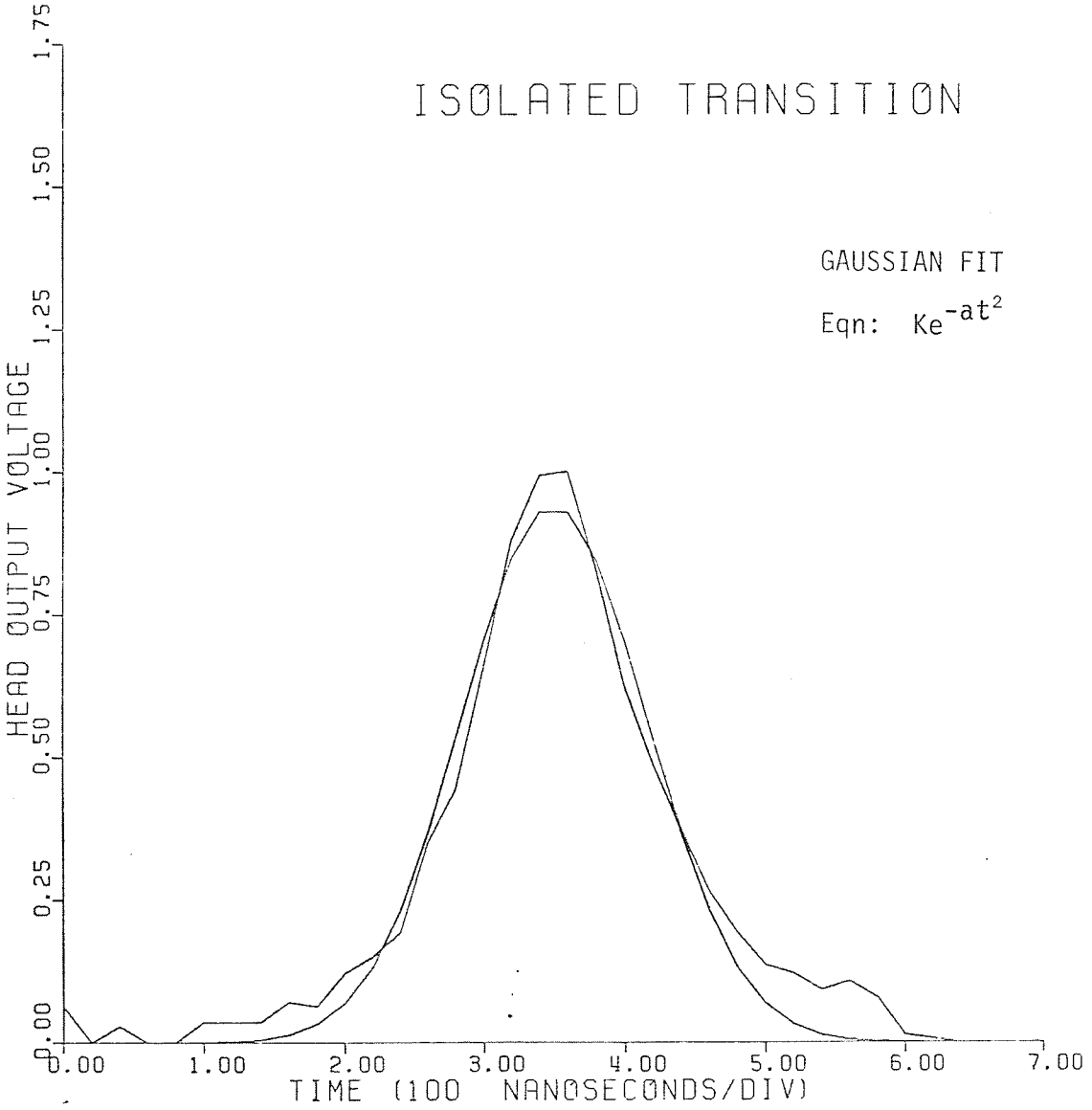

Figure A.4 The least squares fit to the experimentally observed isolated pulse using the Gaussian analytic expression.

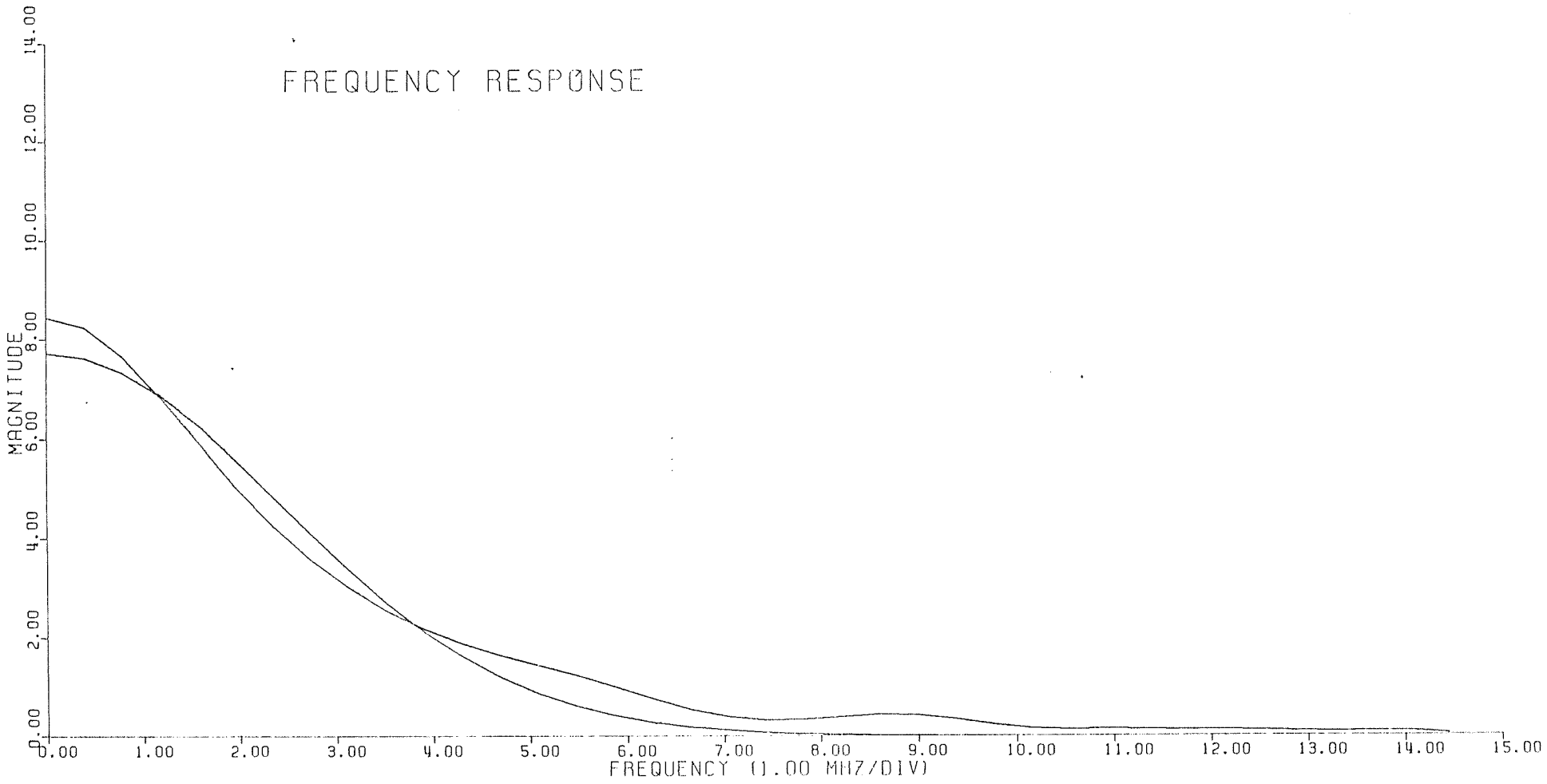

Figure A.5 Magnitude spectrum of the Gaussian analytic expression and the experimentally observed isolated pulse.

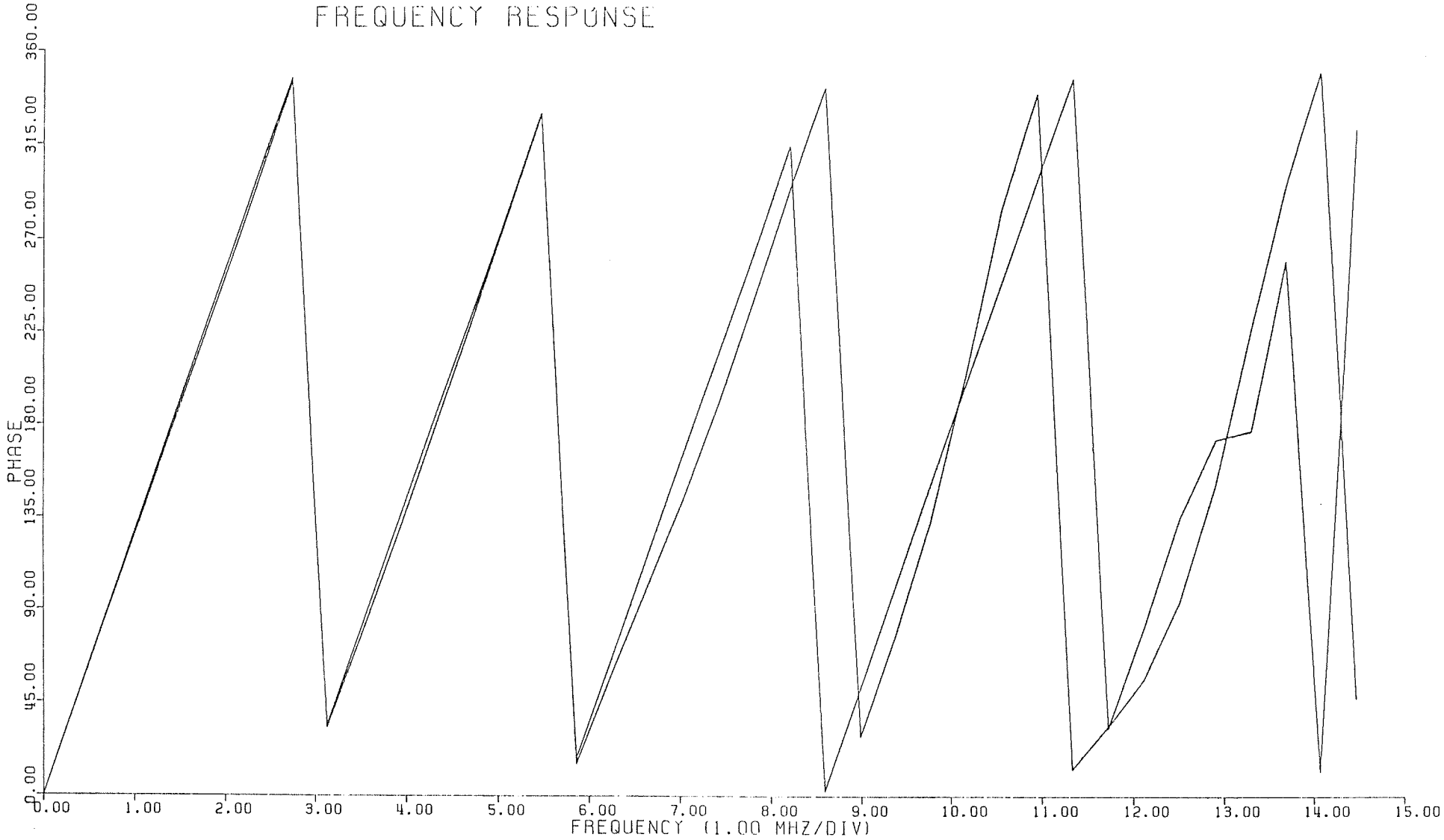

Figure A.6 Phase spectrum of the Gaussian analytic expression and the experimentally observed isolated pulse.

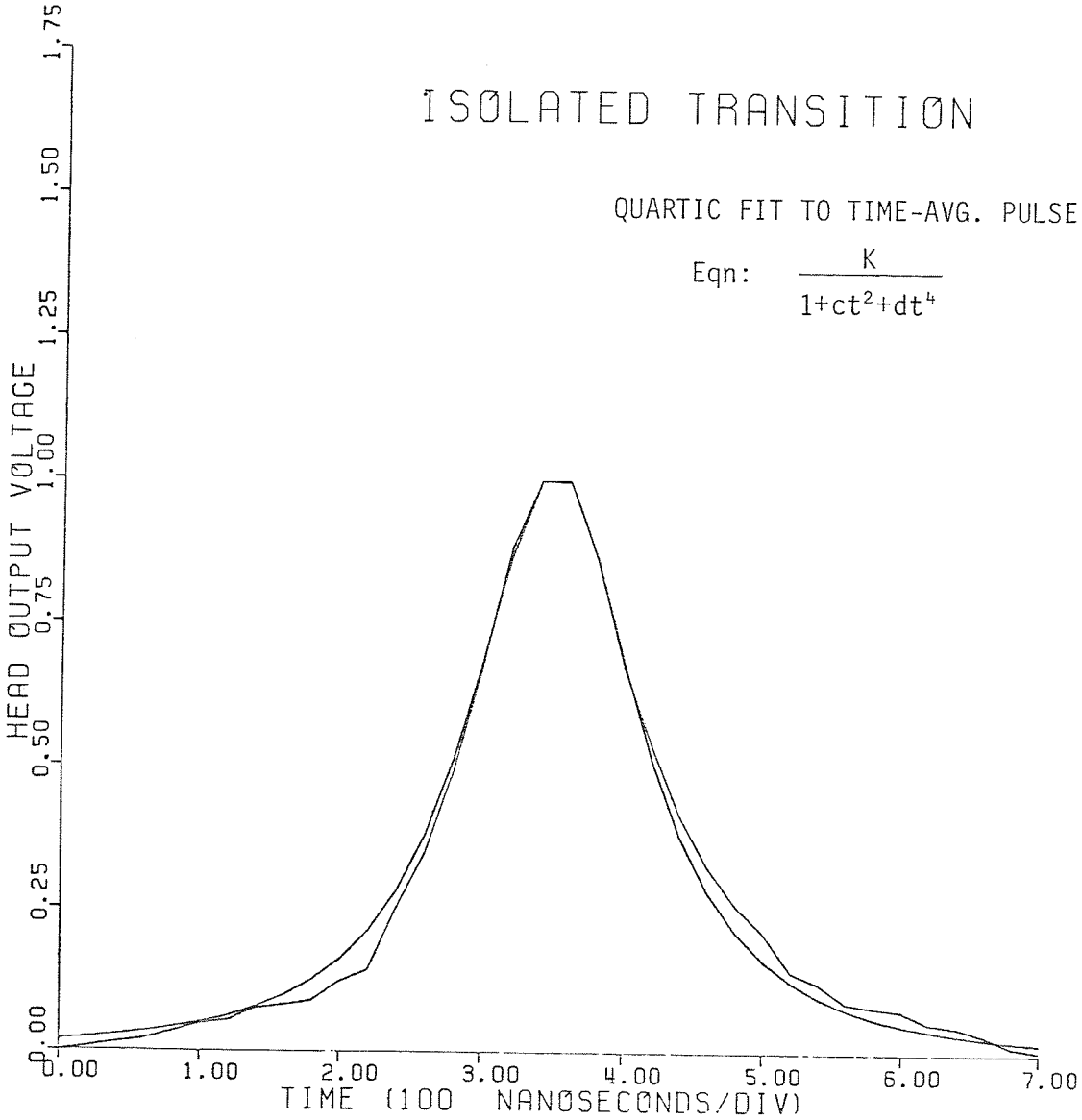

Figure A.7 The least squares fit to the experimentally observed time-averaged isolated pulse using the quartic analytic expression.

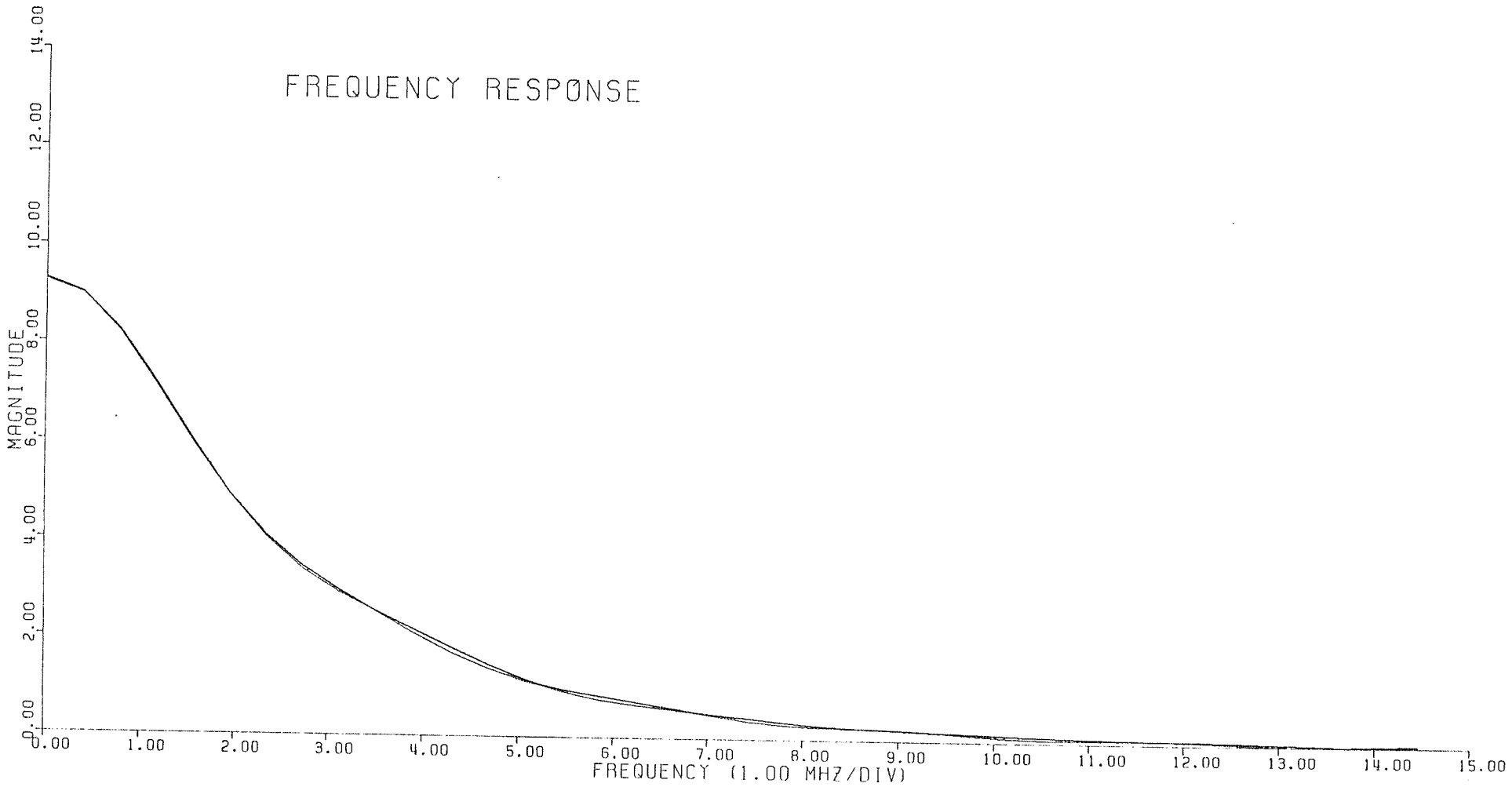

Figure A.8 Magnitude spectrum of the quartic analytic expression and the experimentally observed time-averaged isolated pulse.

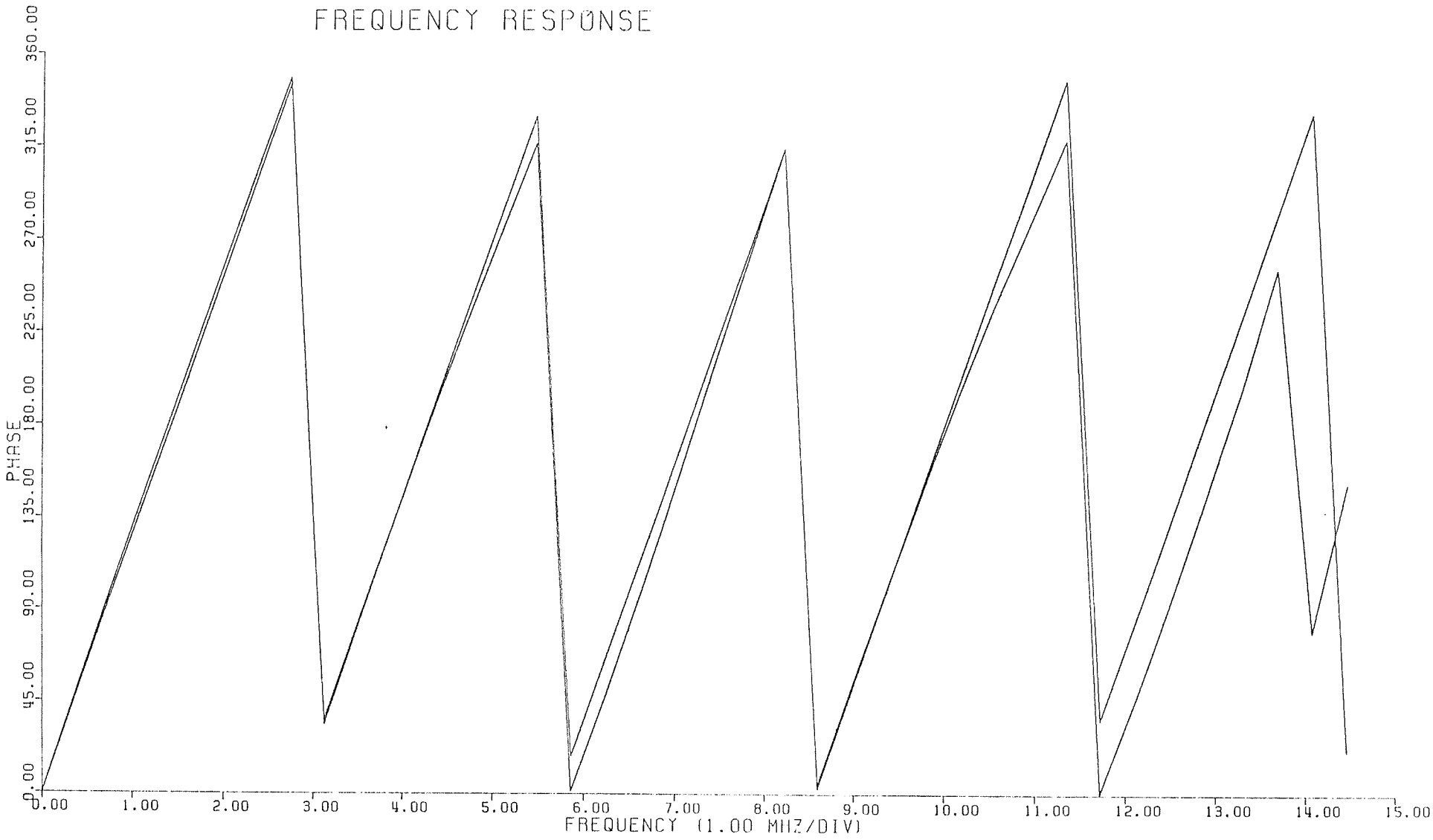

Figure A.9 Phase spectrum of the quartic analytic expression and the experimentally observed time-averaged isolated pulse.

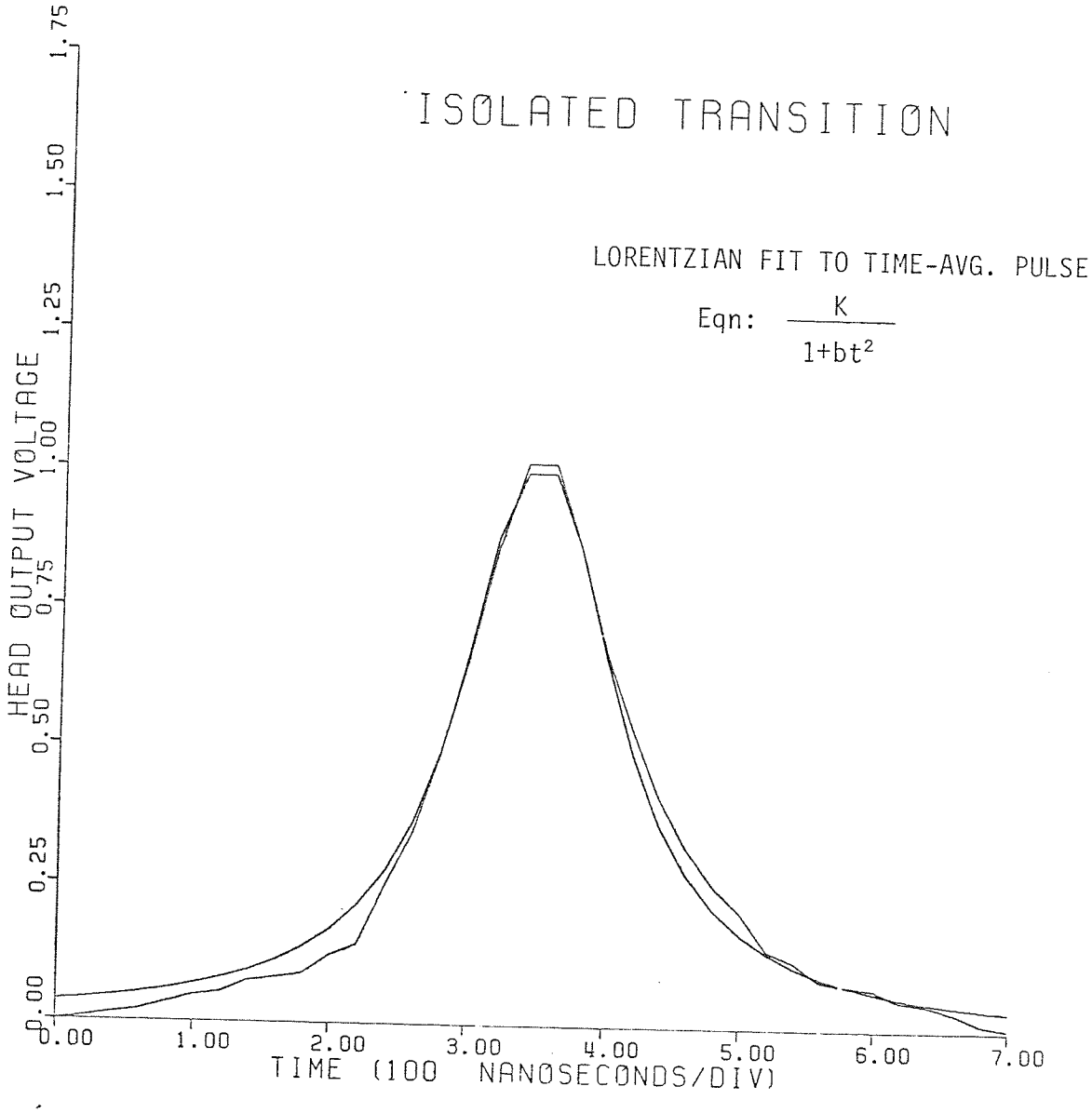

Figure A.10 The least squares fit to the experimentally observed time-averaged isolated pulse using the Lorentzian analytic expression.

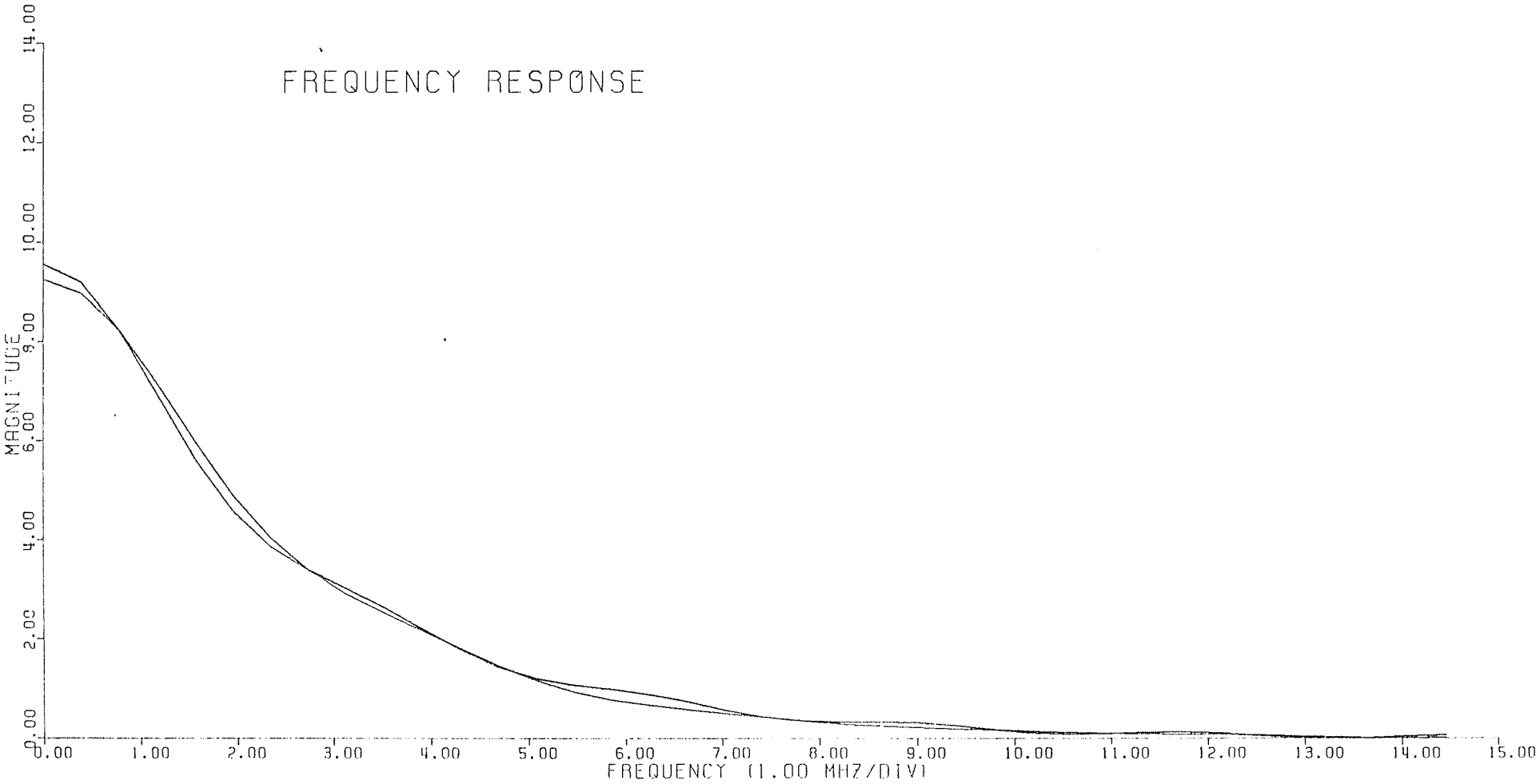

Figure A.11 Magnitude spectrum of the Lorentzian analytic expression and the experimentally observed time-averaged isolated pulse.

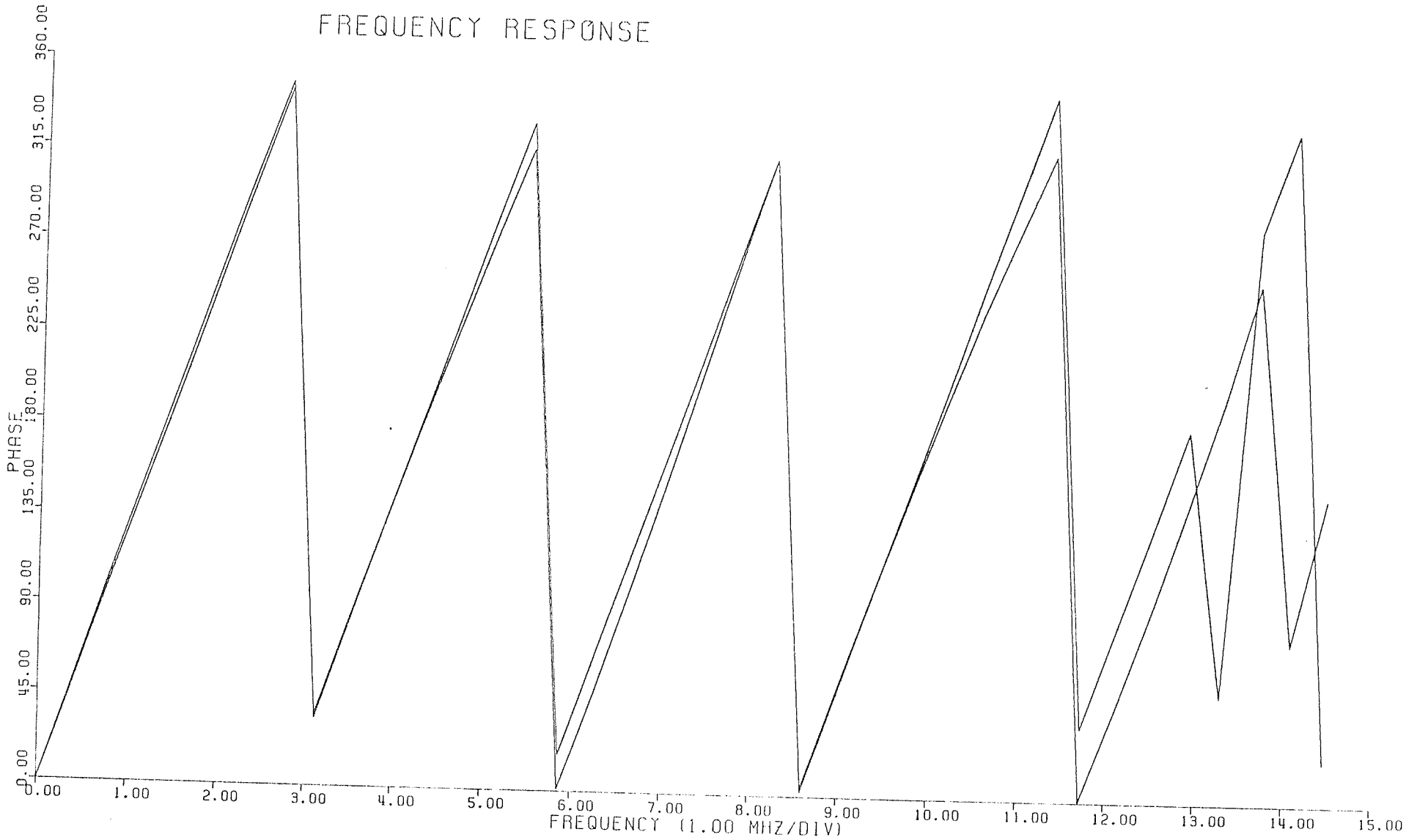

Figure A.12 Phase spectrum of the Lorentzian analytic expression and the experimentally observed time-averaged isolated pulse.

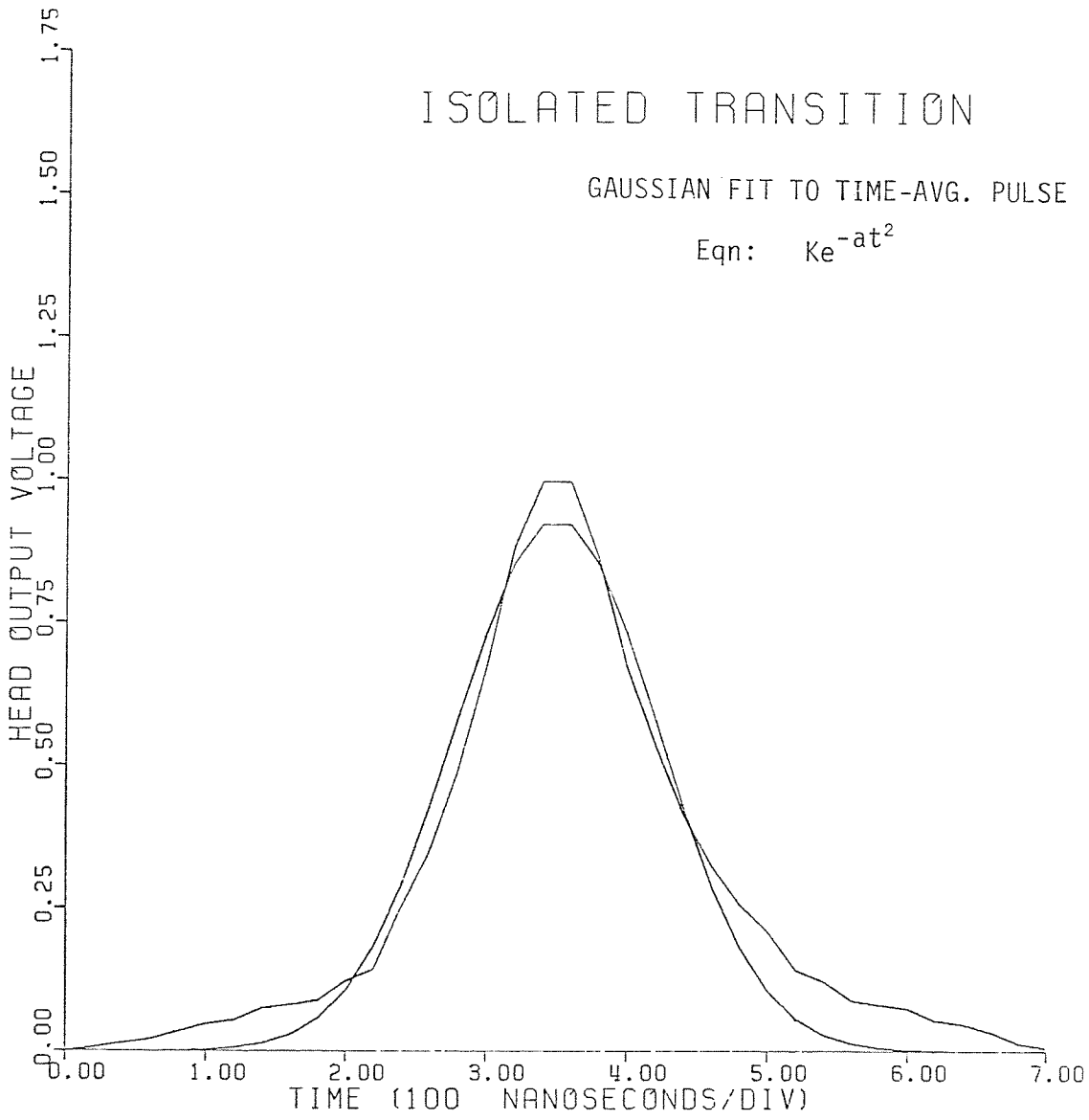

Figure A.13 The least squares fit to the experimentally observed time-averaged isolated pulse using the Gaussian analytic expression.

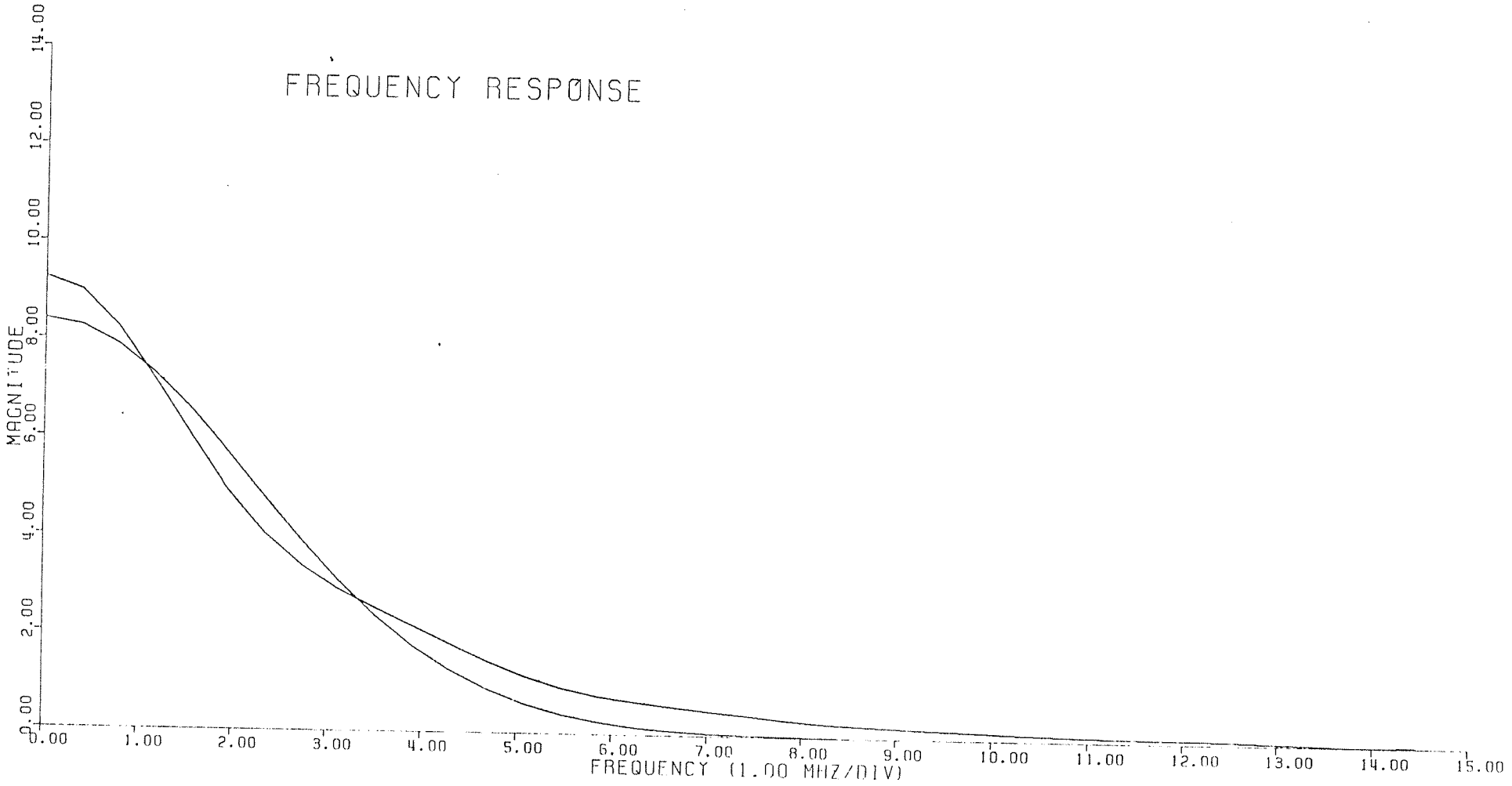

Figure A.14 Magnitude spectrum of the Gaussian analytic expression and the experimentally observed time-averaged isolated pulse.

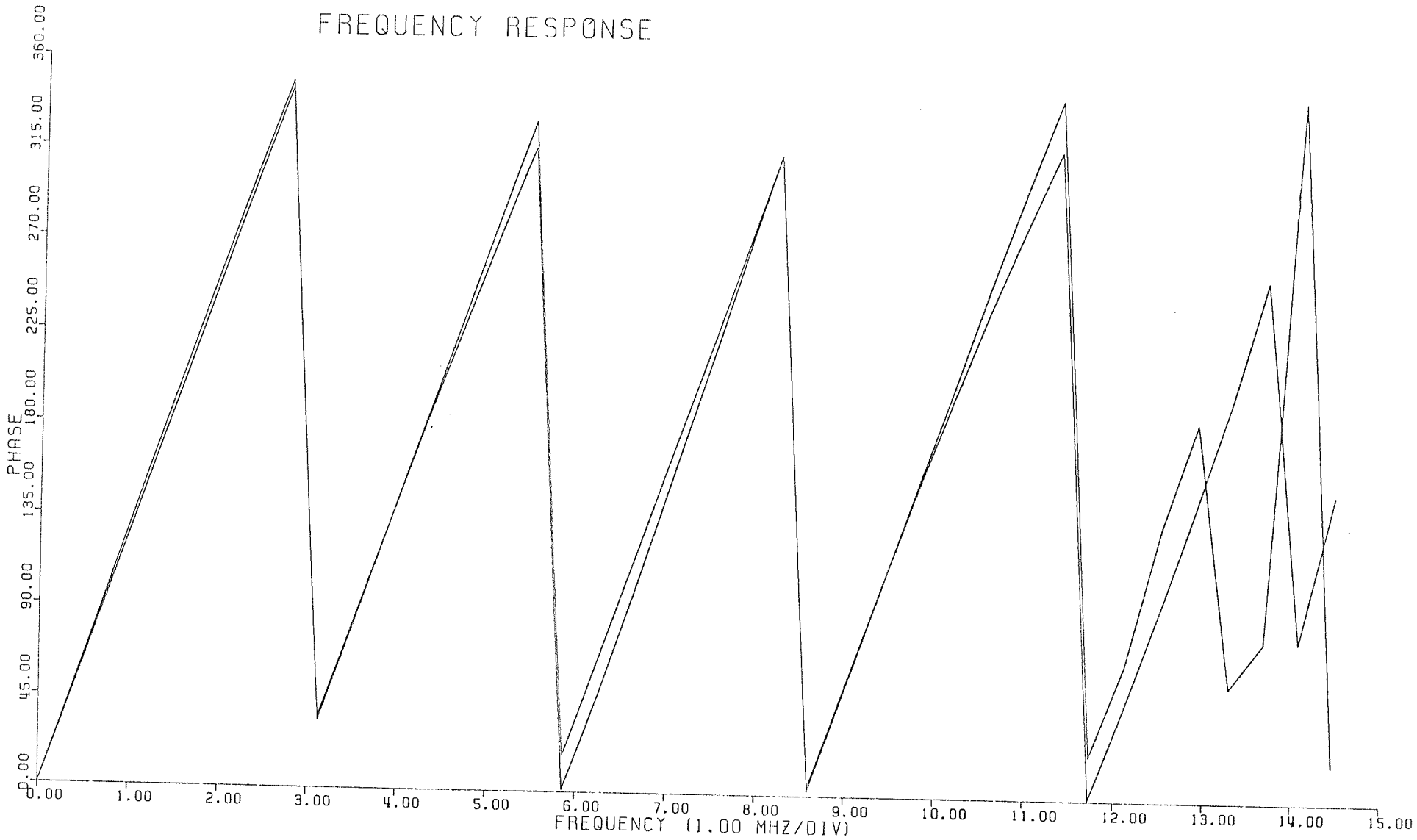

Figure A.15 Phase spectrum of the Gaussian analytic expression and the experimentally observed time-averaged isolated pulse.

APPENDIX B

Least Squares Fit to the Disk Noise Probability Density Function

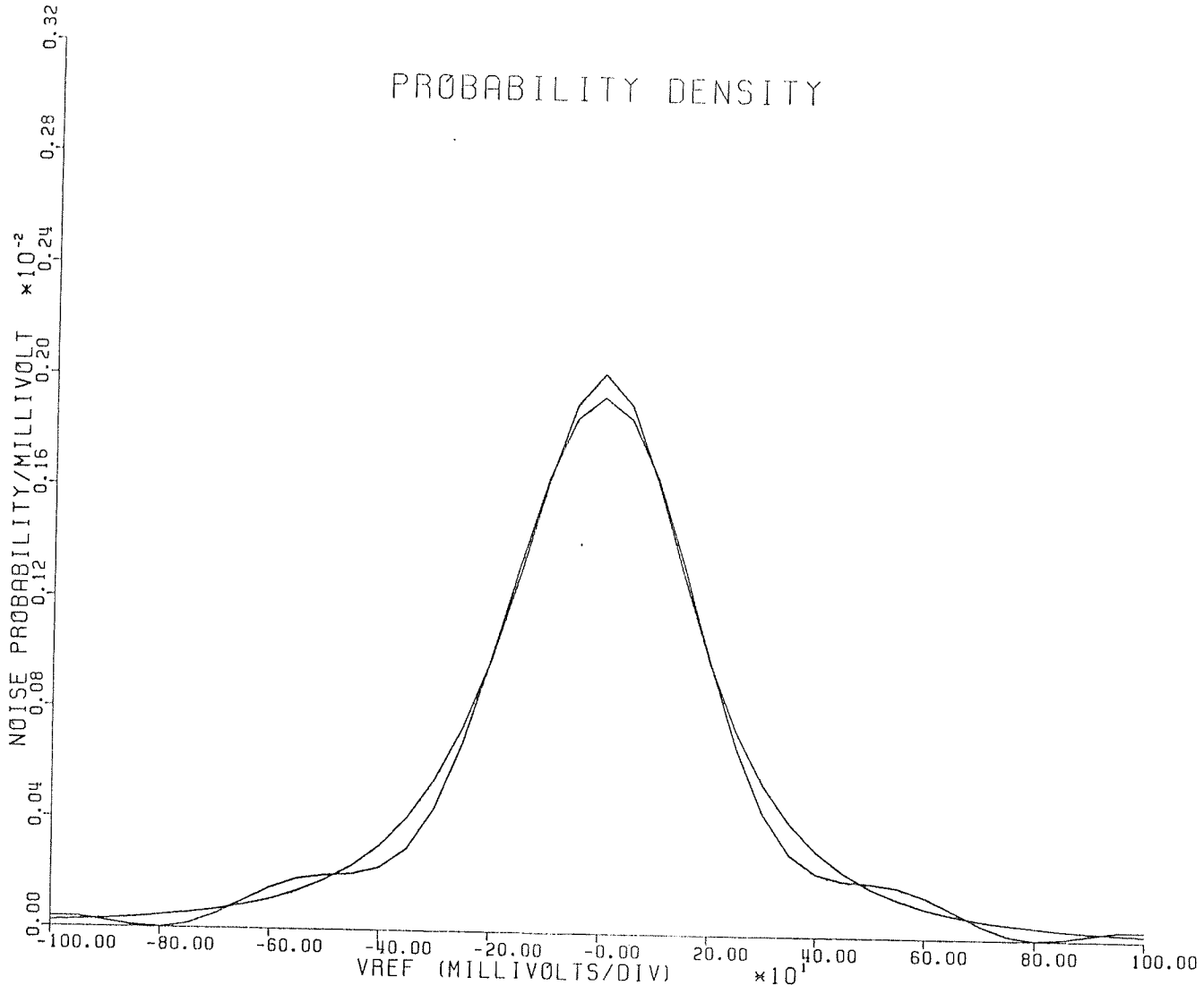

Figure B.1 Least squares fit to the disk noise probability density function using the quartic probability density function.

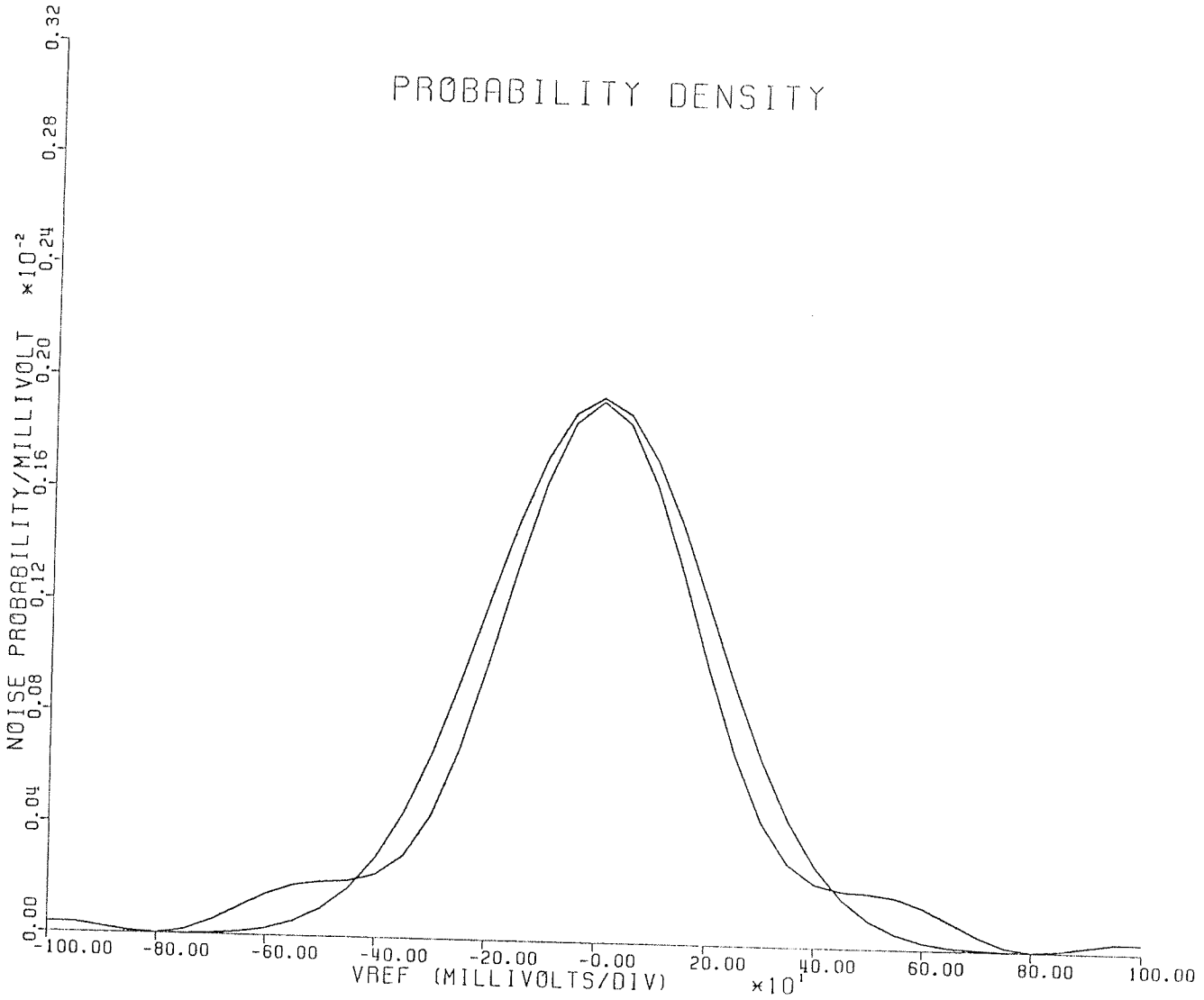

Figure B.2 Least squares fit to the disk noise probability density function using the Gaussian probability density function.

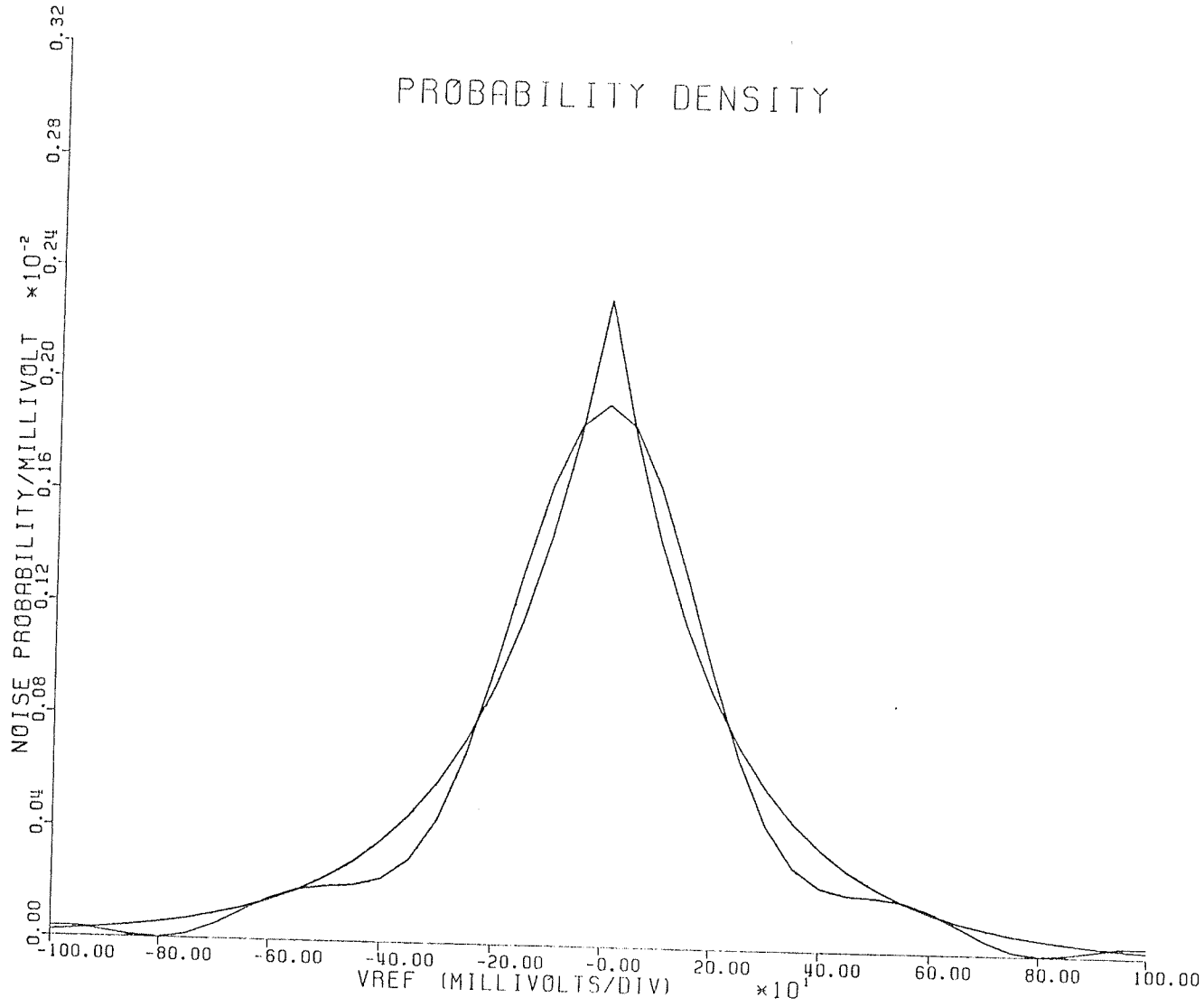

Figure B.3 Least squares fit to the disk noise probability density function using the Laplacian probability density function.

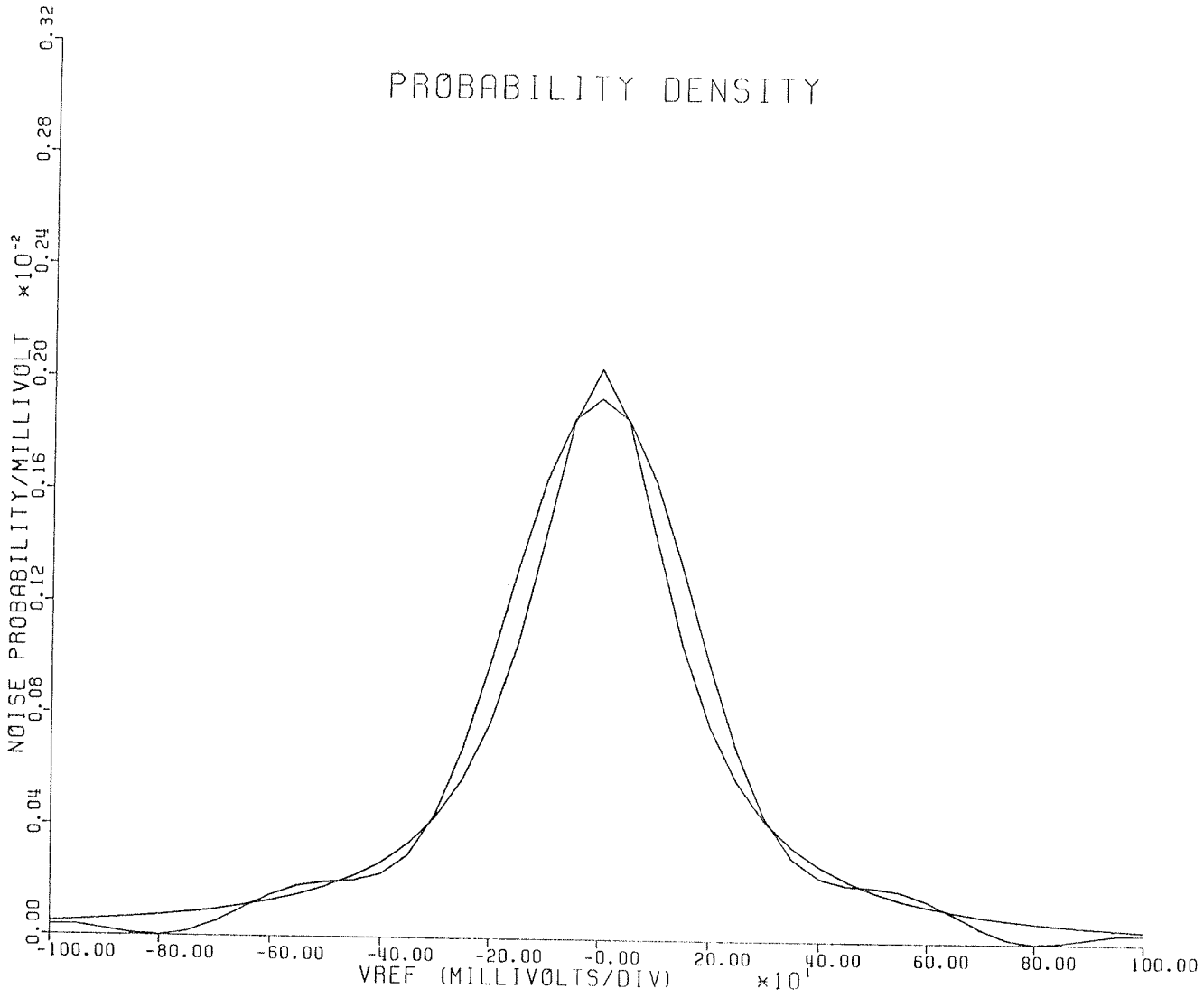

Figure B.4 Least squares fit to the disk noise probability density function using the Lorentzian probability density function.

APPENDIX C

Decision Feedback Equalization Simulation Program

```
      DIMENSION ANALOG(512),XK(512),P(1)
      DATA ANALOG/512*0.0/,XK/512*0.0/
C
C-----------------------------------------------------------------------
C
C     DECISION FEEDBACK EQUALIZATION SIMULATION PROGRAM
C     OF THE BURROUGHS [redacted] DISK DRIVE READ CHAIN
C
C     FEBRUARY 1980
C     DEPARTMENT OF ELECTRICAL ENGINEERING
C     UNIVERSITY OF MANITOBA, WINNIPEG, MANITOBA, R3T 2N2
C
C-----------------------------------------------------------------------
C-----------------------------------------------------------------------
C
C                       PARAMETERS
C
C-----------------------------------------------------------------------
C
      LUNR=5
      LUNW=6
C
      STDEV=0.2617000
      ISEED=12345
      BITS=0.0
      ERRCNT=0.0
      SAVE=0.0
C
      A0=+4.50025
      A1=-0.82720
      A2=-0.42629
      A3=-0.02939
      A4=-0.015384
      A5=-0.037035
      A6=-0.018036
C
      G1=-0.21797
      G2=-0.15030
      G3=-0.06412
      G4=-0.03698
      G5=-0.02557
      G6=-0.01494
C
      FN0=+0.4483
      FN1=+0.3066
      FN2=+0.0680
C
C-----------------------------------------------------------------
C
C                   INITIAL CONDITIONS
C
C-----------------------------------------------------------------
C
      FF1=0.0
      FF2=0.0
      FF3=0.0
      FF4=0.0
      FF5=0.0
      FF6=0.0
      FF7=0.0
      FF8=0.0
      FF9=0.0
      FF10=0.0
      FF11=0.0
```

```
      FF12=0.0
      FB1=0.0
      FB2=0.0
      FB3=0.0
      FB4=0.0
      FB5=0.0
      FB6=0.0
      RN0=0.0
      RN1=0.0
      RN2=0.0
      RN3=0.0
      RN4=0.0
C
C-----------------------------------------------------------------------
C
C     READ PSEUDO RANDOM ANALOG AND BINARY SEQUENCES
C
C-----------------------------------------------------------------------
C
      READ(LUNR,90)  (ANALOG(I),I=1,512)
   90 FORMAT(10X,E12.4)
      WRITE(LUNW,90)  (ANALOG(I),I=1,512)
      READ(LUNR,90)  (XK(I),I=1,512)
      WRITE(LUNW,90)  (XK(I),I=1,512)
C
C-----------------------------------------------------------------------
C
C             CALCULATE SIGNAL-TO-NOISE RATIO
C
C-----------------------------------------------------------------------
C
      VAR=STDEV**2
      E=6.8499
      SNDB=10.00 * ALOG10(E/VAR)
      WRITE(LUNW,1) SNDB
    1 FORMAT(10X,'INPUT SIGNAL-TO-NOISE RATIO = ',F10.5,'DB',/)
C
C-----------------------------------------------------------------------
C
C        CALCULATE PREWHITENED + MATCH FILTERED NOISE SAMPLE
C
C-----------------------------------------------------------------------
C
      DO 50 J=1,2000
      DO 50 I=1,512
      CALL GGUN(ISEED,1,R)
      RN0=R(1) * STDEV
      FNSUM= FN2*(RN0+RN4)+FN1*(RN1+RN3)+FN0*RN2
C
C-----------------------------------------------------------------------
C
C        DECISION FEEDBACK RECEIVER
C
C-----------------------------------------------------------------------
C
      ROFT=ANALOG(I)  + FNSUM
      FFSUM=A6*(ROFT+FF12)+A5*(FF1+FF11)+A4*(FF2+FF10)+A3*(FF3+FF9)
     1      +A2*(FF4+FF8)+A1*(FF5+FF7)+A0*(FF6)
      SK=FFSUM
      BK=FB6*G6+FB5*G5+FB4*G4+FB3*G3+FB2*G2+FB1*G1
      ZK=SK - BK
      THRES=ZK
      IF(THRES.GT.+5.4550)  XKHAT=+9.10
      IF(THRES.LT.-5.4550)  XKHAT=-9.10
```

```
      IF(THRES.LE.+5.4550.AND.THRES.GE.-5.4550) XKHAT=0.0
      DKHAT=SK-XKHAT
      BINOUT=XKHAT/9.10
C     WRITE(LUNW,99) BINOUT
   99 FORMAT(10X,E10.2)
C
C-----------------------------------------------------------------------
C
C          CALCULATE ERROR STATISTICS
C
C-----------------------------------------------------------------------
C
      BITS=BITS+1.00
      IF(BITS.LE.3.0) GO TO 30
      DIFF=ABS(BINOUT-XK(I))
      IF(DIFF.LT.0.01) GO TO 30
      IF(BITS.EQ.SAVE) GO TO 92
      ERRCNT=ERRCNT + 1.00
   92 CONTINUE
C     WRITE(LUNW,91) BITS
   91 FORMAT(20X,E15.8)
      SAVE=BITS + 1.00
   30 CONTINUE
C
C-----------------------------------------------------------------------
C
C     UNIT DELAY TO ALL PARAMETERS   (EXP(-ST))
C
C-----------------------------------------------------------------------
C
      RN4=RN3
      RN3=RN2
      RN2=RN1
      RN1=RN0
C
      FB6=FB5
      FB5=FB4
      FB4=FB3
      FB3=FB2
      FB2=FB1
      FB1=DKHAT
C
      FF12=FF11
      FF11=FF10
      FF10=FF9
      FF9=FF8
      FF8=FF7
      FF7=FF6
      FF6=FF5
      FF5=FF4
      FF4=FF3
      FF3=FF2
      FF2=FF1
      FF1=ROFT
C
   50 CONTINUE
      WRITE(LUNW,35) ERRCNT,BITS
   35 FORMAT('1',10X,E12.5,'ERRORS IN ',E12.5,' BITS READ ',/)
      STOP
      END
```

APPENDIX D

Generation of Pseudo-Random Binary Sequences

Pseudo-random binary sequences have been studied and used extensively for error-correcting codes, multiple access coding, privacy encoding and other similar purposes. In this thesis such sequences were used to simulate a random binary data input stream within the communications channel simulation program.

In the following paragraphs we show how pseudo random binary sequences may be generated through simple operations on matrices. No attempt is made to develop the theory or properties of pseudo-random binary sequences. The discussion will be limited to particular sequences known as maximal length sequences. They are of the most practical interest since they can be generated with a small amount of electronic hardware.

A maximal length sequence is the serially clocked output obtained from a binary linear feedback shift register when certain specific feedback connections are made by a modulo-2 adder. Figure D.1 shows the generalized structure. The coefficients a,b,c, ...,r are binary multipliers or presence coefficients. If, for example, a=1, this signifies a connection is made from the first stage output of the shift register to the modulo-2 adder. The feedback connections for shift registers of up to length 34 are given in Peterson [88].

An equivalent matrix notation may be developed as follows. If each cell of the shift register is represented as intially containing a binary value Y, then the following relations must hold:

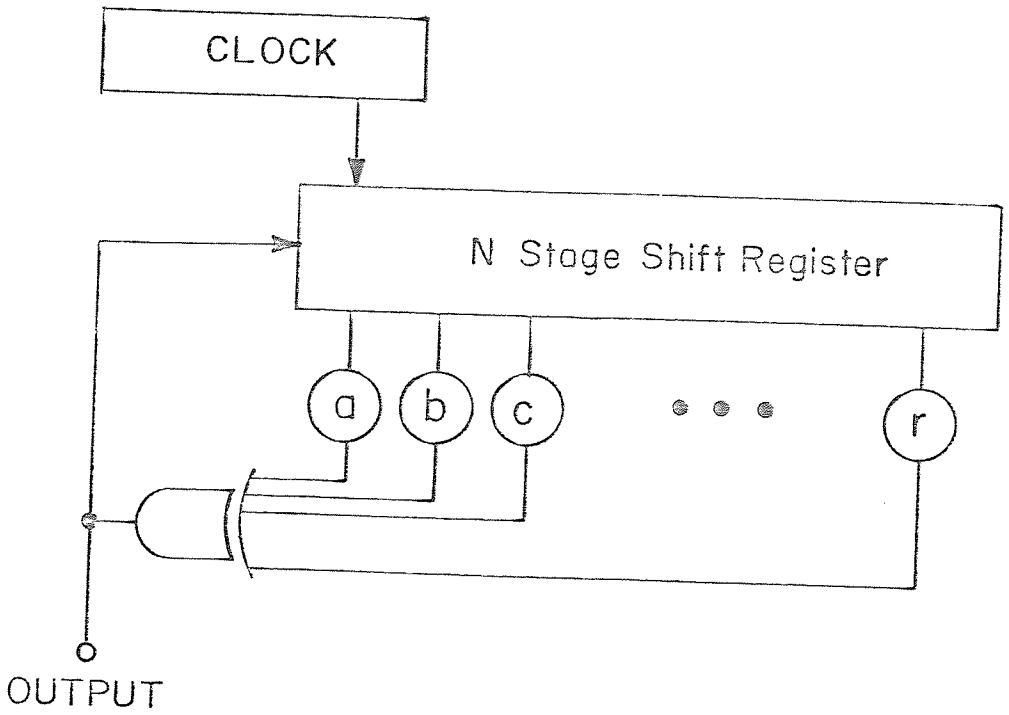

Fig. D.1 . A Binary Linear Feedback Shift Register

$$Y_1' = aY_1 + bY_2 + cY_3 + \ldots + rY_n$$

$$Y_2' = Y_1$$

$$Y_3' = Y_2$$

$$Y_n' = Y_{n-1}$$

where the addition is modulo-2.

These equations can be written conveniently in matrix form as $Y' = TY$ where T is defined as the transition matrix. For the special case of n=4 we can write,

$$\begin{bmatrix} Y_1' \\ Y_2' \\ Y_3' \\ Y_4' \end{bmatrix} = \begin{bmatrix} a & b & c & d \\ 1 & 0 & 0 & 0 \\ 0 & 1 & 0 & 0 \\ 0 & 0 & 1 & 0 \end{bmatrix} \begin{bmatrix} Y_1 \\ Y_2 \\ Y_3 \\ Y_4 \end{bmatrix}$$

where a=1, b=0, c=0, d=1.

If the vector Y is a given state of the shift register, then TY, T^2Y, T^3Y, ... are the following states. If T^{-1} exists, $T^{-1}Y$ is the preceding state.

The maximal cycle length obtainable with n=4 is $k=2^{n-1}=15$ with the all zero state eliminated (since this state is a self-sustaining singleton).